NTNU

Norwegian University of
Science and Technology

Torsion instability of Dynamic Cables during Installation

Marie Finstad Opgård

Norwegian University of Science and Technology
Department of Marine Technology

Preface

This report is the result of a master thesis carried out by stud.techn Marie Finstad Opgård, during the spring semester of 2017 at the Department of Marine Technology, NTNU, under supervision of Prof. Svein Sævik from NTNU. The thesis is a continuation of a specialization project carried out the fall of 2016, in the course TMR4580: *Marine Subsea Engineering, specialization project*. The main findings of the specialization project will be restated in the first chapters of this thesis.

The main topic of this thesis is to study the phenomena of torsion instability during cable installation, and establish parameters which govern the critical behaviour of the cable. This is carried out by following a design procedure proposed by Sævik and Koloshkin. The thesis builds on the findings by Koloshkin in his thesis from 2016.
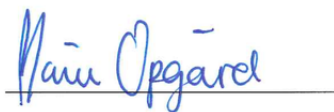
The main dynamic analyses were more time consuming than initially expected. Hence the simulation time was reduced to mange to complete the desirable simulation cases within the time limit. Had I known this beforehand, it would have been preferable to initiate the analyses at an earlier stage.

I would like to express great gratitude to professor Svein Sævik for his guidance and support during the thesis. His help throughout the semester has made the outcome of this thesis very valuable. Due to his expertise and participation in the development of the utilized software SIMLA, he has been of great help when I have encountered programming problems. I also want to thank my co-students at office A2.015 for their encouragement and willingness to discuss theories and results.

The thesis is written with the assumption that the reader has some foreknowledge in the field of marine and structural engineering.

Trondheim, Norway

June 2017

Marie Finstad Opgård

i

Summary

The oil and gas industry today is a heavily regulated segment, and current standard has established restrictions which yields a very limited weather window for offshore cable installations. This is due to experience with cable failure in harsh weather. A limiting factor in current practice is the design criterion for the minimum allowable radius of curvature in the touch down point. In addition, current practice does not allow for occurrence of compression in the touch down zone, since this is associated with loop formation and loss of the functionality of the cable. The main purpose of this thesis is to investigate the validity and conservatism of current practice, by investigating the issues related to torsion instability through a proposed design procedure.

The scope of the thesis comprehends numerical analyses using the SINTEF OCEAN developed software SIMLA. The numerical studies concern a J-lay installation scenario at 100 meters water depth with an implemented cable laying vessel with realistic RAO properties. Two real-life cable cross-sections are evaluated; a single-layered cable without armoring (umbilical 1) and a torsional balanced cable with double-armoring (umbilical 2). The mechanical properties of these are calculated analytically, where the main differences lay in the torsional stiffness of the cross-sections. The effect of installation route is evaluated, and two scenarios are simulated; an end cap turn and a curved route to avoid obstacles.

The results are obtained in two steps. Primarily, the critical values of torsion moment and resultant curvature with respect to loop formation are established. These parameters are determined for both a linear and a non-linear pipe material model. The table below summarizes the main findings with regards to the capacity parameters of the cross-sections.

Torsion capacity parameters for umbilical 1 and 2

	Critical torsion moment [kNm]		Critical resultant curvature [1/m]	
	PIPE31	COMPIPE42	PIPE31	COMPIPE42
Umbilical 1	4.28	3.72	1.30	0.28
Umbilical 2	15.07	52.89	0.90	0.07

Subsequently a range of dynamic analyses with irregular waves are carried out. The irregular waves are applied using a Pierson-Moskowitz wave spectrum with $H_s = 2 - 3m$ and $T_p = 7 - 10s$ with a one hour simulation time. In the dynamic analyses, the torsion moment

and curvature in the cable are analyzed and compared with the capacity parameters for each scenario. For umbilical 1 it is found that the maximum resultant curvature for all sea states exceeds the critical API curvature, while the torsion moment is below the critical torsion moment. The sea states can, due to excess of the API criterion, not be classified as acceptable. It is also concluded that a contributing factor is the low magnitude of the horizontal bottom tension. The maximum resultant curvature for umbilical 2 oscillates around curvature values below the design criterion for minimum radius of curvature for all sea states. The torsion moments are lower than the critical torsion moment. All sea states for umbilical 2 are categorized as acceptable with respect to experienced resultant curvature.

It is in addition investigated whether the cables experience compression in the touch down zone while subjected to irregular waves. For umbilical 1 it is found that compression occurs in the touch down zone for all sea states for both installation scenarios. Umbilical 2 experiences compression in varying degree for all sea states except for $H_s = 2m, T_p = 7s$. The magnitude of the compressive axial force is increasing in accordance with increasing wave height and period. The magnitude of the compressive axial forces experienced are compared with the buckling loads associated with local helix buckling and birdcaging. None of the force values are within the range for the buckling loads for tensile armour buckling. Hence it can be concluded that its possible with occurrence of compression without necessarily associated kink formation nor local buckling.

The effect of wave heading is also investigated. Changing the wave heading impacts the maximum resultant curvature. It is found that the most critical scenario occur when the waves are incoming with a heading of $[\pi, 2\pi]$. This is due to the cable configuration, which experience a slight bend in the touch down zone at the initiation of the dynamics. It is also carried out a study of the effect of additional sea current. A current velocity of $4m/s$ with correspondingly heading of $0°, 90°, 180°, 270°$ is applied. This result in the observation that the most critical scenario is a current heading of 180 ° due to reduction of the cable' effective weight.

It is investigated whether a too low horizontal bottom tension is the reason of the severe curvature levels for umbilical 1. Analyses with a $T_0 = 5kN$ are run for the respective sea states. Resulting from this the curvature levels for umbilical 1 is lowered to acceptable levels for $H_s = 2m$. The same analyses are carried out for umbilical 2, where the resulting curvatures increase compared to lower initial tension. This is due to severe yielding of the friction moment for the case of $T_0 = 5kN$, inducing more severe deformation of the cable.

Sammendrag

Olje- og gassindustrien i dag er en svært regulert industri, og når det gjelder installasjon av fleksible stigerør medfører dagens standard et svært begrenset værvindu for gjennomføring av installasjoner. Dette er grunnet erfaring med kabelsvikt under tøffe værforhold. En begrensende parameter i forbindelse med kabelinstallasjon er et etablert design kriterium som begrenser den tillatte krumningsradiusen i touch down regionen. Samt tillater ikke dagens praksis tilstedeværelse av kompresjon i touch down regionen, da dette er assosiert med dannelse av loop og svikt av kabelens funksjonalitet. Hovedformålet med denne oppgaven er å undersøke gyldigheten og konservatismen til dagens praksis, ved å studere problemer knyttet til torsjonsinstabilitet.

Omfanget av masteroppgaven omfatter i hovedsak numeriske analyser i SIMLA, et ikke-lineært program utviklet av SINTEF OCEAN. De numeriske analysene simulerer et J-lay installasjonsscenario på 100 meters vanndyp. To eksisterende kabeltverrsnitt blir analysert; en ett-lags kabel uten armering (kabel 1) og en torsjonsbalansert kabel med dobbel armering (kabel 2). Kablenes mekaniske og strukturelle egenskaper er beregnet analytisk, hvor den største forskjellen mellom tverrsnittene er torsjonsstivheten. Effekten av installasjonsrute er evaluert, og to forskjellige scenarioer er simulert; en "end-cap" vending på 180 grader nært forankringspunktet og en krum rute pga hindringer på sjøbunnen.

Resultatene blir presentert i to trinn. I første omgang er de kritiske verdiene for torsjonsmoment og resultantkrumning knyttet til loop dannelse for begge tverrsnitt estimert. Disse parameterne er beregnet for både lineære og ikke-lineære materialmodeller. Tabellen nedenfor oppsummerer maksimal verdiene for torsjonsmoment og resultantkrumning respektivt, hvor kritisk krumning er hentet fra tidspunktet hvor maksimum torsjonsmoment oppnås.

Torsjonskapasitetsparametere for umbilical 1 and 2

	Maks torsjonsmoment [kNm]		Maks resultant krumning [1/m]	
	PIPE31	COMPIPE42	PIPE31	COMPIPE42
Kabel 1	4.28	3.72	1.30	0.28
Kabel 2	15.07	52.89	0.90	0.07

Deretter er det blitt gjennomført dynamiske analyser med irregulære bølger. De irregulære bølgene blir påført ved et Pierson-Moskowitz spektrum med $H_s = 2-3m$ og $T_p = 7-10s$, hvor

stimuleringstiden er én time. I de dynamiske analysene blir torsjonsmoment og krumning analysert med respekt på kapasitetsverdiene definert for hvert scenario. For kabel 1 er det funnet at den maksimale resultantkrumningen for alle sjøtilstander overstiger det kritiske API kravet til krumningsnivå, mens det resulterende torsjonsmomentet ligger på et nivå under det etablerte kritiske momentet. De høye krumningsverdiene er funnet til å trolig være knyttet til det lave bunnstrekket i kabelen. For kabel 2 oscillerer den maksimale resultantkrumningen rundt verdier under kriteriet for minimum krumningsradius for alle sjøtilstandene, og torsjonsmomentet er lavere enn kritisk kapasitetsverdi. Ut ifra dette defineres alle sjøtilstandene simulert for kabel 2 som akseptable.

Det er undersøkt om kablene opplever kompresjon i TDP når utsatt for irregulære bølger. For kabel 1 er det funnet tilstedeværelse av aksiell kompresjon i touch down regionen for alle sjøtilstander for begge installasjonsscenarioer. Kabel 2 opplever kompresjon i varierende grad for alle sjøtilstander med unntak av $H_s = 2m, T_p = 7s$. Kompresjonskraften øker i samsvar med økende bølgehøyde og -periode. Størrelsen på kompresjonskraften er sammenlignet med kritiske knekkingsverdier assosiert med lokal knekking av armeringen. Ingen av sjøtilstandene induserer aksialkrefter av samme størrelsesorden som knekklastene. Det kan derfor bli konkludert med at tilstedeværelse av kompresjon i touch down region ikke nødvendigvis medbringer lokal knekking eller loop formasjon, og kan være akseptabelt.

Effekten av bølgeretning er også undersøkt. Dette er gjort for kabel 2, med en sjøtilstand tilsvarende $H_s = 3m, T_p = 10s$. Ved å endre retningen på innkommende bølger påvirkes den maksimale resultantkrumningen. Det er funnet at den mest kritiske tilstanden er når bølgende kommer med vinkel i området $[\pi, 2\pi]$. Dette skyldes kabelkonfigurasjonen i det dynamikken aktiveres, hvor kabelen opplever en bøyning i touch down regionen. En studie knyttet til effekten av strømning er også gjennomført. En strømningshastighet på $4m/s$ med korresponderende vinkel på 0°, 90°, 180° og 270° er påført systemet. Dette resultere i observasjonen av at kombinasjonen av strøm med en retning på 180 ° gir mest kritiske krumningsverdier, grunnet reduksjon av kabelens effektive vekt.

Det er undersøkt om et for lavt bunnstrekk er grunnen til overskridelse av API kriteriet for kabel 1. Analyser med $T_0 = 5kN$ er gjennomført for de respektive sjøtilstandene. Resultatet indikerer at krumningsnivået nå synker til akseptable verdier, under det kritiske krumningskriteriet. Samme analyser med T_0 er også kjørt for kabel 2. I motsetning til kabel 1, opplever kabel 2 høyere krumningsverdier når bunnstrekket økes. Dette skyldes overskridelse av tverrsnittets friksjonsmoment og dermed flytning, noe som medfører mer betydelige deformasjoner av kabelen.

Scope of Work

THESIS WORK SPRING 2017

for

Stud. tech. Marie Finstad Opgård

Torsion instability of Dynamic Cables during Installation

Torsjonsinstabilitet av Dynamiske fleksible stigerør under installasjon

During installation, both dynamic and static cables may be exposed to combined action of severe curvature and axial compression at the touch down point. This may result in local buckling inside the cross-section that causes the cross-section to be unstable in torsion, global loop formation or a combination of these, finally resulting in capacity failure. Current practice is to not allow compression at the TDP, which causes high installation costs due to the limited weather window for installation. Previously the above issue has been addressed by the master thesis of Evgenii Koloshkin (2016), however, without concluding with respect to design criteria.

This master thesis continues on the basis of the project work carried out during Fall 2016 where the primary objective is to formulate and validate a design procedure for handling the installation kinking failure model. The master thesis work is to be carried out as follows:

1. Literature study as performed during the project work, including cable technology, methods for cross-section analysis, failure modes and design criteria. with particular focus on the kinking global modes and the local helix buckling failure modes, analytical and numerical methods for stress and tensile armour buckling analysis of flexible pipes and the non-linear Marintek FE software Simla.

2. Establish a realistic installation scenario including seabed profile, route, weather data and vessel motions. Evaluate the installation route and focus on sections where the relative yaw rotation between the vessel and TDP is large.

3. Based on a conservative estimate of the torsion stiffness of a set of cross-sections, calculate the inherent torque for the different installation scenarios at the critical route sections.

4. Calculate lower and upper bound values of the cross-section friction moment for a the same set of cross-sections. Also calculate the minimum radius of curvature for the selected cross-sections.

5. Predict the critical curvature associated with kink formation for these cases.

6. Perform dynamic analysis with the built-in torque level and based on using a non-linear moment curvature model and the dynamic maximum curvature at TDP as a measure of kink formation

7. Use a sufficient number of cycles to prove that kink formations is not developed due to accumulated plastic deformations. If a stable value of the maximum curvature is obtained without kink formation and the standard maximum curvature design criteria is not exceeded, the sea state is acceptable.

8. If compression occurs during the dynamic analyses, the design check also need to include local helix buckling and birdcaging.

9. Conclusions and recommendations for further work

The scope of work may prove to be larger than initially anticipated. Subject to approval from the supervisors, topics may be deleted from the list above or reduced in extent.

In the thesis the candidate shall present his personal contribution to the resolution of problems within the scope of the thesis work

Theories and conclusions should be based on mathematical derivations and/or logic reasoning identifying the various steps in the deduction.

The candidate should utilise the existing possibilities for obtaining relevant literature.

Thesis format
The thesis should be organised in a rational manner to give a clear exposition of results, assessments, and conclusions. The text should be brief and to the point, with a clear language. Telegraphic language should be avoided.

The thesis shall contain the following elements: A text defining the scope, preface, list of contents, summary, main body of thesis, conclusions with recommendations for further work, list of symbols and acronyms, references and (optional) appendices. All figures, tables and

equations shall be numerated.

The supervisors may require that the candidate, in an early stage of the work, presents a written plan for the completion of the work.

The original contribution of the candidate and material taken from other sources shall be clearly defined. Work from other sources shall be properly referenced using an acknowledged referencing system.

The report shall be submitted in two copies:
- Signed by the candidate
- The text defining the scope included
- In bound volume(s)
- Drawings and/or computer prints which cannot be bound should be organised in a separate folder.

Ownership
NTNU has according to the present rules the ownership of the thesis. Any use of the thesis has to be approved by NTNU (or external partner when this applies). The department has the right to use the thesis as if the work was carried out by a NTNU employee, if nothing else has been agreed in advance.

Thesis supervisor Prof. Svein Sævik, NTNU.

Deadline: June 11, 2017

Trondheim, January, 2017

Svein Sævik

Candidate's - date and signature:

Contents

List of Tables

List of Figures

Nomenclature

Acronyms

API	American Petroleum Institute
CLV	Cable laying vessel
DNV	Det Norske Vertitas
FEM	Finite Element Method
LR	Locking radius
MBR	Minimum Bending Radius
PE	Polyethylene
PVD	Principle of Virtual Displacements
PVW	Principle of Virtual Work
RAO	Response Amplitude Operator
SR	Storage radius
TDP	Touch down point
TDZ	Touch Down Zone
TL	Total Langrangian
UL	Updated Langranian
XLPE	Cross-linked Polyethylene

Greek Letters

α	Lay angle
β	Torsion coupling parameter
β_2	Pipe curvature about the Z^2-axis
ϵ	Strain component
ϵ_{lim}	Maximum allowable strain
η	Sea surface elevation
γ	Peakedness parameter
κ_i	Curvature components
μ	Friction coefficient
ω	Wave frequency
ϕ_{jk}	Phase angles
ψ	Angular coordinate
ρ	Density
ρ_l	Locking radius
σ	Spectrum width
σ	Stress components
τ	Torsion component
θ	Rotation
υ_a	Apparent Poisson's ratio

Roman letters

$\ddot{u}$ Acceleration component

$\dot{u}$ Velocity component

$\ddot{\mathbf{r}}$ Acceleration vector

$\dot{\mathbf{r}}$ Velocity vector

$\mathbf{C}$ Damping matrix

$\mathbf{M}$ Mass matrix

A Cross-section area

A_e Enclosed area

B Buoyancy force

b Wire width

C_a Added mass coefficient

C_D Drag coefficient

D Diameter

d Loop diameter

E_{xx} Green strain

EA Axial stiffness

EI_e Elastic bending stiffness

EI_s Slip bending stiffness

F_f Fill factor

g	Gravitational acceleration
GI_t	Torsional stiffness
H_s	Significant wave height
k	Wave number
l	Beam length
L_p	Pitch length
M_f	Friction moment
M_i	Moment components
M_t	Torsion moment
n	Total number of wires
P	Axial force
q	Shear force per unit length
Q_i	Axial force
R	Radius
S	Spectral density
s	Catenary length
S_η	Wave energy spectrum
t	Time
T_0	Horizontal bottom tension
T_p	Peak period

T_w	True wall axial force
T_z	Zero-up crossing frequency
u	Displacement components
W_e	External work
W_i	Internal work
w_s	Submerged weight
x	Layback length
$\mathbf{K}$	Stiffness matrix
$\mathbf{R}$	External load vector
$\mathbf{r}$	Nodal displacement vector

Chapter 1

Introduction

1.1 Background

A submarine cable is a crucial connection between offshore topside facilities and equipment located on the seabed. The umbilical's function is to provide the control to operate and monitor subsea equipment. The cable normally consists of both a dynamic and a static part. The static part is located on the seabed under stable environmental conditions while the dynamic part hangs freely from topside equipment. The dynamic part is subjected to loading due to vessel motion and environmental loads. Thus, this part of the cable is normally designed to restrain high tensile loading and fatigue mechanisms.

The touch down zone (TDZ), the zone where the umbilical first hits the seabed, is critical with respect to failure of the cable during installation. This region may be exposed to severe curvature and axial compression, which may result in local buckling in the cross-section causing failure. Current practice is to avoid the occurrence of compression at the touchdown point to prevent cable failure. This restricts the weather window for the operation. The limited weather window results in high installation costs. It is therefore of great interest to investigate whether it exists exceptions were compression at the touchdown point not necessarily leads to structural failure and may be tolerated.

1.2 Previous work

The issue of torsion instability during a cable installation has previously been addressed in a master thesis conducted by Evgenii Koloshkin at NTNU during the spring of 2016 [18]. Koloshkin carried out analyses of cables with both linear-elastic and non-linear material properties. His work established that the torsion reaction utilization and heave motion amplitude are of great importance for the kink formation process in the case of an elastic cable model, while for the non-linear model the amount of torsion utilization is of much larger significance than the heave amplitude. Koloshkin also found results which showed that a pipe can experience compression in the touch down zone without necessarily induce loop formation. He was not able to conclude anything with regards to a general design

criterion for cables with respect to kink formation and torsion instability.

As a continuation of the master thesis, Sævik and Koloshkin proposes a analysis procedure for evaluating loop formation in offshore cables during installation [29]. The proposed procedure is the starting point for the present thesis.

1.3 Objective

The objective of this thesis is to validate the design procedure presented by Sævik [29] for evaluation of the loop formation issue related to installation of offshore cables. The design procedure includes the following steps

1. Evaluate the installation route and focus on the sections where the relative yaw rotation between the vessel and TDP is large.

2. Evaluate the torsion balance of the cross-section and calculate the β-parameter.

3. On the basis of the above, calculate the inherent torque for the different installation scenarios at the critical route sections.

4. Calculate lower and upper bound values of the cross-section friction moment.

5. Predict the critical curvature associated with kink formation for these cases.

6. Perform dynamic analysis with the built-in torque level and based on using a non-linear moment curvature model and use the dynamic maximum curvature at TDP as a measure of kink formation.

7. Use a sufficient number of cycles to prove that kink formations is not developed due to accumulated plastic deformations. If a stable value of the maximum curvature is obtained without kink formation and the standard maximum curvature design criteria is not exceeded, the sea state is acceptable.

8. If compression occurs during the dynamic analyses, the design check also needs to include local helix buckling and birdcaging.

By carrying out numerical analyses, the validity and accuracy of the design procedure shall be investigated and discussed.

1.4 Scope and limitations

Identifying the effect of the sea state severity on the torsion stability during cable installation will hopeful lead to some insight in which parameters which are the most critical with respect to torsion buckling. Since the strict limits in the current practice lead to a limited weather window for carrying out installations and hence high installation costs, it's of great interest to investigate whether current practice is reasonable or not.

Due to the limited time scope for the master thesis, some limitations have been made. The number of cross-sections which are to be analyzed are limited to two, as well as the total simulation time for the irregular sea state is chosen as 1 hour for all sea states. The analyses are operational analyses, and its thus assumed that installations in the North Sea will not be carried out in sea states with a significant wave height above 3 meters. Hence six of the most probable sea states with $H_S = 2 - 3m$ is chosen. Number of various installation scenarios are also limited to two, corresponding to two of the most normal scenarios; a 180 ° turn near the anchoring point and curved routing due to obstacles on the sea bed. The time scope also only allows for analyses with a limited number of wave and current combinations.

1.5 Thesis structure

Chapter 2 presents an overview of the most relevant literature and theory related to the field of umbilical installation and related issues. Of relevance are typical design of a dynamic cable and the process of an umbilical installation. In addition, focus is put on relevant failure modes connected to the installation phase, as well as methods for performing analysis with respect to buckling.

In **chapter 3**, the theory behind the finite element method is presented, with a special focus on the non-linear element method as it is applied in SIMLA. The chapter presents the fundamental properties of the method, along with categorization of non-linearities and solution procedures.

Chapter 4 presents the theory of SIMLA. The focus is on the element types applied and the associated material models. Lastly the methodology of the analyses is discussed.

Chapter 5 presents the model parameters, with focus on model dimensions, material properties, installation parameters and load conditions.

In **chapter 6** the results are presented and discussed. The results are presented as either static or dynamic results. The static results comprehend capacity analyses of the various cross-section with respect to kink formation, and determination of parameters which can be

used as measures of the occurrence of loop formation. The dynamic results present the results from the main dynamic analyses where various sea states are tested. The results discuss capacity with respect to critical torsion moment and curvature, as well as occurrence of compression in the touch down zone. The effect of wave heading and current is investigated, as well as the horizontal bottom tension. Lastly a discussion regarding establishing a design criterion is presented, along with a discussion around some uncertainties and limitations of the analyses.

The main conclusions and recommendations for further work are presented in **Chapter 7** and **Chapter 8**.

Chapter 2

Literature study

An umbilical is a connection component between topside facilities and equipment on the seabed, and its main function is to supply control, energy and chemicals to subsea equipment. Thus, the umbilical makes up an important component of an offshore facility, and insurance of acceptable operation is crucial. This thesis will focus on the problems associated with installation of cables. Following a literature study of relevant aspects of the field of dynamic umbilical and the installation process will be given.

2.1 Cable design

Submarine cables can be categorized into either structural cables, signal cables or power cables depending on their application area. An umbilical combine the functionality of each of these categories [27]. The umbilical will when installed normally consist of both a static and dynamic part. The dynamic part of the umbilical is designed to hang as a catenary line from either a floating or a fixed structure. This part is subjected to high tensile loading and fatigue mechanisms due to vessel motion. The static part is the part of the umbilical laying on the seabed [4]. The design of the umbilical cross-section is normally governed by the severity of the loading to which the dynamic part is subjected to, as well as the requirements of the control system.

Figure 2.1 shows a typical cable cross section, with named components [9]. A submarine cable typically consists of (1) a center core of conductors; (2) an insulation system; (3) sometimes an electrical or magnetic shield; (4) a protective armor layer to protect the conductors and to provide strength; (5) an outer sheath as an outside cover [21].

2.1.1 Conductor

The conductor is a part of a cable core designed for transmission of electric current. The conductor is normally made from either copper or aluminum [9]. Copper conductors gives the cable manufacturer the possibility to minimize the cross section compared to aluminium conductor, as well as having the highest electrical conductivity of available materials [21].
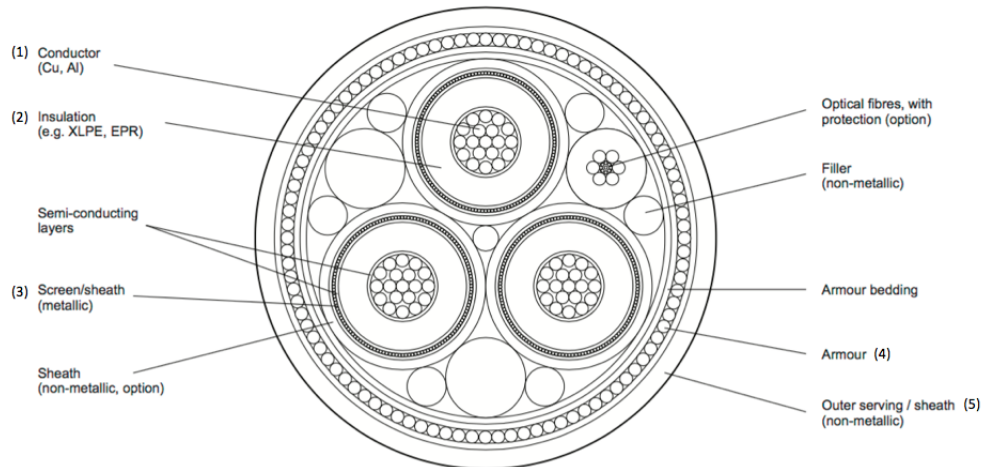
Figure 2.1: Typical 3-phase alternating current power cable cross-section, DNV[9]

Requirements about sufficient flexibility and flexing fatigue strength in subsea applications makes stranded conductors preferred over solid conductors. Stranding is generally of the concentric type in which all wires are of the same diameter, with six wires threaded around a center core wire.

2.1.2 Insulation system

The insulation system functions as a barrier between potential surfaces to prevent loss of current. The insulation wall must be mechanically robust, and resistant to aging and temperature. It is an important component with respect to transferring the load between marine handling equipment and the strength member, and acts as a sheath in contact with the seabed. The insulation material is either polyethylene or cross-linked polyethylene.

Polyethylene

Polyethylene (PE) is available in three density ranges: LDPE (low density), MDPE (medium density) and HDPE (high density). High-density polyethylene is the material of choice for most cables manufactured today. A polyethylene layer around the composite conductor provides dielectric strength. PE cables have a limited operational conductor temperature (70 - 80 °C), which in some application areas make them unfavorable [32].

Cross-linked Polyethylene

PE has subsequently been replaced by cross-linked polyethylene (XLPE) because of its limited conductor temperature limit. A XLPE cable can withstand 90 °C and short-circuit temperatures well above 200°C. The use of XLPE cables for submarine application is limited by the availability of suitable joints [32].

DNV requires a triple-extruded XLPE system for submarine power cables in shallow water applications [9]. This is since the extrusion process of the XLPE layer may generate a local stress enhancement if extruded directly onto the conductor, due to the conductor's grooves, ridges and irregularities. This generation of local stresses will contribute to a reduction in the dielectric strength of the insulation layer. To avoid this, a layer of semi-conductive XLPE is extruded onto the conductor resulting in a extremely smooth dielectric surface towards the insulating XLPE. The triple-extrusion method also provides a semi-conductive layer outside the insulation layer in order to form a stable dielectric surface not being affected by the outer screen layers [32].

2.1.3 Shield

The shield is made of paper or extruded polymer around the cable, to reduce the electric field strength and field concentration zones.

2.1.4 Armoring

The purpose of the armor layer is to provide the necessary tension stability to support the cable during laying as well as mechanical protection to protect the cable core during normal operation. The design of the armoring needs to consider factors such as tension stability, external threat pattern and protection requirements for the planned route. The external threat pattern covers possible impact loads from installation tools, fishing gears or anchors. In the case of armoring, galvanized steel is the preferred material. Galvanized steel fulfills the strength requirements and is the best option with respect to availability and cost. For deep water application, high steel strength in the tensile range of 250,000 psi is utilized, whereas for shallow water applications soft steel in the range of 50,000-70,000 psi is sufficient [21].

The armoring is made from metal wires wound around the cable with a certain lay length. The lay length is defined as the length of cable in which the armoring wire completes one turn around the cable. The armoring lay length must be optimized with respect to the expected tensile forces, the tension stability for the conductor and the torsional requirements of the cable and its installations [32].

2.1.5 Water blocking Sheath

The function of the water blocking sheath is to limit longitudinally seawater penetration along the length of the cable in case of a cable cut on the seabed. The insulation layer is dependent on protection against undue water ingression to maintain the dielectric strength.

The water-blocking sheath is made of a metallic sheath, where materials as aluminum, lead, copper and other metals are used for this purpose [32].

2.2 Cable configurations

Cables can be installed in various configurations. Factors such as cost, environmental conditions, water depth etc., may influence the choice of configuration [3], and Figure 2.2 illustrates some of the most common configurations.

a) Free-hanging Catenary

b) Steep-S

c) Lazy-S

d) Steep Wave

e) Lazy Wave
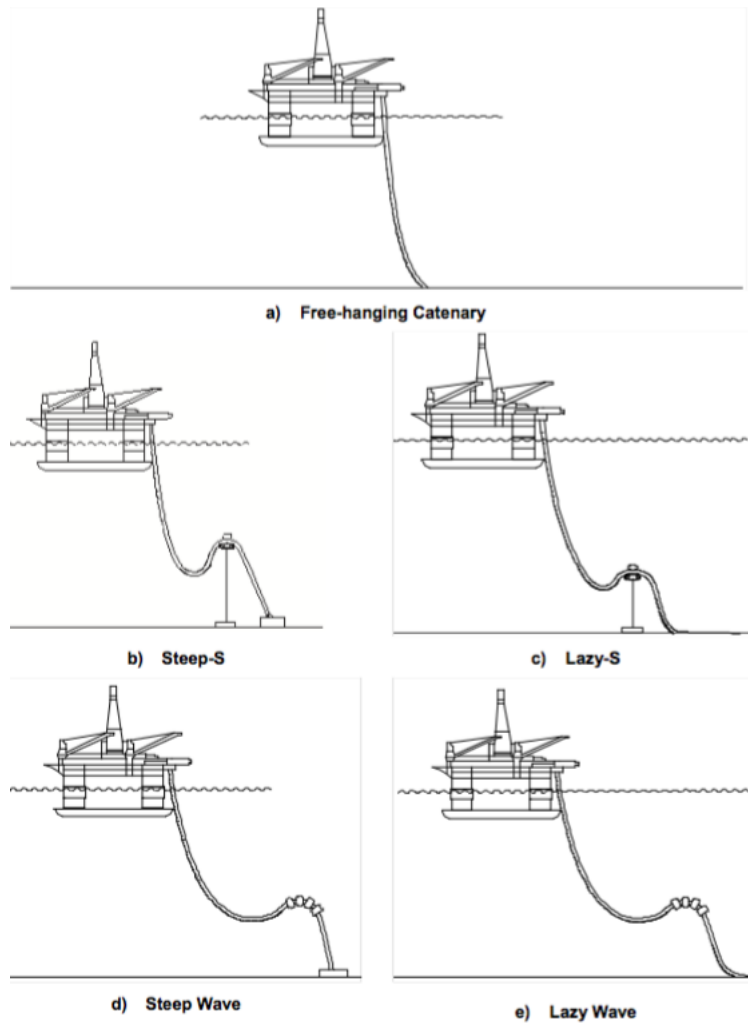
Figure 2.2: Cable configurations [2]

The easiest and most common configuration is the free hanging catenary configuration. The cable then hangs submitted to its own weight [14]. The catenary configuration can be divided into two parts: the suspended part (riser) and the laid part (flowline) [19]. An issue with this configuration, is that in the case of significant first-order wave motions at

the connection between the vessel and the umbilical (particularly heave), these motions are directly transferred directly to the seabed potentially leading to compression at the touchdown point. Consequences of this effect are buckling and over-bending [2]. This configuration does not require any advanced subsea infrastructure, and is therefore in many cases favorable. In some operation areas, there will be a need for additional flexibility in the cable. This has led to development of the lazy and steep wave, as well as lazy- and steep-S configurations. These configurations have additional buoyancy elements, which allows for larger floater motions as well as contributing to a reduction in top tension and loads at the touch down point (TDP).

2.3 Cable installation

A cable installation operation is a complex task. In the planning phase an installation analysis needs to be performed, which considers factors such as cable properties, route characteristics and available installation equipment and capacities [32]. In Figure 2.3 some of the most influential parameters in an installation operation are illustrated [9].
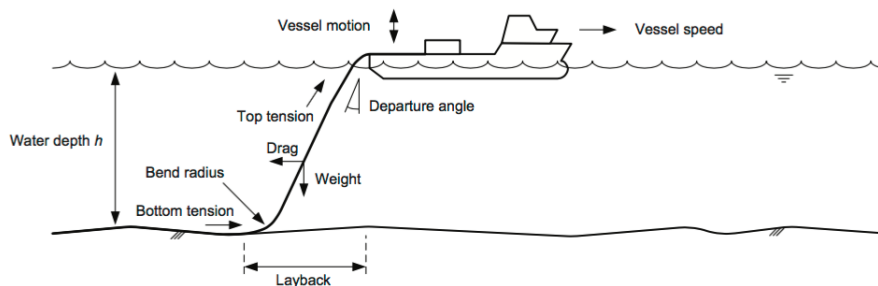
Figure 2.3: Cable laying process [9]

Cables are installed using a cable laying vessel (CLV) or a barge. The CLV needs a turntable or carousel cable storage facility to enable loading, transport and installation of cables. The cable-handling properties of a CLV are defined by the properties of the specific cable to be handled. Factors to be considered are load carrying capability, manoeuvrability properties, deck space for cable handling equipment and jointing shack, crew charter size etc. When using barges, which normally lack propulsion and stabilization systems, extra equipment and vessels need to be implemented into the operation[32].

The cable is run over a laying wheel into the water from the CLV. An important characteristic of the laying wheel is to have a sufficiently large diameter such that the minimum bending radius (MBR) is maintained. The mean bending radius is a value given by the manufacture to ensure avoidance of cable failure. The cable is installed by positioning the cable in a

well-defined catenary line from the laying wheel to the TDP by application of a certain tension in an on-board cable break device. The cable will hit the sea bottom in a flat angle under these circumstances.

The bottom tension is considered a critical parameter for cable laying. A too low tension can cause the cable to build loops or to snake, which generates twisting in the cable. Single-wired armoured cables are not torsional-balanced. This leads to differences between the cable tension at the laying wheel and the bottom tension, resulting in torsion as the cable is lowered to the sea floor. This might lead to loop generation at great water depths [32]. If loop formation has occurred, it is advised to leave the cable in the deformed configuration rather than attempting to straighten it out. Experience shows that the cable will be damaged to such an extent that it has lost all functionality when straightened out.

Installation methods
The most common installation methods for cables are

1. S-lay

2. J-lay

3. Reel lay

In the S-lay method the welded cable is supported on the rollers of the vessel and the stinger, forming the over-bend. Then it is suspended in the water all the way to the seabed, forming the sag-bend. In a J-lay operation, the pipe is welded in a vertical position and lowered to the seabed. The pipeline from the surface to the seabed is one large radius bend. This results in lower stresses than a S-lay system under same conditions. Reel lay is a method of installing pipelines from a giant reel mounted on the CLV. The pipelines are assembled on an spool-base and spooled onto a reel [19].

2.3.1 Loads during installation

The ocean environment induces various loads on offshore structures. These can be categorized into two main categories: static and dynamic loads. For riser structures one can refer to the structure self-weight, the buoyancy and the sea current drag as static loads. With regards to dynamic loading, hydrodynamic loading caused by sea waves and floating unit movement are the main contributions [13].

Static loads

The cable self-weight loading can be modeled as a force per unit reference volume $\mathbf{b_w}$.

$$\mathbf{b_w} = \rho \mathbf{g} \tag{2.1}$$

An element submerged into water will be exposed to a buoyancy force equal to the weight of the displaced water, per Archimedes' law. For a cable segment with length ds the buoyancy force B is defined as

$$B = g\rho_w A_e \tag{2.2}$$

Assuming that the cable is fully submerged, one can consider the resulting static force on the cable, named the "effective weight", to include the self-weight and the buoyancy of the cable [23]. The effective weight is also sometimes referred to as the submerged weight, and can be taken as $w_s = w_p - g\rho_w A_e$. Figure 2.4 illustrates the effective weigh and effective tension concept. The effective tension will have an extra contribution resulting from the external pressure acting on the cable due to hydrostatics, as $+p_e A_e$ [27].
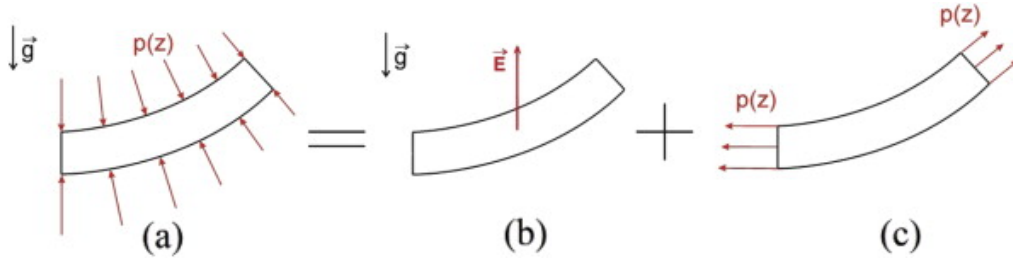
Figure 2.4: Effective weight and effective tension description [14]

Dynamic loads

The contributions from the hydrodynamic loading can be decomposed in a drag and a lift component. The lift actions of the fluid can be neglected for simplifications. To consider a mean hydrodynamic force, a common approach is to consider drag forces using Morsion's model (see [16]). The magnitude of the fluid force dF per unit length of a beam element can be written as

$$dF = \rho_f A\ddot{U} + C_a \rho_f A(\ddot{U} - \ddot{u}) + \frac{1}{2}\rho_f DC_d|\dot{U} - \dot{u}|(\dot{U} - \dot{u}) \tag{2.3}$$

where ρ_f is the fluid density, A is the dislocated fluid per unit length, C_a is the added mass coefficient, D is the external diameter of the cross-section, C_d is the drag coefficient, $\dot{U}$ is the fluid velocity magnitude and $\ddot{U}$ is the fluid acceleration magnitude. The drag forces can then be decomposed in axial (aligned with the beam axis) and orthogonal (normal to the beam axis) contributions[13], yielding

$$D\mathbf{F} = d\mathbf{F_t} + d\mathbf{F_n} \tag{2.4}$$

$$d\mathbf{F_t} = -C_{at}\rho_f A\ddot{u}_t + \frac{1}{2}\rho_f DC_{dt}||\dot{U}_t - \dot{u}_t||(\dot{U}_t - \dot{u}_t) \tag{2.5}$$

$$d\mathbf{F_n} = -C_{an}\rho_f A\ddot{u}_n + \frac{1}{2}\rho_f DC_{dn}||\dot{U}_n - \dot{u}_n||(\dot{U}_n - \dot{u}_n) \tag{2.6}$$

The fluid particle velocity and acceleration are strongly dependent on the severity of the sea state. A sea state can either be represented as regular or irregular waves.

Regular waves
A simplified representation of waves is a regular wave representation. The simplest wave theory is the Airy wave theory where the waves are represented as harmonic sinusoidal waves with linearized boundary conditions. The wave surface elevation is then described as a harmonic motion at the form

$$\eta(x,t) = \eta_0 Re[e^{i(\omega t - kx)}] = \eta_0 \cos(\omega t - kx) \tag{2.7}$$

where ω is the angular frequency of the wave, k is the wave number and η_0 is the wave amplitude.

Irregular waves
Waves are an irregular phenomenon with natural random occurrence. Sea waves are irregular in both time and space, and the distribution of the sea surface elevation caused by waves can be modelled either in the frequency-domain or the time-domain. In the time-domain the wave train are analyzed as a sequence of individual regular waves defined by two main parameters; the wave height H and the wave period T [17]. The randomness of the sea state

is captured by introducing a wave spectrum. A wave spectrum describes the distribution of wave energy as a function of wave frequencies. The spectrum is produced assuming that the sea state is stationary for a short duration of typically 3 hours.

The surface elevation is expressed as

$$\eta = \sum_{j=1}^{N_\beta} \sum_{k=1}^{N_\beta} A_{jk} e^{i(\phi_k t + \phi_{jk}^p + \phi_{jk})} \tag{2.8}$$

$$A_{jk} = \sqrt{2 S_\eta(\beta_j, \omega_k) \Delta\beta \Delta\omega} \tag{2.9}$$

where A_k is the wave component amplitude given in Equation (2.9). ϕ_{jk} are random phase angles, which are sampled from a uniform distribution over $[-\phi, \phi]$, while ϕ_{jk}^p are position dependent phase angles. The random phase angles of the wave time series are generated by defining a starting integer value called seed. Different seeds of random phase angles result in different time series [17]. Thus, to cover the whole range of statistical waves, several different seeds needs to be used.

The duration of the time series is limited to $T = N_t \Delta t \approx 2 N_w \Delta t$. The duration T_{sim} will be adjusted to cover the duration of the dynamic analysis if necessary [28].

It exists various standardized wave spectra, where Pierson Moskowitz and Jonswap are the most commonly used. The two-parameter Pierson Moskowitx spectrum is defined as

$$S_\eta(\omega) = A\omega^{-5} exp[\frac{-B}{\omega^4}], \quad 0 < \omega < \infty$$
$$A = 124.2\frac{H_s}{T_z^4} \tag{2.10}$$
$$B = \frac{496}{T_z^4}$$

where T_z is the zero-up crossing frequency, which relates to the peak period with the following relation $T_p = 1.408T_z$. The three parameter Jonswap spectrum is given as

$$S_\eta = \alpha g^2 \omega^{-5} exp[-\beta(\frac{\omega_p}{\omega})^4]\gamma^{exp[-\frac{(\omega-\omega_p)^2}{2\sigma^2\omega_p^2}]}$$

$$\alpha = 1.2905\frac{H_s^2}{T_z^2}$$

$$\beta = \begin{cases} 1.205 & \text{for} \quad \text{for North Sea Conditions} \\ 1 & \text{for} \quad T_p \geq 5\sqrt{H_s} \end{cases}$$

$$\gamma = \begin{cases} exp[5.75 - 1.15\frac{T_p}{\sqrt{H_s}}] \\ 5.0 & \text{for} \quad T_p < 3.6\sqrt{H_s} \end{cases}$$

$$\sigma = \begin{cases} 0.07 & \text{for} \quad \omega \geq \omega_p \\ 0.09 & \text{for} \quad \omega \leq \omega_p \end{cases}$$

$$\omega_p = \frac{2\pi}{T_p}$$

$$\frac{T_p}{T_z} = 1.407(1 - 0.287\ln\gamma)^{\frac{1}{4}}$$

(2.11)

The wave direction angle is defined relative to the global coordinate system x-axis and counterclockwise, which is shown in Figure 2.5.
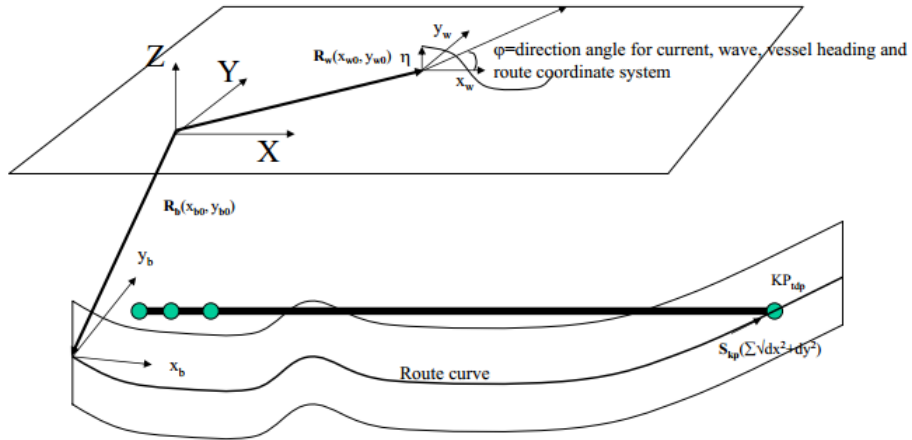
Figure 2.5: Definition of direction angle for current, waves etc. [28]

Current

The presence of current will induce drag forces on the cable. For a fixed cylinder in current along, the flow component perpendicular to the cylinder axis will induce a quadratic drag force, which can be expressed as

$$F_c = \frac{1}{2}\rho U^2 D C_D \sin^2 \kappa \qquad (2.12)$$

where κ in this context is the cone angle between velocity vector and cylinder central axis. This last sin term acknowledges the fact that a current incoming from either 90° or 270° according to Figure 2.5 will yield highest resulting force on the cable [15].

Combination of current and waves

An accepted practice for estimating the effect of a combined current and wave loading is to vertically superpose the current velocity on the velocity resulting from the waves before calculating the drag force [15]. Treating the drag force components from each contribution separately yield an underestimation of the forces, as the drag force is quadratic.

Vessel induced movement

During installation, the cable laying vessel will induce forced motion of the cable top connection. The cable top connection is then subjected to a time-dependent prescribed motion due to the vessel dynamic behavior. This leads to a time-dependent relative velocity between the cable and the seawater, creating hydrodynamic damping forces. The model can be synthesized via a response amplitude operator (RAO), which permits evaluating the movements of the floating vessel, related to a given sea state.

The wave frequent motions are described by a set of complex transfer functions $H_{WFj}(\beta, \omega)$. The transfer function describes how the system responds a wave excitation with unit amplitude for various frequencies ω and wave headings θ, by describing the relation between the response and the excitation

$$H_{WFj}(\beta, \omega) = \frac{x_j(\beta, \omega)}{\zeta_1(\beta, \omega)} \qquad (2.13)$$

where $x_j(\beta, \omega)$ is the response amplitude in dof j and $\zeta_1(\beta, \omega)$ is the surface elevation amplitude [28]. The absolute value of a transfer function is known as the response amplitude operator. The RAO can be estimated using the spectral relation given in Equation (2.14), where $S_{xj}(\beta, \omega)$ and $S_\zeta(\beta, \omega)$ is the energy density spectrum of the response and the incoming

wave spectrum respectively [28].

$$S_{xj}(\beta, \omega) = |H_{WFj}(\beta, \omega)|^2 S_\zeta(\beta, \omega) \tag{2.14}$$

The RAO translates the wave characteristics to vessel movements, and are defined in all six degrees of freedom for a vessel; surge, yaw, heave, roll, pitch, sway. For laying operations, motion in pitch and heave have the largest influence on the vertical movements of the laying wheel. Roll motions will also influence if the laying wheel is located off the vessel's central line [21].

2.4 Failure modes and design criteria

A dynamic cable should be designed to satisfy its functional requirements under relevant loading conditions. Loads acting on items of a cable system can be classified as functional, environmental or accidental. DNV [9] uses the following definitions of the load classes:

1. **Functional loads**: Loads as a result of the physical existence of the cable system and its intended use between manufacturing and decommissioning. Examples include weight of the cable, external hydrostatic pressure etc.

2. **Environmental loads**: Loads induced by environmental conditions acting on the cable, both directly and indirectly. Waves, currents, vessel motion are examples of environmental loads.

3. **Accidental loads**: Loads which are caused directly or indirectly by unplanned activities, such as earthquakes, impact with dragged anchors and trawling gears, installation vessel position failure during installation/recovery.

This section summarizes the relevant failure modes and design criteria for subsea cable applications, with respect to the mentioned load classes.

2.4.1 Design criteria

Design criteria are defined as recommended practice to prevent failure of the system. A cable system has a specific capacity to respond to a range of demands they are subjected to during temporary or permanent phases. The capacity of a system can be described by several limit states, where DNV operates with the limit states defined in table 2.1 [9].

Table 2.1: Definition of limit states according to DNV[9]

Limit State	Examples
Serviceability Limit State (SLS)	Damage to cable sheath (before or after installation) or armour (after installation)
Ultimate Limit State (ULS)	Exceeding cable core emergency temperature rating or compromising minimum bending radius
Fatigue limit state (FLS)	Repeated cable bending and vortex induced vibrations in free spanning section
Accidental limit state (ALS)	Objects dropped onto cables and anchor impact

DNV operates with a range of design criteria for umbilical systems, defined in [9]. Examples of design criteria for cable system components in different life cycle phases are presented in table 2.2.

Table 2.2: Overview of design criteria, and their connection to life cycle phases [9]

Component	Manufacturing	Installation	Operation and maintenance	Decommissioning
Power cable	Manufacturability, testability	Ultimate strength (e.g tension, bending, torsion, impact), on-bottom stability	Electrical strength and conductivity, fatigue strength, thermal conductivity	Residual strength
Optical fibers	Manufacturability, testability	Ultimate strength (e.g tension, bending, torsion)	Transmissivity	
Tubular cable protection system	Manufacturability	Ultimate strength, compatibility with cable	Fatigue strength	

This project focuses on the installation phase, and thus design criteria related to ultimate strength of the system. DNV [8] operates with criteria for the following mechanical parameters, as listed below.

- Strain (elastomer hoses)

- Strain (steel tubing)

- Stress and/or load (reinforcement layers and carcass)

- Stress and/or load (steel tubing)

- Stress and/or load (end fitting)

- Hydrostatic collapse (buckling load)

- Mechanical collapse (carcass induced stresses)

- Crushing collapse and ovalisation (during installation)

- Compression (axial and effective)

- Service life factors.

An important aspect to ensure fulfillment of the design criterion, are applying safety factors during the design phase to ensure a certain margin in the capacity of the system. API 17J presents the safety factors dependent on cable component and operational condition. The most relevant cases with respect to buckling and tensile armour failure are summarized in table 2.3.

Table 2.3: Safety factors for relevant failure modes and operation conditions as stated in API 17J. The table is reduced to comprehend the most critical components of an umbilical, while the failure modes presented focus on tensile armour failure and birdcaging. For full table including all components and failure modes see [1].

Layer	Failure mode	Operating Conditions			Nonoperating conditions		
		Permanent		Abnormal	Temporary		Extreme
		Normal	Extreme		Normal		
					Installation	Test	
Tensile armours	Breakage	0.67	0.85	0.85	0.67	0.91	0.85
	Buckling	0.85					
	Wire disorganization	The cumulative radial gap between each tensile armor and its adjacent layers shall not exceed half the wire thickness					
Antibuckling tape	Birdcaging	0.67	0.67	0.85	0.85	0.85	0.85
Internal pressure sheath	Rupture	The maximum allowable bending strain at nominal dimensions shall be 7.7 % for polyethylene (PE) and polyamide (PA), 7.0 % for polyvinylidene fluoride (PVDF) in static applications and for storage in dynamic applications, and 3.5 % for PVDF for operation in dynamic applications					

Minimum bending radius

As mentioned earlier, a possible consequence of the catenary configuration is buckling and overbending due to high load accumulation at the touchdown point. A measure introduced to intent to avoid this effect, is the minimum bending radius and associated minimum radius of curvature. The minimum bending radius denotes the minimum radius a cable can be bent at a specific load and a specific time. Bending radius below the MBR might induce cable failure, which is to be avoided to the extents possible. DNV and API operate with methods for determining the MBR, as well as presenting safety factors which shall ensure safe operation.

API 17J [1] determines the MBR using the concepts of storage minimum bend radius (SR) and locking radius (LR). The standard states that the "storage minimum bend radius shall be calculated as the minimum bend radius that satisfies all the requirements of the table"[1]. The bend radius required to cause locking, the locking radius, in the interlocked layers shall be calculated. The SR shall be at least 1.1 times the LR, and the MBR must not be smaller than the SR for all loading conditions. Table 2.4 states the safety factors recommended by API to account for different loading conditions.

Table 2.4: Design criterion for minimum bend radius as presented in API 17J for unbounded flexible pipes [1]

Loading type	Load condition			Survival
	Operating		Non-operating	
	Permanent	Abnormal	Temporary	
All types	1.0 x storage minimum bend radius (SR)			
Static	1.1 x locking radius (LR)			
Dynamic supported	1.1 x 1.1x LR	1.1 x LR		
Quasi-dynamic	1.25 x 1.1 x LR	1.1 x 1.1 x LR		1.1 x LR
Dynamic	1.5 x 1.1 x LR	1.25 x 1.1 x LR		

The locking radius is found considering the bending strain needed to close the gap at the tensile or compressive sides of the cable. For interlocked profiles this can be formulated as

$$
\begin{aligned}
\text{At the compression side:} \quad & \frac{L_p}{n}\frac{R}{\rho_l} = \frac{L_p}{n} - \frac{b_{min}}{\sin\alpha} \\
\text{At the tensile side:} \quad & \frac{L_p}{n}\frac{R}{\rho_l} = \frac{b_{max}}{\sin\alpha} - \frac{L_p}{n}
\end{aligned}
\tag{2.15}
$$

For the tensile armour layer, the compressive side applies resulting in

$$\rho_l = \frac{R}{1 - F_f} \tag{2.16}$$

The locking radius for the pipe is taken to be the largest ρ_l for all helical layers. The integrity of the plastic layers is governed by the maximum allowable strain. This yields a limit for the bending radius of the plastic layer as given in equation (2.17). This equation also holds for the armour layers, when determining the bending radius in the case of maximum allowable bending stress.

$$\rho_\epsilon = \frac{R}{\epsilon_{lim}} \tag{2.17}$$

The resulting bending radius is established as the value which yields the smallest radius of curvature, including safety factors as specified in API 17J [1].

2.4.2 Failure modes

Failure is defined as an event or condition where the system fails to fulfill its objective. Because of the complexity of marine cables; electrical, thermal, mechanical and chemical failure modes are possible. This thesis focuses on the structural and mechanical failure modes, with special focus on the failure mode connected to tensile armour failure. Thus, the failure modes presented will be within those limits. Table 2.5 presents some of the main mechanical failure modes for cables. In addition, a full, more detailed description of the failure modes connected to cable operation can be found in API 17B [2].

Table 2.5: Mechanical failure modes according to DNV [9]

Failure mechanism	Limit State	Demand Characteristics	Response characteristics
Torsion	ULS	Tensile force	Strain, opening or closing of armour, bird caging, bonding failure
Bending	ULS	Bending moment	Elongation (outside) and compression (inside), strain, bonding failure
Axial tension	ULS	Twisting moment	Elongation or compression, strain, bonding failure between conductor and insulation
Lateral compression	ULS	Clamping force and area	Compression, strain, bonding failure
Impact	ALS, ULS	Impact force and area	Shear stress and strain
Abrasion	SLS	Lateral and longitudinal forces, surface friction	Abrasion of cable sheath
Vibration	FLS	Current - velocity, direction	Fatigue of cable components
Sheath degradation	SLS	Irradiation - wavelength (e.g. UV), strength	Ageing of outer cable sheath, cracking

2.5 Torsion instability

According to Ermolaeva [10] there exist two classes of torsional instability in a cable:

1. Hockling, loop formation due to too low tension to sustain a torque reaction.

2. Constructional deformation involving damage of individual wires, which forms so-called "birdcaging", caused by local buckling.

Below the two different cases are presented more in detail.

2.5.1 Hockling

The presence of very low tension in the touch down zone, combined with torsion moment can yield structural instability, resulting in the formation of a loop which is known as hockling [14]. Hockling, according to Rosenthal [24], occurs when the tension in the cable is not large enough to sustain a torque reaction applied in the extremes of the cable. If the tension continues to increase after the loop formation, it is possible that the curvature level increases up to a kink, which is considered as failure of the structure [14]. The presence of helical armour laid in opposite directions is to intent to keep the axial rotation at zero during tensioning. External loading such as yaw rotations of the cable-laying vessel or manufacturing

deviations can lead to torsion moments acting on the structure, which might be critical with respect to loop occurrence. The physical explanation of hockling is that torsion strain energy is transformed into bending strain energy, resulting in the formation of a loop.

Loop formation criteria

According to Ermolaeva [10] "Hockling refers to the torsion instability problem of an elastic slender rod, accompanied by large deflections". A straight line is the first (trivial) equilibrium state for a rod, while the next equilibrium state is a loop. Hence hockling occurs when certain load conditions induces a shift in equilibrium states from its trivial straight line state to a loop configuration. Load combinations of tension and torque are known to initiate this shift in configuration. There exist criteria for when loop formation takes place. To derive such a criterion, it is assumed that the cable can be consider an elastic slender beam, and that the criteria for loop formation of an initially straight elastic beam is valid for a cable in catenary configuration [10].

The Greenhill criterion gives an indication of a point of instability if any attempt is made to increase the torque relative to the applied tension, as well as value of the minimum tension needed to prevent loop formation under the introduced amount of torque [10]. The analytical buckling criteria is determined for a beam with length l, with displacements constrained in both extreme points (with exception of the axial direction in one of the extremes, in which loading is applied), bending stiffness EI, subjected to a compression load P and a torsion moment M_t.

The differential equation for the beam in y- and z-direction is given in (2.18), where w and v are displacements in y- and z-direction respectively. The solution of the differential equation is generally given on the form in Equation (2.19) [6].

$$
\begin{aligned}
EIw'' - M_t v' + Pw &= 0 \\
EIv'' + M_t w' + Pv &= 0
\end{aligned}
\tag{2.18}
$$

$$
v = Ae^{iwx}, \quad w = Be^{iwx}
\tag{2.19}
$$

Introducing the general solution into the differential equation yields a system of two homogeneous linear equations, which is presented in Equation (2.20).

$$
\begin{bmatrix} P - EIw^2 & iM_t w \\ -iM_t w & P - EIw^2 \end{bmatrix} \begin{bmatrix} A \\ B \end{bmatrix} = \mathbf{0}
\tag{2.20}
$$

Deflection is possible if the determinant of the matrix is equal to zero [6] which indicates that

$$EIw^2 \pm M_t w - P = 0 \qquad (2.21)$$

By only considering a positive torque, the solution of the equation becomes

$$w_{1,2} = \frac{1}{2EI}(-M_t \pm \sqrt{M_t^2 + 4EIP}) \qquad (2.22)$$

The general solution of the differential equation then includes both the real and the imaginary part of the solution

$$
\begin{aligned}
v &= A_1 e^{iw_1 x} + A_2 e^{iw_2 x} \\
w &= B_1 e^{iw_1 x} + B_2 e^{iw_2 x}
\end{aligned}
\qquad (2.23)
$$

where A_1, A_2, B_1, B_2 are complex constants. Introducing the boundary constraints, the following relation between w_1 and w_2 are found

$$w_w = w_1 + \frac{2\pi}{l} \qquad (2.24)$$

which by combining 2.24 and 2.22 yields the following expression

$$\frac{\pi}{l} = \frac{\sqrt{M_t^2 + 4EIP}}{2EI} \qquad (2.25)$$

Equation (2.25) can be rearranged, and gives the following critical load condition to cause instability[14],

$$\frac{P}{P_{cr}^0} + \left(\frac{M_t}{M_{t,cr}^0}\right)^2 = 1 \qquad (2.26)$$

The critical torsion moment $M_{t,cr}^0$ and critical compressive axial force P_{cr}^0 is given by

$$P_{cr}^0 = \frac{\pi^2 EI}{L^2} \qquad (2.27)$$

$$M_{t,cr}^0 = \frac{\pi k EI}{L} \qquad (2.28)$$

with k = 2 for the mentioned boundary conditions [14]. Equation (2.26) is known as

Greenhill's equation. Liu [20] presented a study concerning the loop formation in electromechanical cables with single and multiple wires. Greenhill's formula is then rewritten in the case of an applied tensile load $T = -P$ which leads to Equation (2.29) if one considers a beam with a large length l, such that $\frac{T}{\frac{\pi^2 EI}{L^2}} \gg 1$.

$$\frac{T}{\frac{\pi^2 EI}{L^2}} = \frac{M_t^2}{\left(\frac{k\pi EI}{L}\right)^2} \tag{2.29}$$

which also can be written as

$$T = \frac{M_t^2}{k^2 EI} = \frac{M_t^2}{4EI} \tag{2.30}$$

$$M_t = \sqrt{4TEI} \tag{2.31}$$

Based on the expression in (2.29), Ross [25] uses energy transfer methods to evaluate the conditions of loop formation. The deduction assumes that the tension/torque conditions leading to loop formation are sustained for a long enough period for the loop to form, as well as that the cable tension is constant during loop formation. The deflection shape is assumed to be formed as a circle, shown in Figure 2.6(a), while the nonlinear buckling process in real-life will lead to the formation of loops of the shape illustrated in Figure 2.6(b).
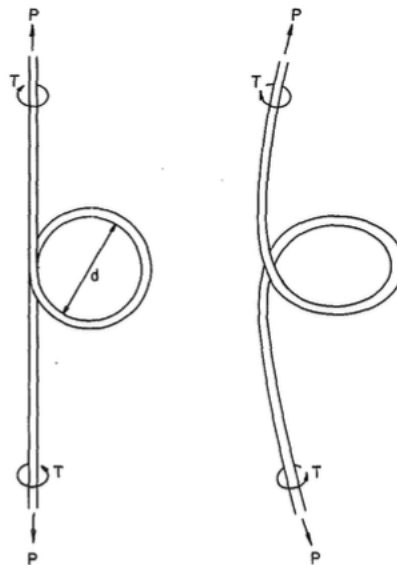
Figure 2.6: (a) Assumed loop shape (b) Actual loop shape [25]

Application of energy methods leads to the following relation between torque T and tension P which will lead to cable kinking

$$T = \frac{EI}{d} + \frac{Pd}{2} \tag{2.32}$$

For the case of a tension-free cable, a loop of diameter d will form dependent on the value of the torsion as given in Equation (2.33)

$$d = \frac{EI}{T} \tag{2.33}$$

The loop diameter that will result in a minimum torsion to produce a loop in the elastic range is found as

$$d = \sqrt{\frac{2EI}{P}} \tag{2.34}$$

Substituting this equation into Equation (2.32), yields the critical torque which will induce loop formation. The critical torque associated with loop formation is defined by Equation (2.35). Loop formation can according to Ross [25] be prevented if the torsion is maintained below the value defined in the equation. If the critical torsion level is exceeded, the loop formed will have a diameter as defined by the relation in Equation (2.36).The results found by Ross [25] yields critical torsion moments half the size of Greenhill.

$$T = \sqrt{2PEI} \qquad or \qquad P = \frac{T^2}{2EI} \tag{2.35}$$

$$d = \frac{\frac{2EI}{T}}{1 + \sqrt{1 - \frac{2PEI}{T^2}}} \tag{2.36}$$

2.5.2 Local buckling of Tensile Armours

The cables are designed to withstand high tensile loads. During installation, the TDP of the cable may experience high compressive loads. The armour wires of the umbilical may then be subjected to large lateral and radial displacements, which may lead to buckling of the tensile wires. Tensile armour failure may develop in either radial or lateral direction. Figure

2.7 shows the damages from radial and lateral failure respectively.

Radial failure mode

Lateral failure mode
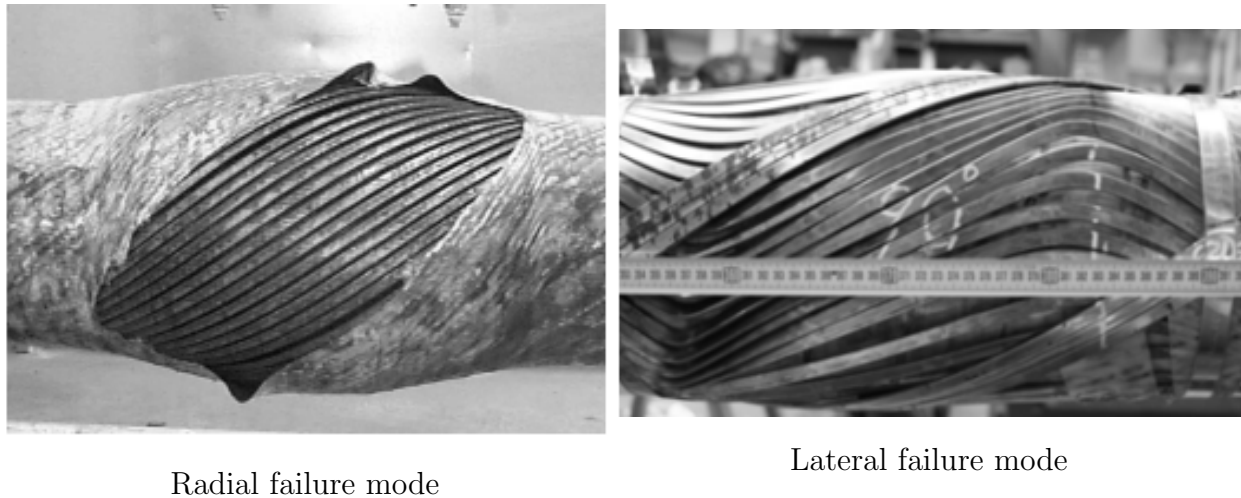
Figure 2.7: Examples of tensile armour buckling [34]

Radial failure

Radial failure of the tensile armours is commonly known as bird-caging. Bird-caging occurs when individual wires unravel under excessive torsional loads that are reverse to the direction in which the wire strands are wound. Radial failure may occur in different ways [27];

1. Failure of supporting layer (anti buckling tape)

2. Elastic buckling without tape failure

3. Yield failure of the wires

Most cables have a supporting layer which function is to prevent radial failure, an anti-buckling tape [27]. When the ultimate strength of the anti-buckling tape is exceeded, a sudden radial expansion of the tensile armour will take place which might induce cable failure. It is the anti-buckling tape alone which must carry the radial pressure due to expansion of the tensile armour, and thus the ultimate strength of the layer will determine the critical external pressure. This radial failure mode is not considered a buckling failure, but simply failure triggered by the loss of support [30].

The external axial force P_{b1} inducing failure of the supporting layer can be defined as [27]

$$P_{b1} = \frac{R}{\tan^2 \alpha}\left[\frac{n_t \sigma_{ut} A_t \sin^2 \alpha_t}{\cos \alpha_t R_t} + 2\pi E_s \epsilon_{ut} t_s\right] \tag{2.37}$$

where R is taken as the mean radius of the tensile armour layers, ϵ_{ut} is the ultimate strain of the anti-buckling tape, E_s is the sheath Young's modulus, σ_{ut} is the tape ultimate stress, n_t is the number of tape filaments, A_t is the cross-section area of the tape filament, α_t is the tape lay angle, t_s is the sheath thickness and R_t is the tape radius.

The second radial failure mode is an elastic buckling mode, where the armour wires deflect radially in a sinusoidal pattern. The critical buckling load is found based on curved beam theory, where both bending of the armour wires and straining of the elastic foundation will contribute to the critical load. The elastic foundation is in this case the outer sheath. The following formulas assume that there is no interaction between the wires, such that each wire behaves equally. The elastic foundation stiffness c has contributions from both the anti-buckling tape and the outer sheath. The contribution from the outer sheath c_1 is found from considering one wire width's contribution to the hoop stiffness

$$c_1 = \frac{q_2}{u_2} = \frac{2\pi}{n} \frac{E_s t_s}{R} \cos \alpha \tag{2.38}$$

where n is the number of armour wires. For the anti-buckling tape, the stiffness parameter c_2 is determined to be

$$c_2 = \frac{q_2}{u_2} = \frac{n_t}{n} \frac{E A_t \sin^4 \alpha_t}{R^2} \frac{\cos \alpha}{\cos \alpha_t} \tag{2.39}$$

By assuming a sinusoidal buckling shape

$$u = u_0 \sin \frac{n \pi X^{-1}}{l} \tag{2.40}$$

the critical buckling load $Q_{1,cr}$ of one single wire can be expressed by using the Principle of Minimum Potential Energy and assuming straight beam theory

$$Q_{1,cr} = \pi^2 E I_2 (\frac{m}{l})^2 + \frac{c}{\pi^2} (\frac{l}{m})^2 \tag{2.41}$$

To determine the lowest buckling load possible, the expression for the critical buckling load is differentiated with respect to $\frac{m}{l}$ which yields

$$Q_{1,cr} = 2\sqrt{E I_2 c} \tag{2.42}$$

The total contribution from all the wires are obtained by multiplying with the factor $n \cos \alpha$,

yielding

$$P_{b2} = n \cos \alpha Q_{1,cr} \tag{2.43}$$

The axial force leading to wire yield failure is calculated as

$$P_{b3} = n \cos \alpha \sigma_y A \tag{2.44}$$

where σ_y is the yield stress of a wire of cross-section area A.

The resultant axial load inducing radial failure is determined based on the reasonable assumption that there will be interaction between the modes of failure, which gives

$$\frac{1}{P_{rad}} = \frac{1}{P_{b1}} + \frac{1}{P_{b2}} + \frac{1}{P_{b3}} \tag{2.45}$$

Lateral buckling

Lateral buckling takes place when the wires becomes transversely unstable below the anti-birdcaging layer. Lateral buckling is hard to detect as it takes place under the outermost layer of the cable. This buckling mode most commonly occurs during cable laying operations in deep-waters [35].

During installation, flexible cables are exposed to axial compression due to hydrostatic pressure on the end cap and repeated bending cycles due to waves, current and vessel motions. These are conditions which are known to lead to lateral buckling.

By the manner a flexible cable is designed to be torsionally stable, the number of wires in the outer layer generally is larger than in the inner layer. Interaction between the layers causes compressive loads to be larger in the inner layer than in the wires contained in the outer layer [34]. Lateral buckling is found to occur when the inner layer of tensile armour wires loses its load carrying capacity due to buckling. This loss of load carrying ability causes bending and compression to couple with the torsion. The coupling leads to a severe twist of the cable in the pitch direction of the outer layer of armour wires. This twist causes further compressive straining of the wires in the inner layer, leading to plastic deformation of the inner layer. This might cause deformations to an extent where the cable will not have sufficient structural integrity to function in operation [35].

Under the assumption of no friction, a conservative estimate of the buckling load can be

obtained from the curved beam differential equation as [27]

$$P_{lat} = n\frac{\cos\alpha}{R^2}[GJ\sin^4\alpha + (4EI_2 + EI_3 - GJ)\sin^2\alpha\cos^2\alpha] \tag{2.46}$$

2.6 Mechanical behaviour of dynamic cables

Submarine cables must be designed to withstand all mechanical stresses during manufacturing, handling, transport, installation and operation. Its ability to withstand loads during the different phases of a cable's design life is dependent on the mechanical characteristics of the cross-section. The cross-sections of subsea cables are complex due to its multiple layers. This multiple layer composition makes the structure able to accommodate large flexural deformations without leading to failure.

An individual component layer of a dynamic cable can be classified in two basic categories: a cylindrical element or a helical element. The former element is used to model homogeneous cylindrical components such as polymer or metal tubes, while the latter element includes armour layers made up of a set of helical strips or wires. metallic conduits and pressure reinforcement layers. The mechanical properties of the generic flexible structure depend on the interaction between the individual components. The main characteristic component of the flexible structure is the helical reinforcement wires or strips. The helical configuration of these elements results in nonlinear mechanical properties with coupling between axial and torsional deformations [31].

The load components acting on the cable cross-section can be divided into the following categories [27]:

1. **Axi-symmetric loads** which only change the diameter and length of the cable and with small relative deformations between wires, i.e torque, tension, internal/external pressure loads.

2. **Bending loads** where straight cable is bent into a torus and where significant relative deformations will occur between wires.

In the following section, analytical methods for stress analysis of a umbilical cross-section will be presented deducted from work presented by Sævik in [27].

2.6.1 Behavior due to axi-symmetric loads

The following analytical expressions assume that the cylindrical straight pipe shape is kept during deformation, such that only the length and diameter of the pipe cylinder are changed

during loading and that the relative deformations between wires are small. Because wires are laid helically, stresses from the axial force in the wires will dominate.

The kinematic quantities related to the analytical expression defined in this section, are defined in Figure 2.8.
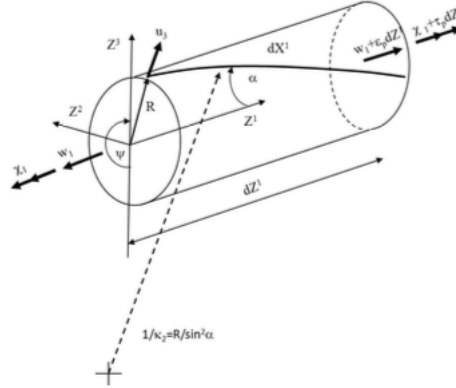
Figure 2.8: Kinematic quantities related to axi-symmetric loading [27]

Axial loading

In an unstressed configuration, the initial torsion and curvatures are directly dependent on the lay angle α and the helix radius R, as defined in Equation (2.47)

$$
\begin{aligned}
\kappa_1 &= \frac{\sin \alpha \cos \alpha}{R} \\
\kappa_2 &= \frac{\sin^2 \alpha}{R} \\
\kappa_3 &= 0
\end{aligned}
\tag{2.47}
$$

where κ_1 corresponds to the initial torsion, while κ_2 and κ_3 corresponds to curvature in binormal and normal direction respectively. The contact line load in radial direction is expressed as a function of the axial force Q_1 alone, since the contributions from shear force and bending moments can be neglected. The contact load is defined by

$$
q_3 = \kappa_2 Q_1 = \frac{\sin^2 \alpha}{R} Q_1
\tag{2.48}
$$

The axial strain in the helix is defined as

$$\epsilon_{11} = \cos^2 \alpha \epsilon_p + \frac{\sin^2 \alpha}{R} u_3 + R \sin \alpha \tau_p \tag{2.49}$$

where ϵ_p and τ_p corresponds to the pipe strain and torsion at pipe center, and u_3 the radial motion of each layer.

Application of the principle of virtual work yields a relation between the internal and external forces along the length of the cable. By expressing the internal virtual work equal to the external virtual work, as the principle of virtual work states, the following relation between forces and motion is obtained

$$T_w \delta u + M_t \delta \theta = n E A_t \int_0^L (\cos^2 \alpha \frac{u}{L} + R \cos \alpha \sin \alpha \frac{\theta}{L})(\cos^2 \alpha \frac{\delta u}{L} + R \cos \alpha \sin \alpha \frac{\delta \theta}{L}) \tag{2.50}$$

Expressing this expression on matrix form yields a stiffness relation on the form of

$$\mathbf{R} = \mathbf{Kr} \tag{2.51}$$

where $\mathbf{R}$ is the vector containing the external loads, $\mathbf{K}$ is the stiffness matrix and $\mathbf{r}$ contains the nodal displacements.

$$\begin{bmatrix} F_x \\ M_x \end{bmatrix} = \begin{bmatrix} EA & \beta EA \\ \beta EA & GI_x \end{bmatrix} \begin{bmatrix} \epsilon_x \\ \kappa_x \end{bmatrix} = \frac{n E A_t}{L} \begin{bmatrix} \cos^3 \alpha & R \cos^2 \alpha \sin \alpha \\ R \cos^2 \alpha \sin \alpha & R^2 \cos \alpha \sin^2 \alpha \end{bmatrix} \begin{bmatrix} u \\ \theta \end{bmatrix} \tag{2.52}$$

The torsion instability will be influenced by a range of parameters such as the cross-section torsion balance, the routing, vessel motions, seabed friction and built-in torque from the manufacturing and installation procedures. The β-parameter in the equation corresponds to the coupling parameter between torque and axial force, given as:

$$\beta = \frac{M_x}{EA\epsilon_x} \tag{2.53}$$

It is noted that for complex cross-sections the β-parameter can vary depending on the load condition. For dynamic cross-sections equipped with two tensile armour layers of opposite lay angles, the β-parameter will be close to zero. For a static umbilical, however, β may be significant and will influence the torsion stability performance by the introduction of a tension dependent torque that adds to other contributions[29]. The matrix in Equation (2.52) gives a β-parameter equal to $\beta = \frac{R}{L}\cos^2\alpha\sin\alpha$ for a single-layer helix umbilical without torsion balance.

The axial stiffness is then obtained by assuming no torsion coupling and assuming positive radial motion, yielding (2.54)

$$EA = nEA_t\cos\alpha(\cos^2\alpha - v_a\sin^2\alpha) \tag{2.54}$$

where the apparent Poisson's ratio v_a is defined by the relation between axial and radial strain.

Torsion

Excessive torsion may give lock-up of the wires causing bird-caging or excessive yielding. The case of excessive torsion is prone to occur during cable installation. The torsional moment M_t is to be balanced by an internal moment caused by an axial tensile force. The axial tensile force consists mainly of contributions from the helically wounded tensile armours. Equilibrium considerations yield that the torsion moment is defined as

$$\sum_{i=1}^{N_a} n_j\sigma_{11}A_tR_j\sin\alpha_j = M_t \tag{2.55}$$

Torsional stiffness for the cable is defined in Equation (2.56), where the overall strain and radial motion effects are disregarded. It is mainly the tensile armours which provide torsional resistance.

$$GI_t = nA_tER^2\sin^2\alpha\cos\alpha \tag{2.56}$$

In Equation (2.56) n is the number of tensile armour wires and R is the mean radius of the armour layers.

2.6.2 Behavior due to bending

For tensile armour layers, the dynamic stresses consist of an axial friction stress associated with slip between layers, axial stresses from dynamic tension and local torsion and bending stresses resulting from the components of global curvature along each wire.

Moment-curvature behavior

The response of a cable subjected to axi-symmetric loads will be linear as long as the loading is within the linear range of the material. This is not the case for the bending behavior. For a subsea cable submitted to an undulated bending, the relation between the bending moment and the cable curvature will follow a hysteresis curve[12], as illustrated in Figure 2.9.
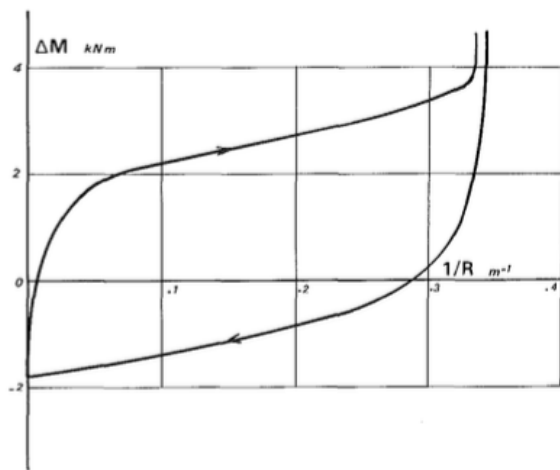
(a) Hysteresis curve
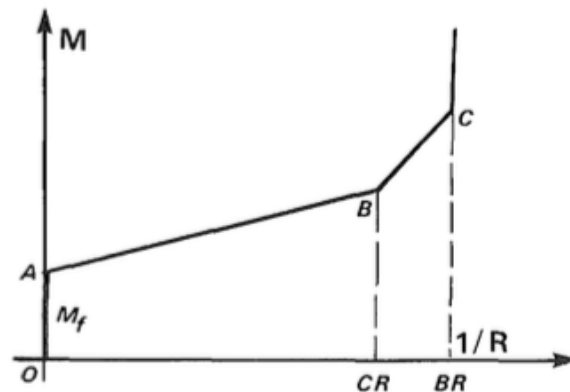
(b)Moment-curvature relation [12]

Figure 2.9: Non-linear material behaviour in bending

When the curvature and the bending moment is small, slip is prevented by the internal friction between layers, leading to a high initial bending stiffness. This is illustrated with region OA in Figure 2.9. In this region, the slope of the curve is defined by the value of the initial tangent stiffness EI_s. For a certain value of the bending moment, the stiffness will drop significantly. This occurs when the bending moment equalizes the friction moment M_f. The friction moment corresponds to the moment necessary to overcome the friction force. For bending moments larger than the friction moment, the cable starts to act flexible. Region AB is characterized by a slope corresponding to the elastic stiffness, later denoted as EI_e. At this level the friction force is not able to maintain the tensile armor wires in place, and the wires starts to slip. The magnitude of the friction moment depends on the

contact pressure between cable layers, and consequently on the loads applied to the cable [12].

For bending moments below M_f the assumption that plane sections remain plane hold, and the bending stiffness can be assessed in the same way as for a composite beam. For bending moments exceeding M_f, the main contribution to the bending stiffness comes from the plastic sheaths, however local straining of the armor wires also contribute to the stiffness.

The "contact radius" CR corresponds to the radius at point B for which the elastic stiffness increases. This coincide with the point of minimum bend radius allowed, and standards require that the structure not can be curved beyond this point. Reverse slip occurs when the bending moment exceeds twice the friction moment. This makes up the formation of a hysteresis loop in the moment-curvature relationship, illustrated in Figure 2.9.

Bending stress in tensile armour
Local bending behavior can be described by assuming that each wire follows an assumed path along the curved pipe and application of differential geometry. Two types of paths are generally defined as below, and illustrated in Figure 2.10.

1. **Geodesic path**: The shortest distance between two points, respectively on the tensile and compressive sides of the cable along the same helix.

2. **Loxodromic path**: The initial path of each wire on the circular cylinder as if the path was fixed relative to the surface.
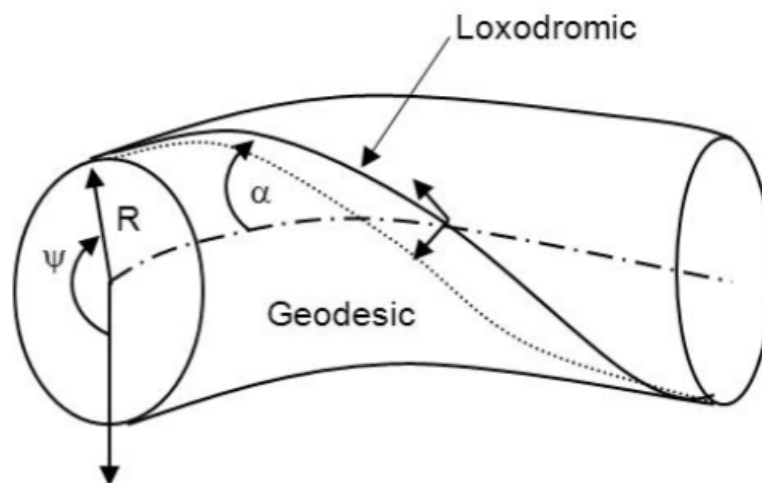
Figure 2.10: Definition of paths [27]

The axial force Q_1 in the wire of cross-section area A_t before slip can be expressed as Equation (2.57), when assuming plane deformation only.

$$Q_1 = -EA_t R \cos^2 \alpha \cos \psi \beta_2 \qquad (2.57)$$

Associated shear force q_1 per unit length needed to fulfill the assumption that plane surfaces remain plane is given by Equation (2.58) when differentiating Equation (2.57) with respect to length coordinate:

$$q_1 = EA_t \cos^2 \alpha \sin \alpha \sin \psi \beta_2 \qquad (2.58)$$

The shear force increases until the pipe neutral axis of bending, and the associated shear stress is then defined as

$$q_{1c} = \mu(q_3^I + q_3^{I+1}) \qquad (2.59)$$

where μ is friction coefficient and the index I and $I+1$ refers to the inner and outer surfaces of the wire. The critical curvature is then found by equating q_1 and q_{1c}, which yields

$$\beta_{2c} = \frac{\mu(q_3^I + q_3^{I+1})}{EA_t \cos^2 \alpha \sin \alpha} \qquad (2.60)$$

By assuming no end effects and harmonic helix motion, an arbitrary cross-section can be divided into two parts; one part which will be in the slip domain (region I) and one which will be in the stick-domain (region II) when exposed to plane bending along Z^2. The cross section zones are visualized in Figure 2.11. The transition between the zones are given by the angle

$$\theta_0 = cos^{-1}(\frac{\beta_{2c}}{\beta_2}) \qquad (2.61)$$

The stress distribution along the slip region can be described by Equation (2.62).

$$\sigma_{11}(\theta) = \frac{\mu(q_3^I + q_3^{I+1})R}{\sin \alpha A_t}\theta \qquad (2.62)$$

At full slip, which corresponds to $\theta = \theta_0 = \frac{\pi}{2}$, the stress reaches its maximum value
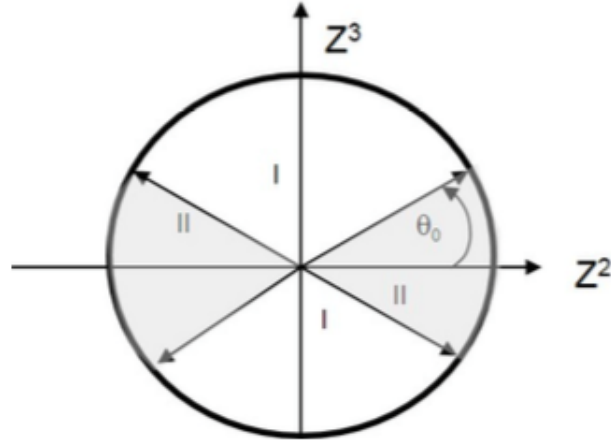
Figure 2.11: Slip and stick-domains for an arbitrary cross section [27]

corresponding to

$$\sigma_{11} = \frac{\pi}{2} \frac{\mu(q_3^I + q_3^{I+1})R}{\sin \alpha A_t} \tag{2.63}$$

Associated bending moments for the start slip and full slip region respectively are found by integration, see Equation (2.64).

$$M = 4F_f \cos^2 \alpha \left[\int_0^{\theta_0} \frac{\mu(q_3^I + q_3^{I+1})R}{\sin \alpha A_t} \theta + \int_{\theta_0}^{\frac{\pi}{2}} E \cos^2 \alpha \beta_2 (\sin \theta - \sin \theta_0) + \frac{\mu(q_3^I + q_3^{I+1})R}{\sin \alpha A_t} \theta_0 \right] t R^3 \sin \theta \mathrm{d}\theta \tag{2.64}$$

Application of Equation (2.61) and (2.64) yields a moment-curvature relation, as the one illustrated in Figure 2.12 [27]. The bending stiffness contribution from each tensile armour layer is then given by

$$EI_s = \begin{cases} \pi R^3 t F_f \cos^4 \alpha & \beta_2 \leq \frac{4}{\pi} \\ 0 & \beta_2 > \frac{4}{\pi} \beta_{2c} \end{cases} \tag{2.65}$$

The total bending stiffness becomes the sum of contributions from all layers, expressed by
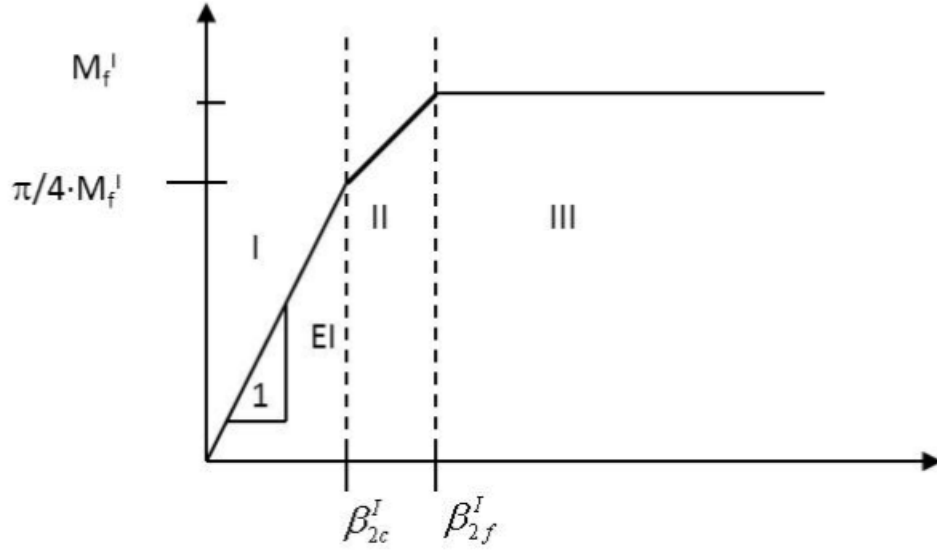
Figure 2.12: Moment curvature diagram for each layer of the cross-section

Equation (2.66)

$$EI = EI_e + \sum_{i=1}^{N_t} \pi R_i^3 t_i F_{fi} \cos^4 \alpha_i f(\beta_2, \beta_{2ci}) \tag{2.66}$$

where $f(\beta_2, \beta_{2c})$ is a function which is equal to 1 for $\beta_2 \leq \frac{4}{\pi}\beta_{2c}$. For $\beta_2 \geq \frac{4}{\pi}\beta_{2c}$, $f(\beta_2, \beta_{2c}) = 0$, meaning that the structural bending has no contribution to stiffness after the initiation of the slip process. For simplicity, the fill factor F_{fi} is assumed to be equal to 0.9 for the tensile armour layers, while for the helical layers the effect of the fill factor is considered by describing the bending stiffness with the help of the effective thickness. Then the bending stiffness EI_s for helical layers can be written as Equation (2.67).

$$EI_s = \frac{1}{2}E \sum_{i=1}^{N_{helix}} A_{tot_i} R_i^2 \cos^4 \alpha_i \tag{2.67}$$

The stiffness EI_e corresponds to the sum of elastic contributions from the plastic layers and local wire bending. By assuming the loxodromic curve representation for the tensile armour,

an estimate for EI_e may be established by the following formula

$$
\begin{aligned}
EI_e = &\sum_{j=1}^{N_{pl}} \frac{\pi}{4}[(R_j^0)^4 - (R_j^i)^4] \\
&+ \frac{1}{2}\sum_{j=1}^{N_t} n_j[G_j J_j 4\sin^2\alpha_j\cos^5\alpha_j + E_j I_{2j}\cos^3 2\alpha_j + E_j I_{3j}\cos\alpha_j(1 + 2\sin^2\alpha_j + \sin^4\alpha_j)] \\
&+ \sum_{j=1}^{N_t} F_{fj}\sigma_{11}\pi R_j^3 t_j[9\cos^4\alpha_j\sin^2\alpha_j + 6\cos^6\alpha_j + \frac{\cos^8\alpha_j}{\sin^2\alpha_j} + \frac{cos^4\alpha_j}{\sin^2\alpha_j} + 4]
\end{aligned}
$$

$$(2.68)$$

where for each tensile armour layer j, the wire torsion rigidity is denoted by $G_j J_j$, $E_j I_{2j}$ is the wire bending stiffness about the weak axis and $E_j I_{3j}$ is the wire bending stiffness about the strong axis.

Chapter 3

Non-linear Finite Element Method

SIMLA is a finite-element program using the nonlinear finite element method to analyze problems with slender beams. The following chapter includes a representation of the basics of the non-linear finite element method and nonlinearities to cover the relevant aspects of the theory which SIMLA is based upon. The theory presented is mainly based on the material given in the SIMLA - theory manual [28], if not otherwise stated.

3.1   Fundamental principles

The finite element method (FEM) is a numerical method for establishing approximate solutions to boundary value problems. FEM is a numerical method which is based on application of the following three main principles

1. Equilibrium

2. Kinematic compatibility

3. Constitutive equations

3.1.1   Equilibrium

Equilibrium is expressed by application of the principle of virtual displacements (PVD). The principle states that the equilibrium of a body requires that for any compatible small virtual displacements imposed on the body in its state of equilibrium, the total internal virtual work is equal to the total external work [5]. Excluding volume forces, the principle of virtual work of an arbitrary equilibrium state of a body with deformed volume V and surfaces S reads [28]

$$\int_V (\rho \ddot{\mathbf{u}} - \mathbf{f}) \delta \mathbf{u} \mathrm{d}V + \int_V \sigma : \delta \epsilon \mathrm{d}V - \int_S \mathbf{t} \delta \mathbf{u} \mathrm{d}S = 0 \tag{3.1}$$

where ρ is the material density, $\ddot{\mathbf{u}}$ is the acceleration field, $\mathbf{f}$ is the volume force vector, σ is the Cauchy stress tensor, ϵ is the natural strain tensor, $\mathbf{t}$ is the surface traction and $\mathbf{u}$ is the

displacement vector.

The stresses may either be expressed with reference to the deformed structure or its initial configuration. True stresses referred to the deformed configuration are denoted σ_{ij} (Cauchy stresses), while stresses referred to the initial configuration are denoted S_{ij} (2nd Piola-Kirchoff stresses). 2nd Piola-Kirchhoff stress is consistent with Green strain which also refers to the initial configuration. In SIMLA, all quantities are referred to the initial configuration, C^0, i.e. 2nd Piola-Kirchoff stress and Green strain are applied.

3.1.2   Kinematic compatibility

Kinematic compatibility indicates that the adjacent cross-sections experience the same displacement and deformations. This means that the structure will remain continuous during deformation, and that the strain will be finite. Application of continuous interpolation functions to describe the displacement distribution over the elements along with proper boundary conditions, ensures that compatibility of an element is obtained [22].

SIMLA applies the assumption of Bernouilli-Euler and Kirchoff-Navier's hypothesis. The hypotheses state that plane sections perpendicular to the neutral axis remains plain and perpendicular to the neutral axis after loading. This indicates no shear deformations. Further, the Green strain tensor is used as strain measure when formulating the incremental equilibrium equations. The 2nd order longitudinal engineering strain is neglected according to von Karman [28]. However, all terms related to coupling between longitudinal strain and torsion are included

The Green strain can thus be defined as

$$E_{xx} = u_{,x} - yv_{,xx} - zw_{,xx} + \frac{1}{2}(v_{,x}^2 + w_{,x}^2) + \theta_{,x}\left(yw_{,x} - zv_{,x}\right) + \frac{1}{2}\theta_{,x}^2\left(y^2 + z^2\right) \qquad (3.2)$$

3.1.3   Constitutive equations - stress strain relationship

The stress strain relationship is defined by a material model. The most common material models are elastic and elasto-plastic material modes. For linear elastic materials, Hooke's law defines this relationship and is given by Equation (3.3).

$$\begin{bmatrix} \sigma_{11} \\ \sigma_{22} \\ \tau_{12} \end{bmatrix} = \frac{E}{1 - v^2} \begin{bmatrix} 1 & v & 0 \\ v & 1 & 0 \\ 0 & 0 & \frac{1-v^2}{2(1+v)} \end{bmatrix} \begin{bmatrix} \epsilon_{11} \\ \epsilon_{22} \\ \gamma_{12} \end{bmatrix} \qquad (3.3)$$

For a pipe, it is necessary to utilize an elasto-plastic material formulation to consider both the stresses in axial and hoop direction [28]. To take into account the effect of material softening beyond the stress proportionality limit, an application of plasticity theory is needed. Plasticity theory states that the total strain can be divided into two components; elastic and plastic contributions. The elastic contribution can be derived from the elastic material law as Hooke's law. The plastic strain is calculated based on the following three criteria [28]:

1. **Yield criterion**: The yield criterion defines the state of stress in which plastic deformation first occurs. For metals, the yield criterion is generally expressed by the von Mises criterion. The yield criterion is expressed in general form as

$$f(S, \kappa) = 0 \tag{3.4}$$

   where f is a scalar function, κ is a strain-hardening parameter and $\mathbf{S}$ is the 2nd Piola-Kirchoff stress tensor.

2. **Hardening rule**: A hardening rule describes how the material hardens after plastic deformation starts. Two types of hardening is generally applied during unloading:
   (i) Kinematic hardening: the distance between the yield limit points never exceeds $2\sigma_Y$
   (ii) Isotropic hardening: the material remembers the hardening prior to unloading, and renewed yielding occurs at a stress level $|\sigma| = \sigma_B$
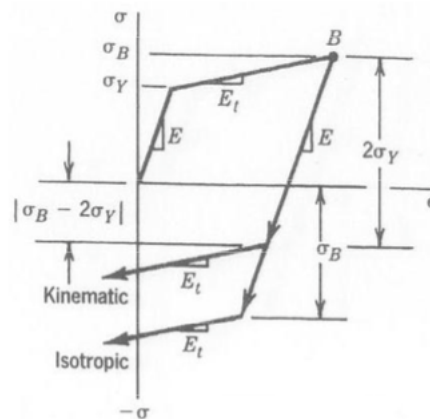
Figure 3.1: Kinematic and isotropic hardening [22]

3. **Flow rule**: Defines a relation between stress increments $d\sigma$ and strain increments $d\epsilon$. The relationship between stress and strain can be described by two different plasticity theories; the flow theory and the deformation theory. SIMLA is based on flow theory.

The program also assumes that the material follows the Drucker's postulate for a stable material, which gives the following requirement

$$\dot{\mathbf{E}}^{(p)} = \dot{\lambda}\frac{\partial f}{\partial S} \tag{3.5}$$

where $\dot{\mathbf{E}}^{(p)}$ is the plastic part of the rate of Green's strain tensor, and $\dot{\lambda}$ is a scalar function depending on the current stress and strain, and on the stress rate [28].

3.2 Nonlinearities

Linear FEM assumes infinitesimally small displacements and linearly elastic material behaviour. The nature of the boundary conditions is also assumed to remain unchanged during the application of loads. This does not hold for all situations. When the ultimate strength of structures that buckle and collapse is to be calculated, the assumptions about small displacements and linear material need to be modified by including nonlinear effects [22].

The following categories for non-linearities are defined [5]:

1. **Material non-linearity**: Governed by a nonlinear stress-strain relation, mainly concerning structures undergoing non-linear elasticity, plasticity, viscoelasticity, creep and inelastic rate effects. Displacements are infinitesimal.

2. **Geometrical non-linearity**: Displacements are large compared to the initial dimensions of the structure. From this it follows that the stiffness and loads will change as the structure deforms. Linear or nonlinear material relation.

3. **Nonlinear boundary condition**: Change in boundary condition at displacement Δ, where a large displacement leads to contact. Included is both force and displacement boundary conditions.

For the case of subsea cables, it exists several nonlinear effects. The umbilical will experience large deformations when laid from the CLV, and the umbilical material will behave non-linearly with elastic-plastic material behaviour. The hydrodynamic loading will act non-linearly; waves and currents are proportional to the square of the relative velocity, according to Morrison's equation. The pipe-soil interaction corresponds to a nonlinear contact problem, and the boundary conditions will also vary.

3.3 Lagrange Formulations

The two most common modes of describing the deformations of solids and fluids are the *Eulerian* and the *Lagrangian* approaches, where the Eulerian description refers to what happens at a certain place in space while the Lagrangian description refers to what happens at a material particle. Two formulations are widely used in analysis of large deformation problems; the Total Lagrangian (TL) and the Updated Lagrangian (UL). The main difference lies in the reference system used for calculating stresses and strains.

The TL formulation is based on a fixed reference system (C^0), while for the UL formulation the local coordinate system is assumed to follow the rigid body displacements as the structure deforms. Thus, the reference system for each calculation refers to the last obtained equilibrium configuration (C^n). SIMLA is based on the co-rotational formulation referring all quantities to the C^0 configuration. The last obtained reference configuration is described by the current strains. The strains are assumed to be small, allowing large rigid body motions to occur. The incremental form of the PVW is obtained by studying the virtual work in an infinitesimal increment Δ

$$\int_V \mathbf{C} : (\epsilon - \Delta\mathbf{E})\delta(\epsilon - \Delta\mathbf{E})\mathrm{d}V_0 - \int_S (\mathbf{t} + \Delta\mathbf{t})\delta\mathbf{u}\mathrm{d}S_0 = 0 \tag{3.6}$$

where $\mathbf{E}$ is the Green strain sensor. Equation (3.6) is used as basis for the stiffness matrix. The first term of the equation gives the material stiffness matrix, while the second term gives the initial stress stiffness matrix, also called the geometric stiffness matrix.

3.4 Solution procedures

SIMLA gives the possibility to solve both static and dynamic problems. The differences between the two procedures are visible when comparing the equilibrium equations. Dynamic analysis considers inertia and damping forces, in addition to the equilibrium of stiffness forces which is common for both procedures. A dynamic equilibrium analysis gives a time dependent solution, while the static solution is independent of the time. The equilibrium equations for the two cases are presented in Equation (3.7),

$$\begin{aligned} \textit{Static:} &\quad \mathbf{Kr} = \mathbf{R} \\ \textit{Dynamic:} &\quad \mathbf{M\ddot{r}} + \mathbf{C\dot{r}} + \mathbf{Kr} = \mathbf{R(t)} \end{aligned} \tag{3.7}$$

where $\mathbf{K}$, $\mathbf{M}$, and $\mathbf{C}$ is respectively the stiffness, mass and damping matrix, $\mathbf{R}$ is the external

load vector and $\mathbf{r}$, $\dot{\mathbf{r}}$ and $\ddot{\mathbf{r}}$ is the displacement, velocity and acceleration vectors.

3.4.1 Static problems

The solution procedure for static problems is based on the widely used iteration method, the Newton-Raphson technique. Figure 3.2 illustrates the iteration process of the Newton-Raphson method. The equations utilized in a Newton-Raphson iteration are given by the following equations [5],

$$^{t+\Delta t}\mathbf{K}^{(i-1)}\Delta\mathbf{U}^{(i)} = {}^{t+\Delta t}\mathbf{R} - {}^{t+\Delta t}\mathbf{F}^{(i-1)} \tag{3.8}$$

$$^{t+\Delta t}\mathbf{U}^{(i)} = {}^{t+\Delta t}\mathbf{U}^{(i-1)} + \Delta\mathbf{U}^{(i)} \tag{3.9}$$

with initial conditions

$$^{t+\Delta t}\mathbf{U}^{(0)} = {}^{t}\mathbf{U}; \ {}^{t+\Delta t}\mathbf{K}^{(0)} = {}^{t}\mathbf{K}; \ {}^{t+\Delta t}\mathbf{F}^{(0)} = {}^{t}\mathbf{F} \tag{3.10}$$
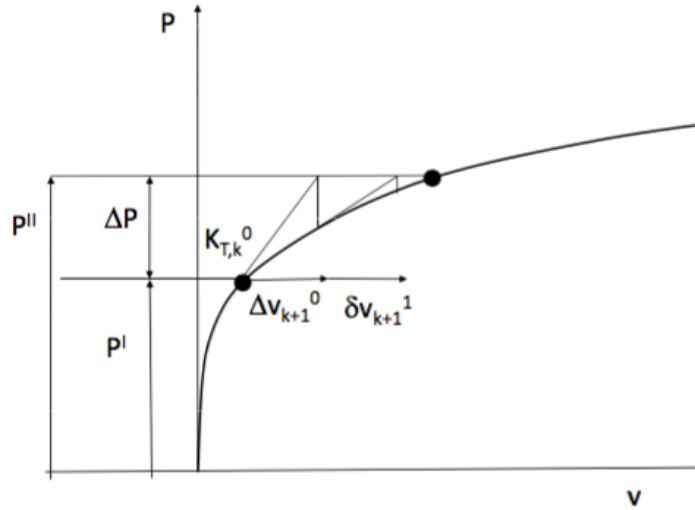
Figure 3.2: Illustration of Newton-Raphson method [28]

3.4.2 Dynamic problems

Nonlinear dynamic problems cannot be solved by modal superposition, thus direct time integration of the equation of motion is used. This can be performed by either an explicit

or an implicit method.

In an explicit method, the displacements at the next time step is determined based on information from the current time steps and previous time steps. This can be expressed by Equation (3.11). Explicit methods are conditionally stable where very short time steps must be applied to obtain convergence.

$$\mathbf{r_{k+1}} = \mathbf{f}(\ddot{\mathbf{r}}_k, \dot{\mathbf{r}}_k, \mathbf{r_k}, \mathbf{r_{k-1}}) \tag{3.11}$$

In an implicit method, the displacements depend on information from the next time step as well as quantities from the current step. Since implicit methods use information from the next time step they will have a better numerical stability than explicit methods. These methods are unconditionally stable.

$$\mathbf{r_{k+1}} = \mathbf{f}(\ddot{\mathbf{r}}_{k+1}, \ddot{\mathbf{r}}_k, \dot{\mathbf{r}}_{k+1}, \dot{\mathbf{r}}_k, \mathbf{r_k}) \tag{3.12}$$

3.5 Incremental time integration

SIMLA applies the HHT-α-method in the time integration scheme [28]. An incremental approach is applied since the system solves a nonlinear problem. The HHT-α-method defines a modified equilibrium equation, which is given as

$$\mathbf{M}\ddot{\mathbf{r}}_{k+1} + (1-\alpha)\mathbf{C}\dot{\mathbf{r}}_{k+1} - \alpha\mathbf{C}\dot{\mathbf{r}}_k + (1-\alpha)\mathbf{R^I_{k+1}} - \alpha\mathbf{R^I_k} = (1+\alpha)\mathbf{R^E_{k+1}} - \alpha\mathbf{R^E_k} \tag{3.13}$$

where $\mathbf{R^I}$ is the internal load vector and $\mathbf{R^E}$ is the external load vector. The subscript k refers to current time step, while $k+1$ refers to the next. Both Rayleigh-damping and a diagonal damping matrix is included in the total damping matrix:

$$\mathbf{C} = \mathbf{C_0} + \alpha_1\mathbf{M} + \alpha_2\mathbf{K} \tag{3.14}$$

By applying the Newmark-β method, the acceleration and velocity at time step $k+1$ is found

$$\Delta\ddot{\mathbf{r}}_{k+1} = \Delta\ddot{\mathbf{r}}_{k+1} - \Delta\ddot{\mathbf{r}}_k = \frac{1}{\Delta t^2\beta}\Delta\mathbf{r}_{k+1} - \frac{1}{\Delta t\beta}\dot{\mathbf{r}}_k - \frac{1}{2\beta}\ddot{\mathbf{r}}_k \tag{3.15}$$

$$\mathbf{\Delta\dot{r}_{k+1}} = \mathbf{\Delta\dot{r}_{k+1}} - \mathbf{\Delta\dot{r}_k} = \frac{\gamma}{\mathbf{\Delta t}\beta}\mathbf{\Delta r_{k+1}} - \frac{\gamma}{\beta}\mathbf{\dot{r}_k} - \mathbf{\Delta t}(\frac{\gamma}{2\beta} - 1)\mathbf{\ddot{r}_k} \tag{3.16}$$

By subtracting the equilibrium equation at time step k from Equation (3.13) the following relation is obtained

$$\mathbf{\hat{K}_k\Delta r_{k+1}} = \mathbf{\Delta\hat{R}_{k+1}} \tag{3.17}$$

The effective load vector is then given as

$$\mathbf{\Delta\hat{R}_{k+1}} = (\mathbf{1}+\alpha)[\mathbf{R^E_{k+1}} - \mathbf{R^E_k} + \mathbf{Cb^E_k}] + \mathbf{Ma_k} + \mathbf{R^E_k} - \mathbf{R^I_k} - \mathbf{C_k\dot{r}_k} \tag{3.18}$$

$$\text{where} \quad \mathbf{a_k} = \frac{\mathbf{1}}{\mathbf{\Delta t}\beta}\mathbf{\dot{r}_k} + (\frac{\mathbf{1}}{2\beta} - \mathbf{1})\mathbf{\ddot{r}_k} \tag{3.19}$$

The solution of Equation (3.17) yields the displacement at time step $k + 1$, which is used in Equation (3.16) and (3.15) to obtain the velocity and acceleration at time step $k + 1$ respectively. Solution of Equation (3.18) gives the unbalanced forces at time step k, such that the iteration is performed until balance is achieved in Equation (3.13).

Chapter 4

SIMLA

To investigate the concept of torsion instability of a dynamic cable, the SINTEF OCEAN developed simulation program SIMLA is utilized to simulate cable installation scenarios. SIMLA is a finite element method based program system for non-linear static and dynamic analysis of pipelines. The software allows for solution of a broad aspect of pipeline engineering problems [28]. The system architecture of SIMLA is illustrated in figure 4.1. The work process utilized is mainly divided into three main steps;

1. Development the input file of .sif format. The input file defines the composition of the model with focus on element and material properties of the various components, as well as load and boundary conditions and analysis properties.

2. Run the static and/or dynamic analysis.

3. Post-processing of results from analysis using either XPOST or SIMPOST. The results from SIMLA are stored in the file format .raf, which might be further processed by SIMPOST. The SIMPOST input-file are of format .spi.
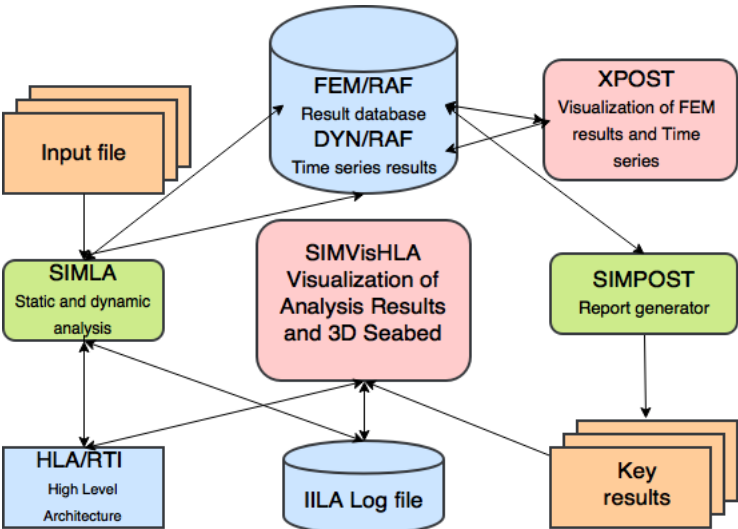
Figure 4.1: SIMLA system architecture [28]

4.1 Model definition

The installation model consists of four main components; the cable, a cable-laying vessel, the sea surface and the seabed. To model these components four different element types are implemented. These element types are listed in Table 4.1. The cable is either made up of linear or nonlinear pipe element, depending in the type of analysis carried out. Figure 4.2 illustrates where which element type is applied in the simulation model. Following the properties of each element will briefly be presented along with the associated material model describing the material properties of the element. The following theory presented is based on theory given in the SIMLA theory manual [28], if not otherwise stated.

Table 4.1: Description of the elements applied in the simulation model

Element	Description
PIPE31	Linear elastic pipe element
COMPIPE42	Elastic-plastic pipe element which includes nonlinear material properties
CONT126	Contact elements to model sea bed and stinger contact
SEA150	Sea element to model sea surface
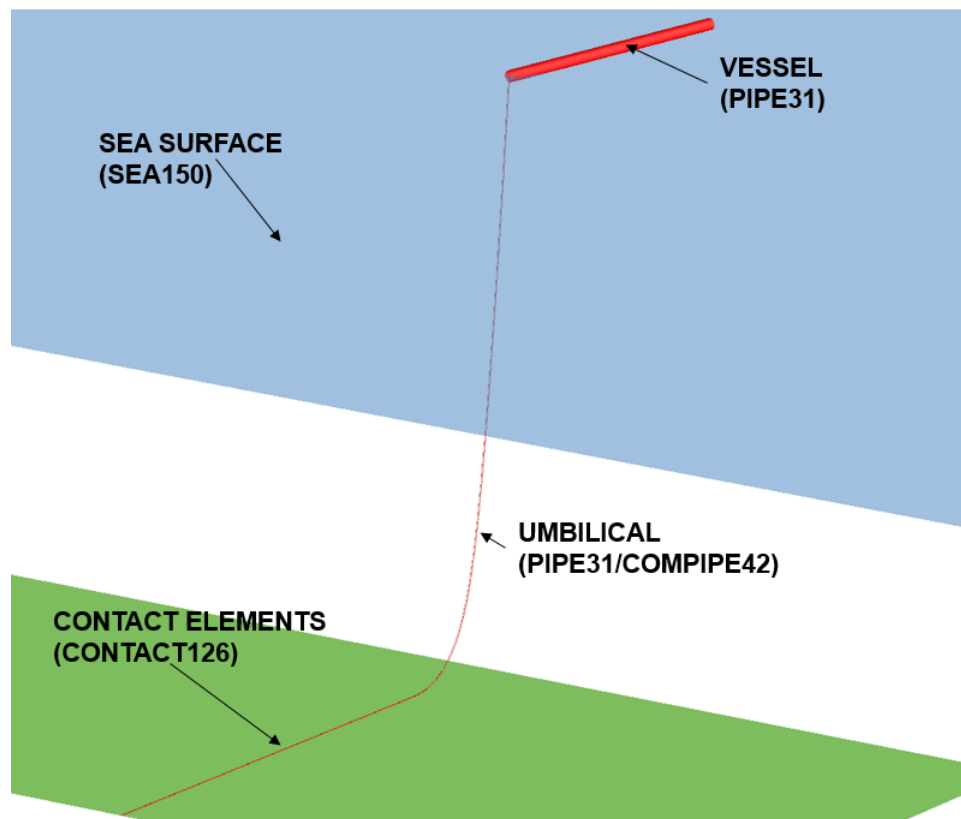
Figure 4.2: SIMLA model set-up

4.1.1 Pipe elements

Each pipe element includes six degrees of freedom per node. The orientation and motion of the beam node is referred to a global coordinate system with base vectors $\mathbf{I_i}$. The element deformations are measured relative to a local beam element system $\mathbf{j_i}$ which is connected to each element. Rotational motion is defined by using an orthonormal base vector triad $\mathbf{i_i^n}$ attached to each node. This leads to the possibility of eliminating rigid body motion. The nodal system $\mathbf{i_i}$ and elemental system $\mathbf{j_i}$ are in the initial state parallel to the global base vectors $\mathbf{I_i}$, and moves along with the node during deformation. Motion of the beam modes is shown in Figure 4.3.
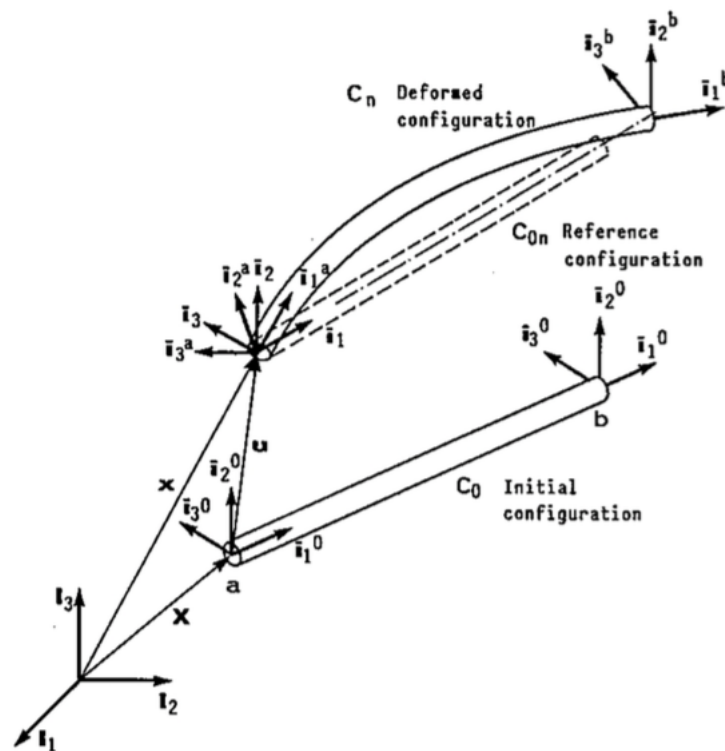
Figure 4.3: Motion of beam nodes [28]

PIPE31

PIPE31 is an elastic 3D pipe element with constant axial strain and torsion consisting of 2 nodes. Each element includes six degrees of freedom per node. The element has a thin-walled tubular cross-section with constant radius and thickness along each element. The associated material type is the LINEAR material model. The LINEAR material type consists of linear material properties for elastic pipe elements. The material model is based on the Bernoulli-Euler and Navier hypothesis. The Green strain tensor is used as a strain

measure in the incremental equilibrium equations. The second order longitudinal strain term in the Green strain tensor is neglected according to von Karman. The same governs for coupling terms between longitudinal strain and torsion. Shear deformations are also neglected.

COMPIPE42

COMPIPE42 is a non-linear material based element, based on the RESULTANT material model. The RESULTANT material model allows for user-defined material curves in each direction. as well as definition of variations in the axial-, torsional - and bending stiffness. This is used to capture the slip behavior of the cables presented in Section 2.6.1. These variations are defined using EPCURVE or HYCURVE commands. EPCURVE describes elastoplastic material behavior with kinematic or isotropic hardening, while HYCURVE describes hyper-elastic material behavior.

4.1.2 Contact elements

Contact elements are virtual elements which simulate the connection and relative displacements between two bodies. Two conditions may occur when considering contact between two bodies A and B; gap opening and contact. Gap opening is defined by Equation (4.1), while contact is defined by Equation (4.2)

$$g = (\Delta \mathbf{u_{CB}} - \mathbf{u_{CA}}) \cdot \mathbf{n_3} + g_0 \geq 0 \tag{4.1}$$

$$g = (\Delta \mathbf{u_{CB}} - \mathbf{u_{CA}}) \cdot \mathbf{n_3} + g_0 < 0 \tag{4.2}$$

where g is the current gap at time $t + \Delta t$ in the direction of $\mathbf{n_3}$ and g_0 is the gap at time t.

CONT126

CONT126 is a contact element in SIMLA used to simulated general pipe-soil interaction modelling on original seabed. The CONT126 elements are 1-noded contact elements which are linked to the contact surface definition. Friction transverse displacement is measured from the position where last contact was obtained. Contrary to other contact elements, CONT126 includes the torsion coupling parameter β. For contact behavior described by CONT126 elements, R_CONTACT is a user defined material property which describes material curves in x-, y- and z-directions for seabed contact elements. Torsion moment is introduced by skin

friction without coupling to transverse displacements. This is enabled by multiplying the force components in x- and y-direction with the z-component and a friction coefficient.

4.2 Analysis methodology

The analysis is built up of two parts; a static analysis to build up the catenary configuration and a dynamic analysis where the dynamic loads are applied. The reference configuration is assumed to be a straight beam with a length equal to the cable initial length. In the static analysis, the cable self-weigh load is imposed and a tension load T is applied in horizontal direction at node 1 to induce necessary tension in the cable. By inducing prescribed translation at the connection node, the cable along with the vessel is pulled up to the sea surface. This yields establishment of the catenary configuration. In the static analysis, no memory effects can be included, which indicates that there is no axial stiffness present as well as that no sliding along the seabed can occur. Figure 4.4 shows the steps of the analysis graphically. The script given in Appendix B illustrates how an input file in SIMLA is defined.

The dynamic analysis is performed as a RESTART of the initial static configuration. The torque level corresponding to an installation scenario is applied gradually in the first step of the dynamic analysis. Lastly the wave loading is applied over a period of one hour. The time scheme is illustrated in Table 4.2

Table 4.2: Time scheme for dynamic analysis

Time interval	Function
0 - 5 sec	Build-up of static configuration
6 - 10 sec	Rotation imposing to obtain torsion level
10 - 3600 sec	Dynamic wave loading simulation

(a) Initial set-up at t = 0.1 s

(b) Catenary configuration at t =5 s
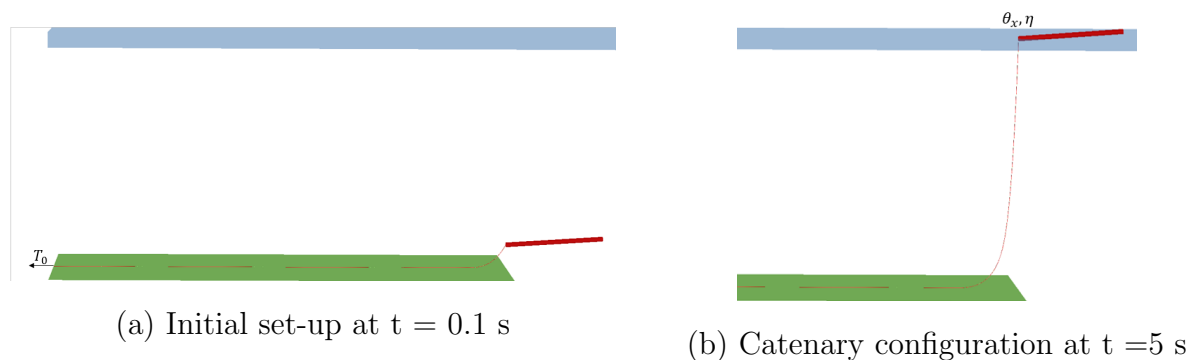
Figure 4.4: Model set-up with main loads

An important aspect of this thesis is to perform a parametric study of the effect of wave parameters. To simplify the execution of this parametric study, the analysis is carried out with the help of *Cygwin*. With Cygwin it is possible to make scripts which run consecutive analyses. With the help of built-in functions, one can change the relevant parameters before each run. The script *go-analyze*, given in Appendix D, shows an example of how the various input files are changed to represent the desired sea state and then run in SIMLA. The script replaces certain predefined text strings with values of the significant wave height and return periods with the help of the function *erzatz*.

The results from SIMLA are post-processed in XPOST or by using SIMPOST together with Matlab. In XPOST the results from SIMLA can be visually presented, and the program offers some possibilities for plotting. More extensive treatment of the results are performed by extracting numerical values from SIMLA for the desired parameters using SIMPOST. SIMPOST creates a result file with the values, which can be treated in MATLAB for a more detailed presentation of the results. An example of a SIMPOST file is given in Appendix C.

Table 4.3 describes the programs used to carry out the analyses, as well as the programs utilized to post-process the results

Table 4.3: Software programs

Program	Description
Cygwin	Cygwin is a large collection of GNU and Open Source tools which provide functionality similar to a Linux distribution on Windows [7]
Matlab	Extensive mathematical program, where some of the most relevant features in this case are treatment of large text files and plotting.
SIMLA	Nonlinear FEM program performing the static and dynamic analysis of the installation procedure. Developed by SINTEF OCEAN.
SIMPOST	A SIMLA post-processor which export predefined results to a result file of format .mpf. Developed by SINTEF OCEAN.
XPOST	Program which gives a visual representation of the SIMLA analysis.

Chapter 5

Model Parameters

This chapter describes the model parameters, which are implemented in SIMLA. The cross-section properties of two cable models are discussed, along with the installation routes and the loading applied to the cable during the operation.

5.1 Umbilical properties

To realistically present the properties of a dynamic cable, the cross-sections of two existing umbilical are chosen as the umbilical input in the simulations. The two cross-sections are shown in Figure 5.1. The umbilical in 5.1 (a) is a single-layered umbilical without armouring, while (b) is a double-layer armoured cable with two helical layers. The latter is torsional balanced, while the lack of armouring makes umbilical 1 unbalanced in torsion. The main structural characteristics of each layer is given in Appendix A. There the dimensions of each layer are presented, along with characteristic area, moment of inertia and mass per unit length.
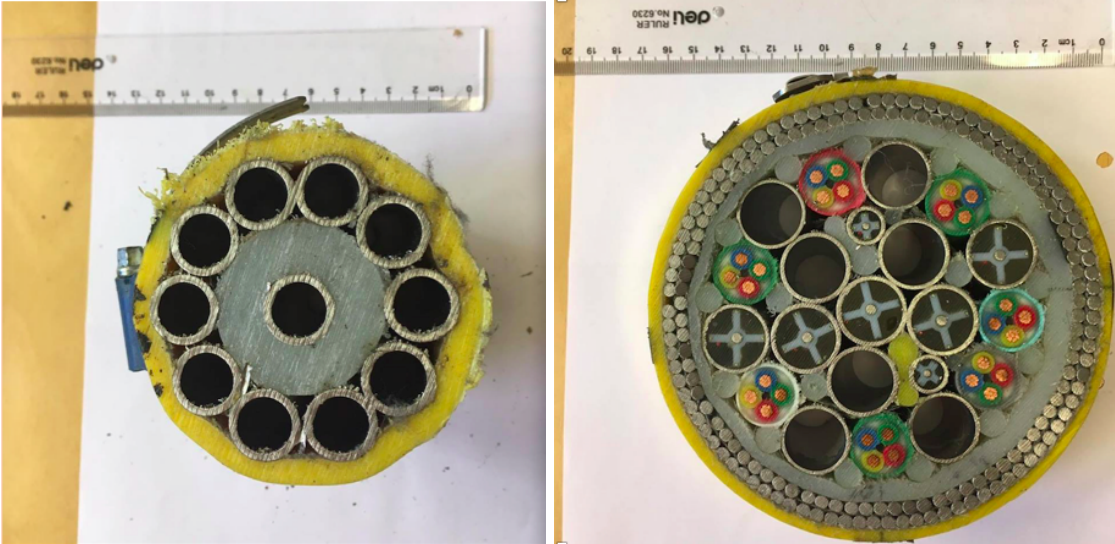
(a) Umbilical 1   (b) Umbilical 2

Figure 5.1: Cable cross-sections

The main strength components of the cross-sections are made of steel, while the insulation layer and the outer sheath are composed of cross-linked polyethylene (XLPE) and polyethylene (PE) respectively. The material properties for the mentioned materials are presented in Table 5.1

Table 5.1: Material properties for umbilical materials

	Symbol	Unit	Normal strength steel	PE	XLPE
Density	ρ	kg/m^3	7850	958	930
Youngs's modulus	E	GPa	200	0.883	0.3
Poisson's ratio	υ	-	0.3	0.46	0.3
Yield stress	σ_y	MPa	450	20	20

The simulations will be carried out with either linear or non-linear pipe elements. The differences lay mainly in the behavior of the cross-section, where the non-linear material model considers the slip behavior of the cable. This yields in different stiffness' for the linear and the non-linear model. The values of the axial-, torsional- and bending stiffness are calculated with the use of the expressions deducted in Section 2.6.1. The elastic cross-section properties are summarized in Table 5.2, while the non-linear properties will be presented in the next chapter. The most apparent difference lies in the magnitude of the torsional stiffness, which is of a factor 10^4 greater for umbilical 2, which is caused by the lack of armouring layers for umbilical 1.

Table 5.2: Elastic cross-section properties

Material parameter	Symbol	Unit	Umbilical 1	Umbilical 2
Axial stiffness	EA	N	$1.94 * 10^8$	$7.6 * 10^8$
Bending stiffness	EI	Nm^2	$6.1261 * 10^3$	$2.4535 * 10^4$
Torsional stiffness	GI	Nm^2	$2.86 * 10^3$	$8.27 * 10^7$
Torsion coupling parameter	β	m	0.023	0

The hydrodynamic properties of the umbilical is presented in Table 5.3. The same properties are applied to the vessel model.

Table 5.3: Hydrodynamic properties

Parameter	Unit	Value
Radial drag coefficient	-	1.0
Tangential drag coefficient	-	0.1
Radial added mass coefficient	-	2.0
Tangential added mass coefficient	-	1.0

5.2 Installation conditions

The installation scenario to be simulated is a J-lay in shallow waters in the northern North Sea. The installation is carried out at a water depth of 100 m.

5.2.1 Minimum radius of curvature

A dimensioning parameter during a cable installation is the minimum radius of curvature. Based on the formulas for MBR presented in API 17J, see Section 2.4.1, the minimum bending radius criterion for the various layers can be calculated. Table 5.4 summarizes the obtained results of the MBR for the two cross-sections.

Table 5.4: Minimum bend radius and radius of curvature for the two cross-sections

Limiting layer	Umbilical 1		Umbilical 2	
	MBR [m]	κ_{min} [1/m]	MBR [m]	κ_{min} [1/m]
Tensile armour layer	0.27	3.70	0.635	1.58
Outer sheath	0.474	2.1	0.905	1.1
Helix layer	5.08	0.1968	6.98	0.1432

As is apparent in the table, the bending capacity in the tensile armour will be the limiting parameter. The minimum radius of curvature is found as $\kappa = \frac{1}{R_{min}}$ which yields that the maximum MBR gives the minimum radius of curvature. Thus, umbilical 1 can experience a curvature radius of 0.197 [1/m] while a minimum curvature radius of 0.143 [1/m] is acceptable for umbilical 2. To ensure fulfillment of this design criterion, safety factors established in API 17J are applied. The analysis performed are fully dynamic, such that a safety factor of $1.1 * 1.25$ is implemented in the radius of curvature. Adding the safety factors from API to the results obtained above yield the minimum acceptable radius of curvature as given in Table 5.5.

Table 5.5: Minimum radius of curvature for the cross-sections, with safety factors

	Minimum radius of curvature [1/m]
Umbilical 1	0.1432
Umbilical 2	0.1041

5.2.2 Catenary configuration

The cable is installed in a catenary configuration. Equation (5.1) presents the parameters defining the catenary shape, while Figure 5.2 illustrates how the parameters relate to the

cable configuration.

$$\text{Catenary length} \quad s = \sqrt{d^2 + \frac{2dT_0}{w_s}}$$

$$\text{Upper angle} \quad \alpha = \tan^{-1}(\frac{w_s s}{T_0})$$

$$\text{Horizontal bottom tension} \quad T_0 = \frac{w_s d}{\tan^2 \alpha}(1 + \sqrt{1 + \tan^2 \alpha}) \tag{5.1}$$

$$\text{Curvature at TDP} \quad \frac{1}{R_{min}} = \frac{w_s}{T_0}$$

$$\text{Layback length} \quad x = \frac{T_0}{w_s} ln[(1 + \frac{w_s d}{T_0}) + \sqrt{1 + \frac{w_s d}{T_0})^2 - 1}]$$
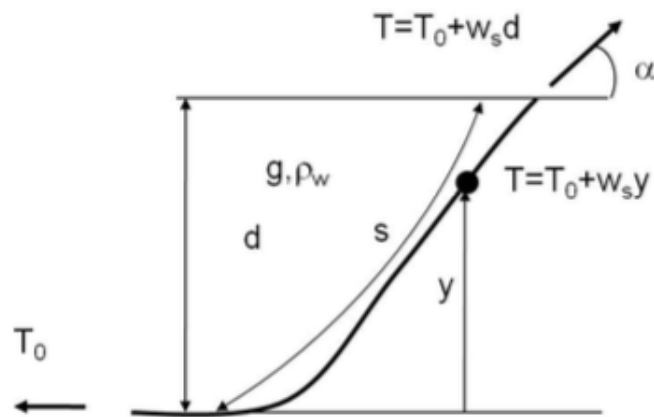
Figure 5.2: Catenary parameters

Table 5.6: Catenary configuration parameters, without safety factors

	Symbol	Unit	Umbilical 1	Umbilical 2
Catenary length	s	m	105	107
Upper lay angle	α	°	87.23	86.26
Layback length	x	m	18.78	23.9
Horizontal bottom tension	T_0	N	236	983
Top tension	T	N	4883	15072

The catenary parameters for the two umbilical cross-sections are calculated and presented in Table 5.6. The parameters are calculated based on the criterion of minimum bending radius/curvature at the TDP as defined in in API 17J [1]. The horizontal bottom tension T_0 gives the minimum tension which must be applied to the system to ensure sufficient tension

in the cable during the static analysis. It is desirable to have as small tension as the MBR criterion allows to improve the maneuverability for the system. Hence a T_0 corresponding to the radius' in Table 5.5 is applied to the cables to ensure allowable curvature initially. This corresponds to a bottom tension of $T_0 = 324.6N$ and $T_0 = 1352N$ for cross-section 1 and 2 respectively, with the recommended safety factors implemented.

Figure 5.3 illustrates the initial configuration of the two cables in the xz-plane. Due to the difference in minimum bending radius as well as in the composition of the cross-sections, the catenary configuration will differ slightly for the two cases.
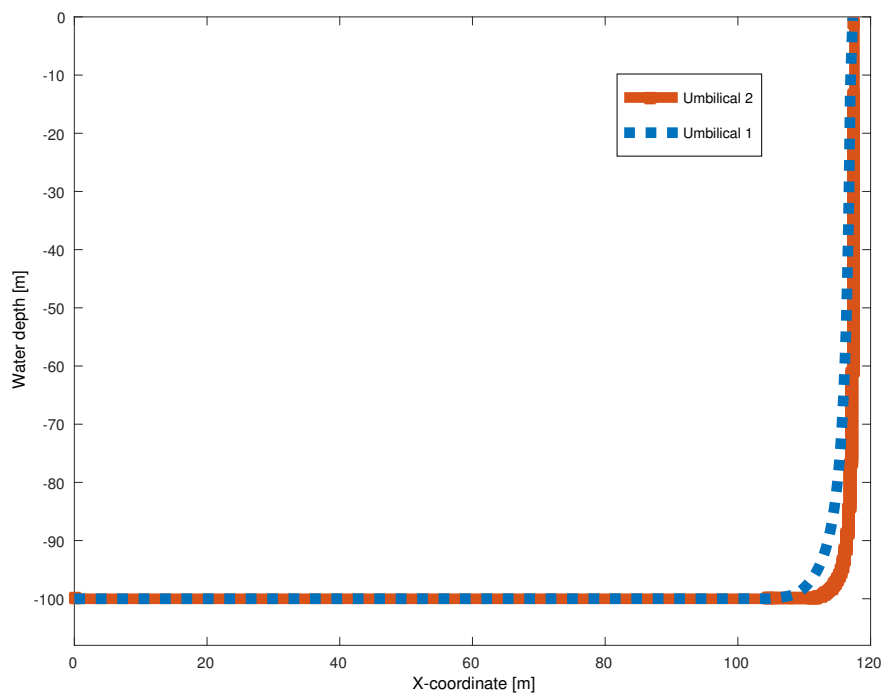
Figure 5.3: Static configuration in the xz-plane for umbilical 1 and 2

5.2.3 Route scenarios

The umbilical is installed in a catenary configuration on an even seabed with constant water depth. Two installation routes are to be analyzed. The routes are chosen due to their large relative yaw rotation between the vessel and the touchdown point. The two installation routes investigated are listed below, and illustrated in Figure 5.4.

1. **End cap turn**; where the cable is laid on the seabed with a 180° turn near the anchoring point.

2. **Curved routing**; route with vessel heading variations to avoid obstacles or objects on the seabed far away from ends. The heading change is chosen as 20 °.

(a) End cap turn

(b) Curved routing
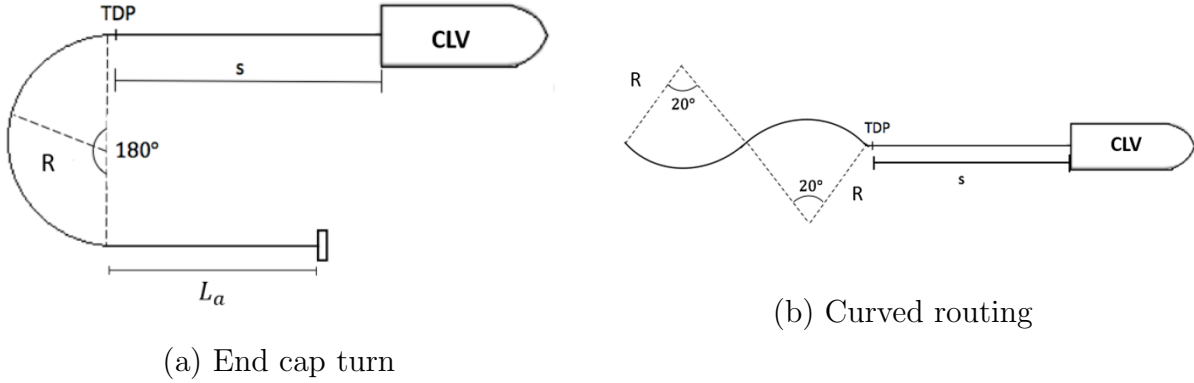
Figure 5.4: Illustration of installation scenarios and main parameters involved

When performing the heading changes, it is important to ensure lateral stability to avoid sliding on the seabed. The tension in the cable must be less than the soil friction force. The soil friction force exhibited by the soil is defined as $F_f = \mu w_s R$ where μ is the soil friction factor, w_s is the submerged weight of the cable and R is the bending radius of the cable associated with the heading change. Thus, the allowed minimum bending radius will be limited by the following relation [27]

$$T_o < \mu w_s R \implies R_{min} > \frac{T_0}{\mu w_s} \tag{5.2}$$

The installation routes are simulated by inducing torsion moments corresponding to the moments induced by the change in route. The relation between the torsion moment and the applied rotation is given as

$$M_x = GI_t \frac{\partial \theta_x}{\partial x} = GI_t \frac{\theta}{L_{tot}} \tag{5.3}$$

where L_{tot} is the total length of the cable including catenary length, length due to turn as well as anchoring length.

The torsion moment is constant in the elements of the cable since the stiffness is equal along all axis [27]. Moment equilibrium yields the following relation between the imposed rotation

due to heading variation and the torsion moment in the cable

$$\frac{M_x^2}{\mu w_s R} + M_x L_c + G I_t \theta = 0 \tag{5.4}$$

This yields a second order equation which can be solved for the torsion moment M_x for a given known rotation θ, which for the case of curved routing is 20°.

5.2.4 Static loads

The cable self-weight, buoyancy and hydrostatic pressure are referred to as the static loads in this context. The umbilical is considered to be fully immersed in water and the combined effect of the structure self-weight, buoyancy and internal pressure can be looked upon as a resulting force named the effective weight[13]. The effective weight for the two cross-sections are presented in Table 5.7.

Table 5.7: Effective weight

	Symbol	Unit	Umbilical 1	Umbilical 2
Dry weight	w_{dry}	N	302.22	95.72
Buoyancy	F_b	N	161.35	49.23
Effective weight	w_s	N	46.47	140.88

5.2.5 Dynamic loads

The dynamic loading scenario will consist of loading from an irregular sea state as well as induced motion of the cable due to the vessel's response to the sea state.

Waves

The waves are modelled as irregular waves described by a two-parameter Pierson Moskowitz spectrum. The defining parameters are the significant wave height H_s and the spectral peak period T_p. A scatter diagram gives the joint probability of the occurrence of a given combination of the significant wave height and wave period, and thus indicating which sea states are the most probable [11]. The probability is given as parts per thousand. The scatter diagram for the northern North Sea is restated in Figure 5.5.

The wave heading is for the main analyses set to 0 degrees, but will be varied in a wave direction study, where the heading direction is defined according to Figure 2.5.

Significant wave height [m]	Spectral peak period [s]																			
	3	4	5	6	7	8	9	10	11	12	13	14	15	16	17	18	19	21	22	SUM
1	59	403	1061	1569	1634	1362	982	643	395	232	132	74	41	22	12	7	4	2	2	8636
2	9	212	1233	3223	5106	5814	5284	4102	2846	1821	1098	634	355	194	105	56	30	16	17	32155
3	0	8	146	831	2295	3896	4707	4456	3531	2452	1543	901	497	263	135	67	33	16	15	25792
4	0	0	6	85	481	1371	2406	2960	2796	2163	1437	849	458	231	110	50	22	10	7	15442
5	0	0	0	4	57	315	898	1564	1879	1696	1228	748	398	191	84	35	13	5	3	9118
6	0	0	0	0	3	39	207	571	950	1069	885	575	309	142	58	21	7	2	1	4839
7	0	0	0	0	0	2	27	136	347	528	533	387	217	98	37	12	4	1	0	2329
8	0	0	0	0	0	0	2	20	88	197	261	226	138	64	23	7	2			1028
9	0	0	0	0	0	0	0	2	15	54	101	111	78	39	14	4	1			419
10	0	0	0	0	0	0	0	0	2	11	30	45	39	22	8	2	1			160
11	0	0	0	0	0	0	0		0	2	7	15	16	11	5	1				57
12	0	0	0	0	0	0	0			0	1	4	6	5	2	1				19
13	0	0	0	0	0	0	0				0	1	2	2	1	0				6
14	0	0	0	0	0	0	0					0	0	1	0	0				1
15	0	0	0	0	0	0	0					0	0	0		0				0
SUM	68	623	2446	5712	9576	12799	14513	14454	12849	10225	7256	4570	2554	1285	594	263	117	52	45	100001

Figure 5.5: Scatter diagram for northern North Sea [11]

Vessel motion

The movement of the cable is mainly determined by the properties of the cable laying vessel. The main purpose of modelling the CLV is to implement realistic motions of the cable due to the presence of the vessel. The vessel is built up of stiff beam elements, using PIPE31. The vessel's response to a sea state is described by RAOs for the six degrees of freedom; surge, yaw, heave, roll, pitch and sway. The RAOs describe how the vessel move because of wave excitation of a certain wave frequency. An example of the outlook of RAOs for the modelled CLV in surge and heave is presented in Figure 5.6. The RAOs are from an existing CLV, which due to confidentiality cannot be named.
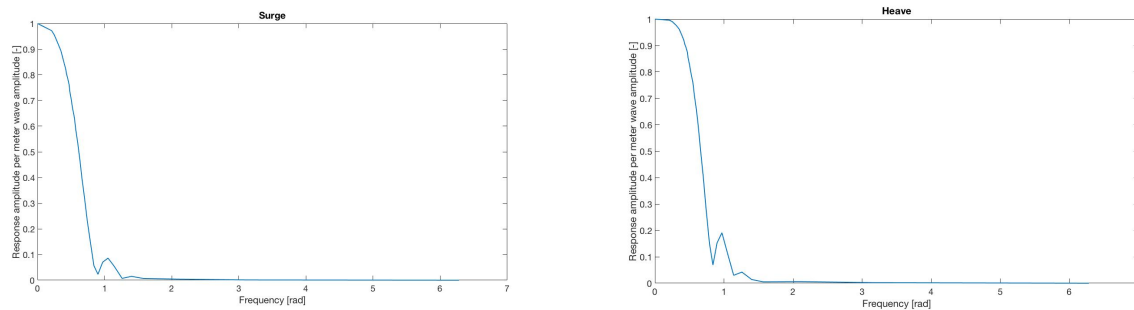
(a) Surge motion

(b) Heave motion

Figure 5.6: RAO properties

5.2.6 Current

To isolate the effect of the sea state, the main analyses are carried out with only wave loading and associated vessel motions. One of the parametric studies presented later will contain additional current loading to investigate the effect of this.

The current velocity profile is then assumed to be as in Figure 5.7. The current velocity is assumed to be constant until a water depth of 50 meters, where it linearly decreases until the sea bottom. A current velocity of 0.4 m/s is chosen. Since this is an operational analysis, there is no need for carrying out analyses with extreme state conditions. The same heading definitions as for waves applies, see Figure 2.5.
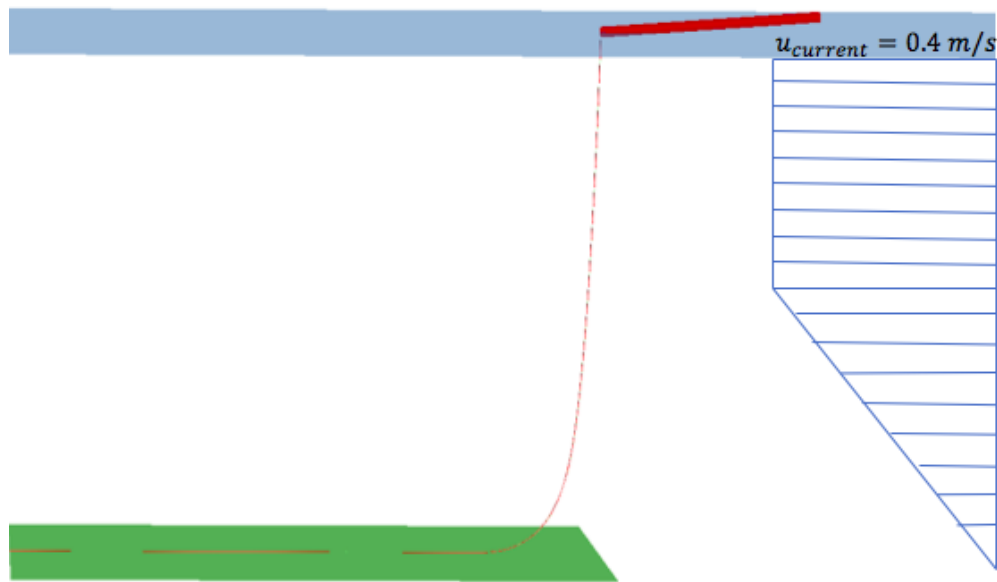
Figure 5.7: Current profile

5.2.7 Soil properties

The soil in the northern North Sea is generally compact. The upper layers usually consist of stratified dense sands and hard clays, followed by further overconsilated clays, silts and sands [26]. Table 5.8 presents soil stiffness and friction coefficient for cables in contact with the seabed, as presented by DNV[2].

The soil properties are defined by the CONTACT material model. This model allows for user-defined friction coefficients in different directions. The soil resistance is defined in three directions; vertically, lateral and axially. In the static analysis, since no memory effects can be included, the seabed must be modelled linearly in all directions, with exception of the axial friction which is zero. The dynamic analysis uses the RESTART function to correct

Table 5.8: Typical soil stiffness and friction coefficient [2]

Seabed type	Direction	Stiffness	Friction coefficient
	Axial	50 to 100	0.2
Clay	Lateral	20 to 40	0.2 to 0.4
	Vertical	100 to 5,000	-
	Axial	100 to 200	0.6
Sand	Lateral	50 to 100	0.8
	Vertical	200 to 10,000	-

for physical dynamic effects. The seabed is now modelled using nonlinear springs, and the transverse and axial soil resistance is modelled as bi-linear functions as illustrated in Figure 5.8(a) and (b). The vertical soil friction is still represented by a linear function, see Figure 5.8(c). For the soil resistance in vertical direction the HYCURVE material model is implemented, while EPCURVE is used to describe the soil resistance in lateral and axial directions.

The Coulomb friction coefficients chosen, in agreement with supervise, to represent the soil conditions in the northern North Sea are

$$\mu_x = 0.4$$
$$\mu_y = 0.7$$
$$\mu_z = 1.0$$
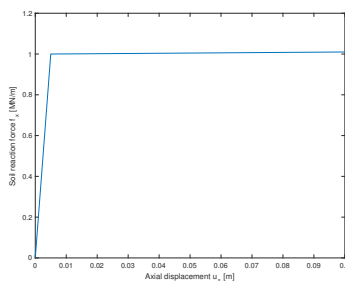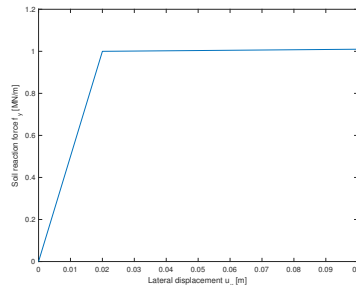
(a) Axial resistance   (b) Lateral restistance   (c) Vertical resistance
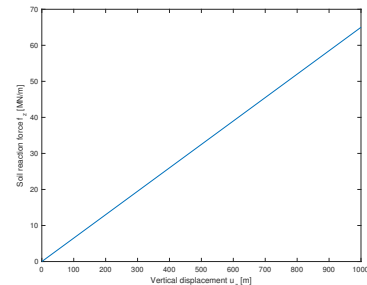
Figure 5.8: Soil resistance components

Chapter 6

Presentation and Discussion of Results

This chapter presents and discusses the main findings obtained when investigating the effect of torsion instability in relation with cable installation. The results are obtained by following the design procedure proposed by Sævik in [29]. The first part of the chapter presents the capacity parameters with respect to curvature and torsion moment, while the latter presents the results from the dynamic analyses. The files used to obtain the results in this chapter are attached in a .zip-file.

6.1   Static results

6.1.1   Cross-section friction moment

The non-linear material behavior of an umbilical is mainly described by the moment-curvature relation. Based on the analytic expressions presented in Section 2.6.1, the moment-curvature relation of the cross-sections were established, capturing the non-linear slip behavior of the cables. Figure 6.1 shows the relations for umbilical 1 and 2 respectively, while Table 6.1 summarizes the main results.

(a) Umbilical 1   (b) Umbilical 2
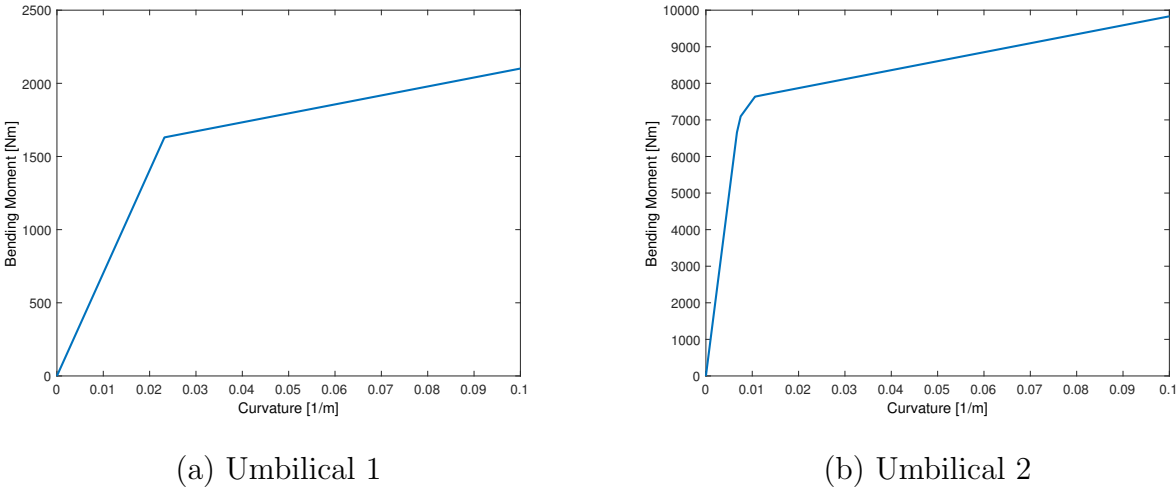
Figure 6.1: Moment curvature relations for both cross-sections

Since umbilical 1 only consists of one helical layer, the moment-curvature curve will only contain one slip curvature. For umbilical 2 both armouring layers as well as the helical tube layers and centre core tube will slip before the cable experience full slip. The bending stiffness decreases as each layer slips. As apparent from the figure the friction moment for umbilical 1 is much lower than for umbilical 2, which is due to a generally lower bending stiffness for both the elastic and the plastic contributions.

Table 6.1: Flexural properties of the umbilical cross-sections

	Parameter	Unit	Value
Umbilical 1	Slip curvature	[1/m]	0.0232
	Friction moment	[Nm]	217.69
	Elastic bending stiffness	$[Nm^2]$	$5.1261 * 10^3$
	Plastic bending stiffness	$[Nm^2]$	$4.245 * 10^3$
Umbilical 2	Slip curvatures	[1/m]	
	- armour 1		0.0067
	- armour 2		0.0075
	- helical layer		0.0107
	- center core		0.0128
	Friction moment	[Nm]	1770
	Elastic bending stiffness	$[Nm^2]$	$1.0573 * 10^3$
	Plastic bending stiffness	$[Nm^2]$	
	- armour 1		$4.47 * 10^5$
	- armour 2		$3.73 * 10^5$
	- helical layer		$1.4825 * 10^5$
	- center core		$1.24 * 10^3$

Effect of layer friction coefficient

For the main analyses, the mean value of the friction coefficient, $\mu = 0.2$ is utilized. At the same time friction coefficients in the range 0.1 - 0.3 are realistic. Hence a study regarding the effect of the layer friction coefficient on the torsion capacity is carried out. The upper and lower bounds of the friction moment are calculated, and the associated moment-curvature relations are established.

Figure 6.2 illustrates how the moment-curvature relation depends on the layer friction coefficient for both cross-sections. The friction coefficient affects mainly the value of critical slip curvature for the cable layers, which increases with increasing friction coefficient. An increase in the friction moment follows an increase in the slip curvatures. The bending stiffness is independent of the friction coefficient. Table 6.2 presents the slip curvatures and friction moment for the bounds of the friction moment. Since the slip curvatures and friction moments make up the moment-curvature relation describing the cable capacity in bending,

one can imagine that this will affect how the cable behaves in torsion. This effect will be investigated further on by evaluating the torsion moment and curvature associated with loop formation.

(a) Umbilical 1   (b) Umbilical 2
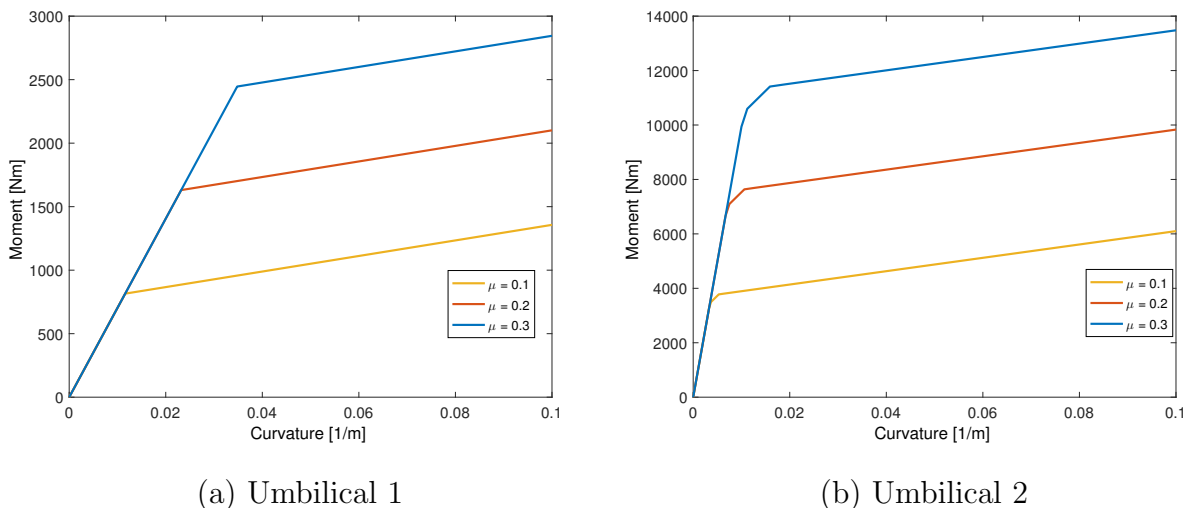
Figure 6.2: Upper and lower bounds for moment curvature relation

Table 6.2: Flexural properties of the umbilical cross-sections with varying friction coefficient

	Parameter	Unit	$\mu = 0.1$	$\mu = 0.2$	$\mu = 0.3$
Umbilical 1	Slip curvature	[1/m]	0.0116	0.0232	0.0348
	Friction moment	[Nm]	0.9574	1.7016	2.4458
Umbilical 2	Slip curvatures	[1/m]			
	- armour 1		0.0034	0.0067	0.0101
	- armour 2		0.0038	0.0067	0.0113
	- helical layer		0.0053	0.0107	0.0160
	- center core		0.0064	0.0128	0.0192
	Friction moment	[Nm]	3334.5	6659.0	9994

6.1.2 Critical torsion moment associated with kink formation

The inherent torque of the cable is found by gradually applying prescribed axial rotation θ_x at the vessel connection node of the cable, and monitoring the torsion moment. By keeping the two orthogonal directions to the applied axial rotation fixed, the torsion moment is conservative [14]. Figure 6.3 shows the torsion moment as a function of the imposed rotation for umbilical 1 and 2 respectively with a non-linear material model. In Appendix E.1 similar plots are found for analyses with a linear material model. The peak value of the torsion moment distribution corresponds to the critical torsion moment for the load case. Torsion buckling is said to occur when the peak value is surpassed. The shape of the cable then

forms into a loop when loading the cable further beyond this point. In the process torsion strain energy is transformed into bending strain energy yielding the change in configuration. It should be noted that due to its low torsional stiffness, umbilical 1 requires much more imposed rotation to obtain loop formation than umbilical 2.

The Greenhill equation, presented in Equation (2.31) in Section 2.6.1, is an analytic estimate of the critical torsion moment yielding loop formation. The analytic critical torsion moment is calculated initially by using the horizontal bottom tension T_0 as the reference value. In addition, the axial force in two elements in the TDZ are excerpted from SIMLA to capture the effect of gradually increasing the imposed rotation.

(a) Umbilical 1   (b) Umbilical 2
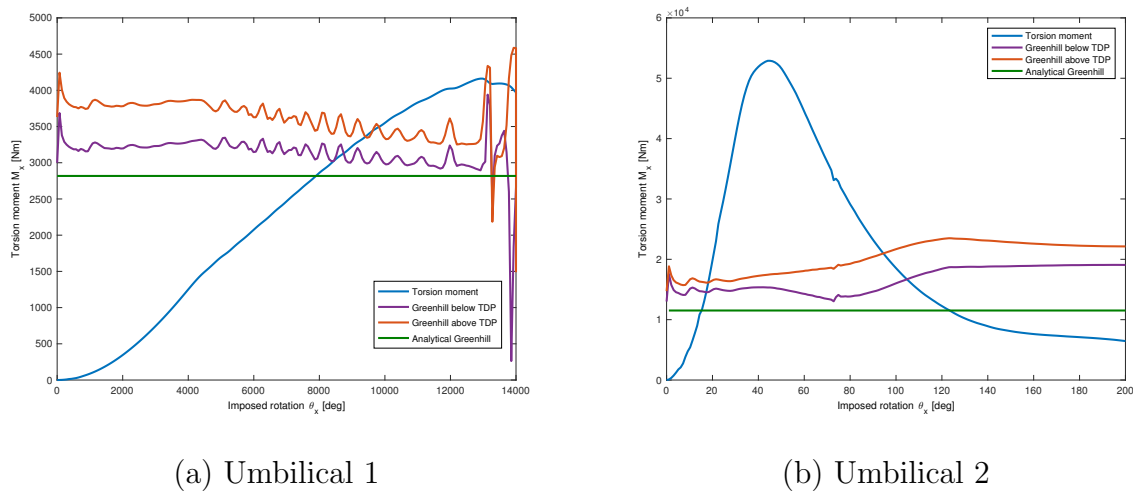
Figure 6.3: Critical torsion moment for both cross-sections from SIMLA, including analytical Greenhill estimates based on various bottom tensions.

Table 6.3 presents the values of both the results from the numerical and the analytic approaches at the load step of maximum torsion moment in SIMLA.

Table 6.3: Critical torsion moment for the cables with COMPIPE42

Method	Critical torsion moment [kNm]	
	Umbilical 1	Umbilical 2
SIMLA	4.16	52.89
Greenhill' equation, initial T_0	2.81	11.5
Greenhill, T_0 from elem. 300	2.47	17.66
Greenhill, T_0 from elem. 280	2.19	15.05

It can be seen from Figure 6.3 that the Greenhill estimates based on the initial horizontal bottom tension T_0 yield an underestimate of the critical torsion moment compared to the results from SIMLA. This is since the tensile force is not uniformly distributed along the cable length. Introducing the tension values excerpted from SIMLA into the Greenhill equation yields higher values of the critical torsion moment, which is more in agreement with SIMLA. The difference between the analytical and numerical results are more significant for umbilical 2 than for umbilical 1. For umbilical 2 Greenhill estimates are of magnitude 20 kNm while the peak value is equal to 52 kNm. For umbilical 1 the numerical differences between the results are smaller. At the point of maximum torsion moment, the time varying Greenhill estimates coincide well with SIMLA. The time varying tensile force excerpted from SIMLA exhibits a snappy behaviour due to rapid changes in configuration. This is most likely due to the relation between the bending moment and torsion moment, which for umbilical 1 is very low due to its low torsional stiffness.

The differences between the numerical and analytical results might be explained with the fact that the Greenhill criterion is derived with the assumption of an elastic straight beam with infinite length. Hence the elastic bending stiffness is utilized in the equation, not considering the non-linear behavior of the cable. The validity for curved beams is not either well established [14], and due to coarse mesh, all elements can not necessarily be considered as straight beams. The coarse mesh can yield greater differences between the numerical and analytical results for umbilical 2 due to a sharper bend in the touch down zone. Hence the elements in the touch down zone experiences higher curvature, limiting the validity of the Greenhill criterion.

Effect of material model

For the scope of this thesis the effect of linear material model is investigated with respect to cable capacity, in addition to the realistically non-linear material behaviour. Hence a comparison of the torsion capacity for both material models is carried out. The development of torsion moment as a function of imposed rotation is given graphically in Figure 6.4, while Table 6.4 presents the extreme values of the graphs.

Table 6.4: Critical torsion moment with respect to PIPE31/COMPIPE42 elements

Cable no.	Umbilical 1		Umbilical 2	
	$M_{x,crit}$ [kNm]	θ_{crit} [°]	$M_{x,crit}$ [kNm]	θ_{crit} [°]
PIPE31	4.2880	8010	15.074	74.8
COMPIPE42	3.7022	12917	52.892	45.1

(a) Umbilical 1   (b) Umbilical 2
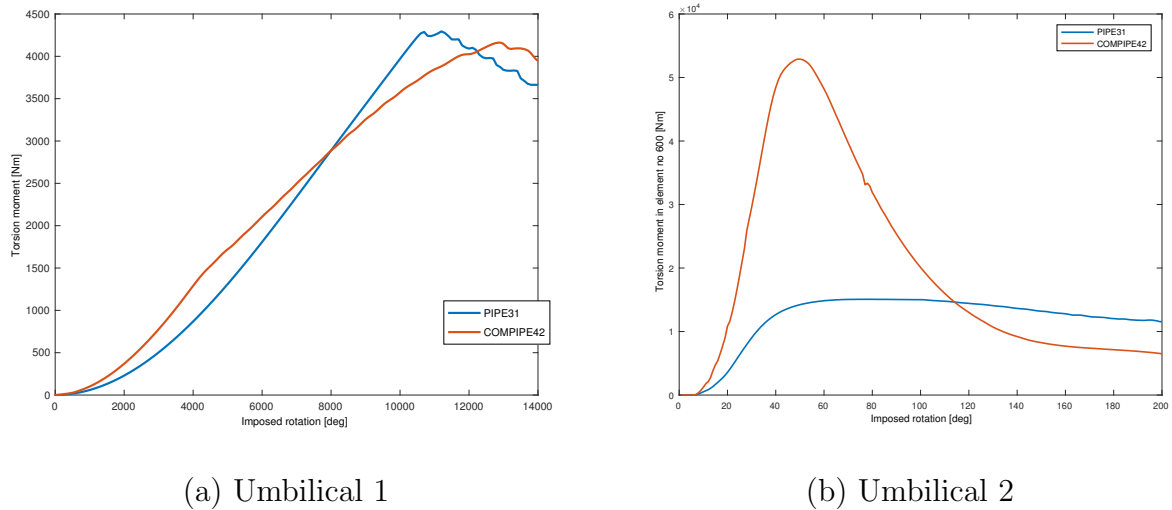
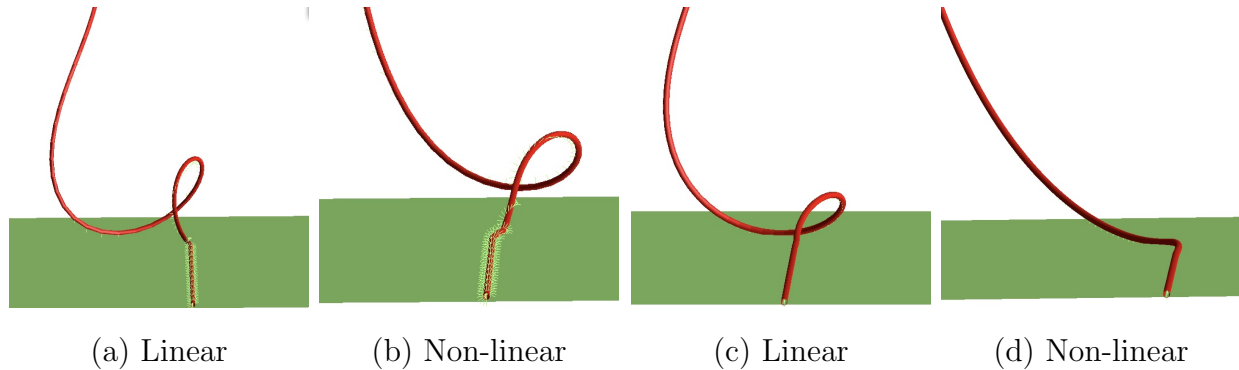**Figure 6.4:** Critical torsion moment for both cross-sections with PIPE31 and COMPIPE42

For umbilical 1, PIPE31 pipe elements yield a higher critical torsion moment than when utilizing COMPIPE42. The difference in the torsion moment for the two cases is of magnitude 0.5 kNm, hence a difference of 13.6 %. COMPIPE42 yield a higher capacity with respect to amount of imposed rotation necessary to reach critical torsion moment, compared to PIPE31. This is apparent from the value of imposed rotation at the point of maximum moment. One would expect that the non-linear properties yield a higher torsion moment, and the low relation between the bending and torsion moment might explain this behaviour for this cable. For umbilical 1 with its low torsional stiffness, the cable suffers from severe deformation at the point of critical torsion moment

For umbilical 2, application of COMPIPE42 elements yields a higher critical torsion moment than with PIPE31. A moment which is 72 % larger is obtained with COMPIPE42 compared with PIPE31. This indicates that an analysis with linear material properties underpredicts the torsion capacity of the cable. Due to the activated non-linear moment versus curvature relationship in COMPIPE42, the bending stiffness is reduced when the slip curvatures are overstepped. This effect is not accounted for in the linear model with PIPE31. After the initial configuration umbilical 2 experience torsion moments of magnitude 10^2, which yields curvature of the dimension 10^{-2} which exceeds the slip curvature. Hence umbilical 2 with COMPIPE42 operates with a lower bending stiffness than PIPE31, yielding higher resulting moments.

Figure 6.5 illustrates the differences in the deformation pattern for the cases of linear and non-linear material models for the two cross-sections. All cases except umbilical 2 with

68

COMPIPE42 experience loop formation at the point of critical torsion moment. Loop formation for non-linear umbilical 2 occurs at a loading level beyond the critical torsion moment. Hence umbilical 2 has yet to reach critical deformation levels at the point of maximum critical torsion moment, while the other cases indicate severe deformation at the same point.

| (a) Linear | (b) Non-linear | (c) Linear | (d) Non-linear |

Figure 6.5: Deformation patterns at point of critical torsion moment

Effect of friction moment

The effect of layer friction coefficient on the torsion capacity of the cable is investigated. This is carried out by analyzing the cross-sections with the cases of moment-curvature relations presented in section 6.1.1. The results obtained for umbilical 1 and 2 can be found in Figure 6.6. The critical torsion moment is found to be dependent on the cross-section friction moment, as is apparent in both the figure and in Table 6.5.

| (a) Umbilical 1 | (b) Umbilical 2 |
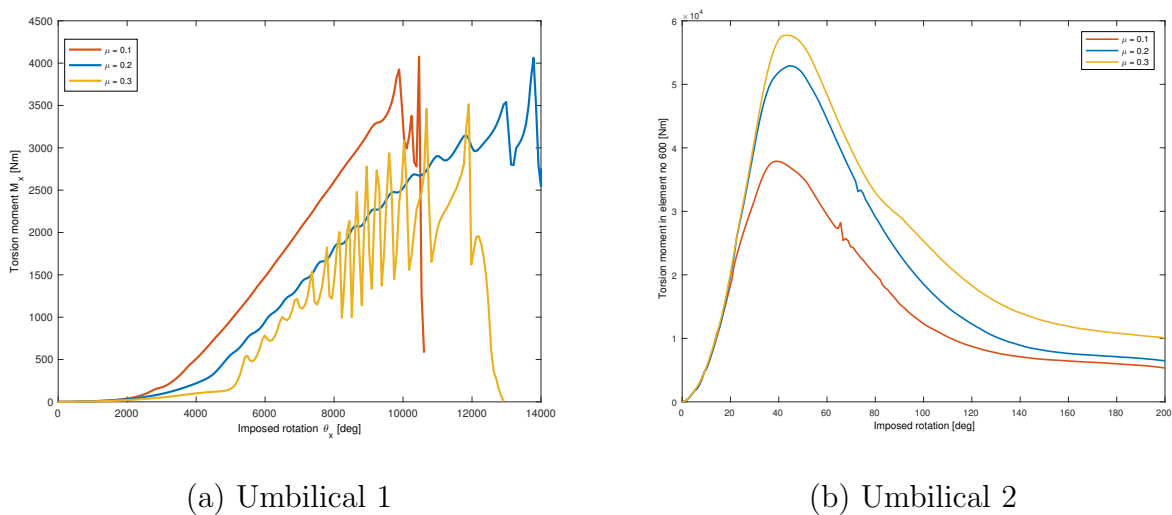
Figure 6.6: Torsion moment for both cross-sections with varying friction coefficient

As is apparent in Figure 6.6 (a) umbilical 1 is highly affected by the changes in friction moment. When applying the lowest friction layer factor, the highest torsion moment is obtained, followed by $\mu = 0.2$ and $\mu = 0.3$. For all cases a drastic drop in torsion moment is experienced when the cable forms into a loop. Both the cases of $\mu = 0.1$ and $\mu = 0.3$ experience torsion buckling at a lower level of imposed rotation than the mean value of the friction coefficient.

The upper bound of the friction moment yields the most interesting results. The cable experience severe deformation when the cable is rotated 8000 degrees, but the torsion moment continues to grow until its maximum is reached at approximately 12 000 degrees. Between these two points, the cable' torsion moment in shifting rapidly. This is due to promptly changes in the cable configuration where the cable coils and uncoils at each load step due to the extremely large imposed rotation. This has a large impact on the experienced curvature.

For umbilical 2 the opposite is apparent. An increase in the friction coefficient yields an increase in the critical torsion moment. The point of critical torsion moment appears at approximately same value of imposed rotation for all three cases, varying between $\theta_x = 43 - 45°$. Umbilical 2 lacks the typically drop in moment after the critical torsion moment is reached. This can be reasoned with the deformation pattern at the point of critical torsion moment, see Figure 6.7. The cable has yet to produce a loop, which occurs in the end of the analyzed period. Hence the capacity of the cable is not associated with a loop as for umbilical 1.

Table 6.5: Critical torsion moment with varying friction moment, umbilical 1 and 2

Friction coefficient	Umbilical 1		Umbilical 2	
	$M_{x,crit}$ [kNm]	θ_{crit} [°]	$M_{x,crit}$ [kNm]	θ_{crit} [°]
$\mu = 0.1$	4.711	10175	37.89	44.1
$\mu = 0.2$	4.16	12917	52.89	45.1
$\mu = 0.3$	3.71	13206	57.72	43.1

Figure 6.7 show how the cable deforms for the different cases of friction coefficients for umbilical 1 and 2. It is apparent from the figures that the non-linear deformation patterns for the two umbilical are very different. The low torsion stiffness of umbilical 1 allows it deform into a more loop shaped configuration at point of critical torsion moment, while the deformation for umbilical 2 is more of a slight bend in the configuration than a loop. It should be commented that the deformation that umbilical 1 experiences is at a imposed rotation of between 10000-13000 degrees, which is highly unrealistic. Hence torsion moments in the range of the critical value is not expected to occur.

| (a) $\mu = 0.1$ | (b) $\mu = 0.2$ | (c) $\mu = 0.3$ | (a) $\mu = 0.1$ | (b) $\mu = 0.2$ | (c) $\mu = 0.3$ |

Umbilical 1   **Umbilical 2**
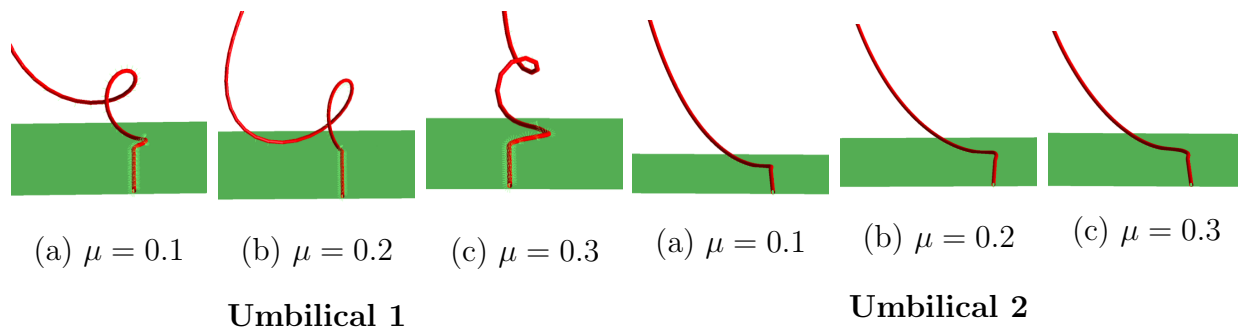
Figure 6.7: The dependency of deformation patterns on cross-section friction moment

6.1.3   Critical curvature associated with kink formation

The resultant curvature in the cable at the point of critical torsion moment is a possible indicator of loop formation. The resultant curvature in a cable element is defined as

$$\kappa_t = \sqrt{\kappa_y^2 + \kappa_z^2} \tag{6.1}$$

where κ_y and κ_z are the curvature components in y- and z-direction respectively. The region which experiences the maximum resultant curvature is the TDZ. Graphs presenting the variation of the maximum resultant curvature as a function of element coordinate and imposed rotation can be found in Appendix E.2.

In his thesis, Koloshkin connected the resultant curvature in the system to the torsion moment by plotting the maximum curvature of each time step against the moment utilization $M_x/M_{x,crit}$, where $M_{x,crit}$ is the critical torsion moment found in Section 6.1.2. The same process is performed for the results obtained in this thesis. Figure 6.8 illustrate the relation between maximum total curvature and moment utilization, for both material models. The figures also include the API determined minimum radius of curvature, to compare how the obtained results correlate with the industry standards. Table 6.6 summarizes the main findings related to critical curvature.

Table 6.6: Critical curvature for umbilical 1 and 2 with linear and non-linear material models

	Umbilical 1		Umbilical 2	
	PIPE31	COMPIPE42	PIPE31	COMPIPE42
SIMLA	1.3084	0.9009	0.2784	0.0731

(a) Umbilical 1   (b) Umbilical 1
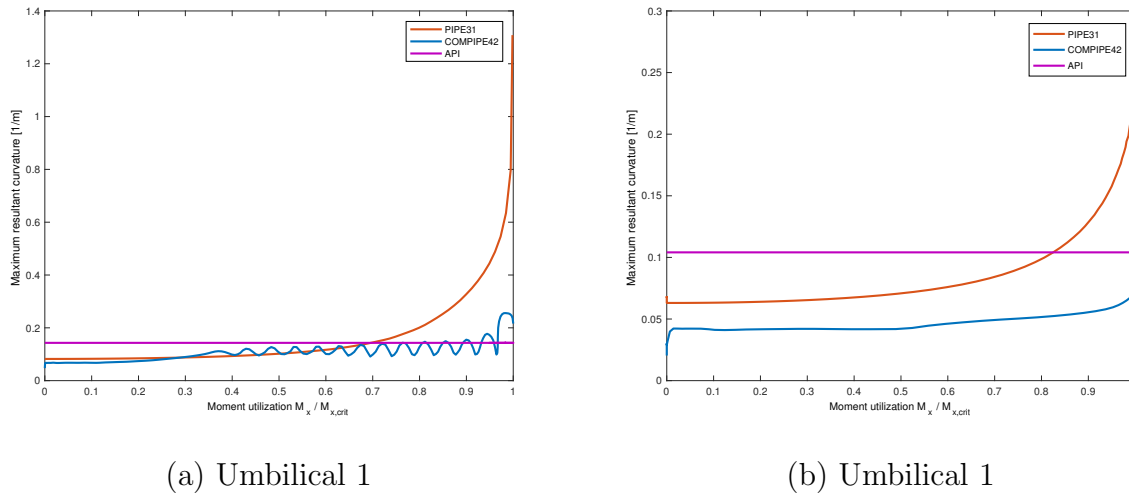
Figure 6.8: Resultant curvature versus moment utilization, PIPE31/COMPIPE42

Both the linear and non-linear cases are analyzed with respect to critical curvature. For umbilical 1 with PIPE31 elements the curvature smoothly increases when increasing the imposed rotation. The API minimum radius of curvature is exceeded at moment utilization of 70 % critical torsion moment. The deformation at this point is determined as acceptable. Implementation of non-linear material behavior exhibits a maximum resultant curvature lower than with PIPE31, and which exceeds the API criterion at a value of 77 %. The resultant curvature starts to oscillate with a gradually increasing amplitude after approximately 37 % moment utilization. This is due to rapid changes in the configuration, where the cable fluctuates to each side of the cable center line. As Figure 6.5 (b) illustrates, the deformation of the cable at the point of critical torsion moment is apparent, with clear loop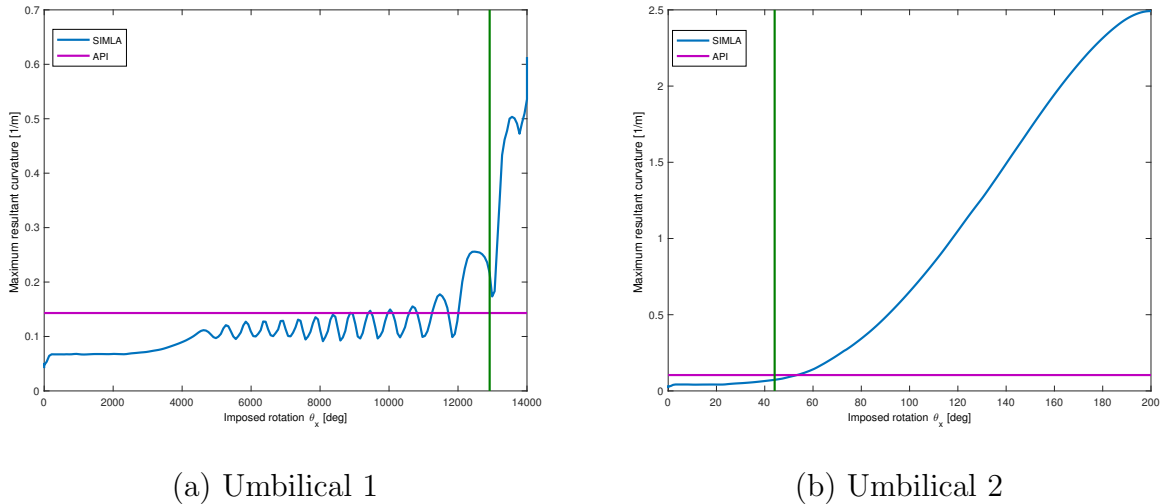 formation. Plotting the resultant curvature as a function of imposed rotation yields Figure 6.9 (a). The figure illustrates how the maximum resultant curvature increases rapidly after the peak of torsion moment is reached. The point of critical torsion moment is illustrated by the green line.

For umbilical 2, linear material properties yield a resultant curvature of 0.27 1/m at the point of the critical torsion moment. Hence the API criterion is surpassed at a moment utilization of 82 %. The maximum resultant curvature obtained with non-linear material properties is below the API criterion for the whole range of moment utilization. As Figure 6.9 (b) illustrates the curvature continues to increase almost exponentially after the critical torsion moment is surpassed, and the magnitude of the curvature exceeds the API criterion at a time step slightly after the critical rotation level. Even though the curvature for the non-linear case is below API, XPOST indicates that the configuration has not shifted into

a loop but only experiences a bend in the touch down zone. A critical cable configuration is yet not reached. This indicates that the curvature at full moment utilization is a difficult measure when desiring to predict loop formation for umbilical 2.

(a) Umbilical 1   (b) Umbilical 2

Figure 6.9: Resultant curvature as a function of imposed rotation

Both graphs in Figure 6.9 illustrates that the moment utilization does not function well as a measure of loop formation. The cable has not necessarily reached a configuration corresponding to anything resembling a loop, as is the case for umbilical 2, and the drastic changes in configuration occur at rotation levels beyond the one associated with critical torsion moment. For umbilical 1 the cable experiences critical deformation before the maximum moment is reached, and thus limiting the validity of the critical torsion moment as a loop formation measure. It is also apparent from the figures that the API functions better as a safe operation limit than the resultant curvature at the point of critical torsion moment. This is because the curvature is highly dependent on deformation pattern and cross-section properties.

Effect of nonlinear friction moment
As proven earlier, changing the friction layer coefficient impacts the critical torsion moment in various degree for the two cables. The development of the maximum resultant curvature for umbilical 1 and 2 as a function of the moment utilization is presented in Figure 6.10, while Table 6.7 presents the numerical extremes of the figures.

Table 6.7: Critical resultant curvature with varying friction coefficients

| Friction coefficient	Maximum total curvature [1/m]	
	Umbilical 1	Umbilical 2
$\mu = 0.1$	2.5740	0.0966
$\mu = 0.2$	0.2162	0.0731
$\mu = 0.3$	1.7351	0.1307
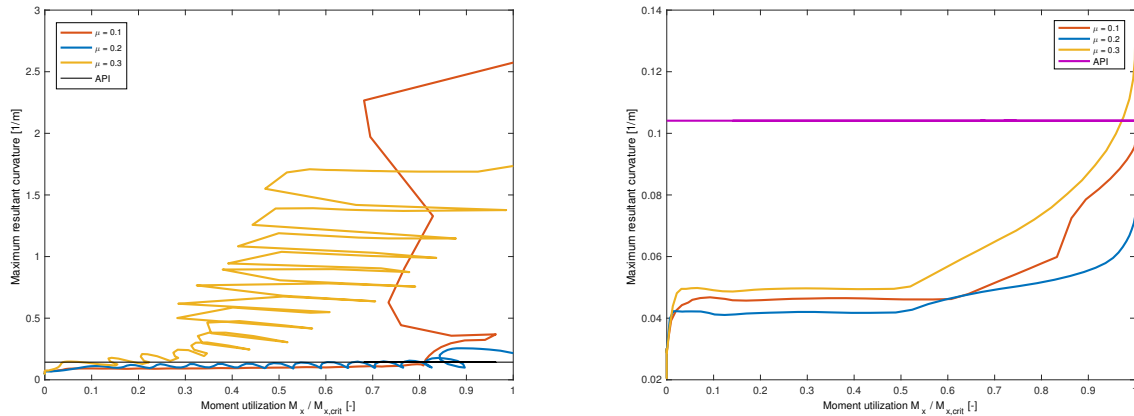
Figure 6.10: Maximum total curvature as a function of moment utilization, umbilical 2

The resultant curvature and torsion moments are closely connected. For umbilical 1 varying the non-linear friction moment impacts the torsion moment and resultant curvature greatly. The highest value of curvature at the point of maximum moment utilization is obtained with $\mu = 0.1$, while $\mu = 0.3$ follows close behind. The critical curvature for $\mu = 0.2$ is barely above the API criterion. The differences in the curvature values at point of full moment utilization can be explained in the different ways the cable deforms, as seen from Figure 6.7. For $\mu = 0.3$ it is observed that the torsion moment shifts rapidly in values, due to coiling and uncoiling of the cable in subsequent load steps. Due to this, the same curvature values are obtained at different values of the moment utilization. This is the reason for the "horizontal" oscillation of the curvature. The API criterion for this case is exceeded at a very low value of the moment utilization, at approximately 15 %. This correlates with the deformation visualized in XPOST, where its visible that the cable deforms critically right after exceeding the curvature criterion. This indicates that the critical capacity of the cable is reached long before the cable experiences its maximum value of torsion moment. This illustrates once again that utilizing critical torsion moment and resultant curvature as indicators of loop formation complicates things, as the cable might fail before these critical parameters are reached.

For umbilical 2 all nonlinear cases with various friction coefficient exhibits curvatures which are below the API criterion when maximum torsion moment is reached. At the point of critical torsion moment and thus critical curvature for these load cases, the cable has not formed a loop. Once again the measure of moment utilization leaves out the main characteristics of the curvature behavior, which takes place after the critical torsion moment value is reached. Figure 6.11 (b) shows that the resultant curvature increases drastically after the critical torsion moment is reached at $\theta_x = 44deg$, where the lowest friction moment yields the highest value of the curvature in the end.

(a) Umbilical 1   (b) Umbilical 2
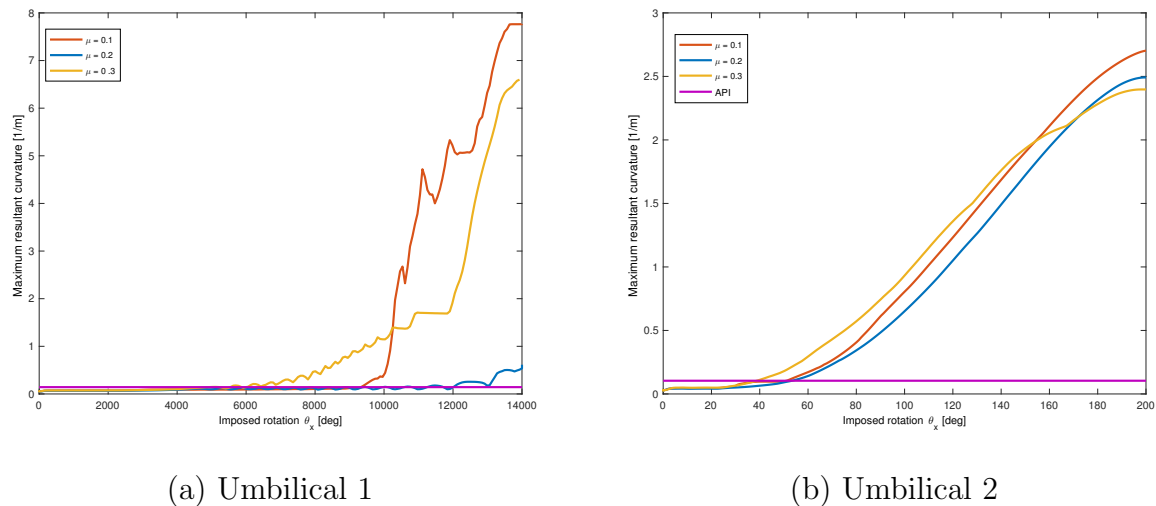
Figure 6.11: Resultant curvature as a function of imposed rotation

6.2 Dynamic results

The dynamic analyses are performed using a built-in torque level along with the established non-linear moment curvature model. The dynamic analyses include dynamic wave loading and induced vessel motions. Installations will seldom be carried out in severe sea states, thus it is assumed that installations will not be performed in conditions with a H_s above 3 meters. Based on this assumption, the most probable sea states from the scatter diagram valid for the northern North Sea, see Figure 5.5, are chosen. Table 6.8 presents the chosen sea states which will be simulated in the dynamic analyses.

Table 6.8: Sea states for dynamic analyses

Significant wave height [m]	Spectral peak period [s]			
2	7	8	9	10
3	-	-	9	10

The main goal with these analyses is to determine whether the given sea states are acceptable for umbilical 1 and 2. The dynamic maximum curvature at the TDP will be used as a measure of kink formation. It is desirable to prove that kink formations are not developed due to accumulated plastic deformations by utilizing a sufficient number of cycles.

6.2.1 Evaluation of installation route

Two different installation scenarios will be implemented in the dynamic analyses and investigated; an end cap turn and the case of curved routing. The installation scenarios are simulated by applying a torsion level corresponding to the moment induced by the route. Table 6.9 shows the torsion levels of each installation scenario along with the moment utilization with respect to torsion capacity.

Table 6.9: Torsion levels corresponding to the load cases

Load case	Cross-section no.	Torsion moment	Moment utilization
Curved routing	Umbilical 1	0.0092 kNm	0.25 %
	Umbilical 2	14.19 kNm	26.84 %
End cap turn	Umbilical 1	0.050 kNm	1.42 %
	Umbilical 2	1520.71 kNm	1504 %

The torsion moment for umbilical 2 corresponding to an end cap turn will be of magnitude 1520 kNm. This moment is much larger than the critical torsion moment of 52.9 kNm. Thus, applying this moment to the model will definitively induce deformation which is not viable for the cable. Hence this scenario is defined as unfeasible for a cross-section with these properties at this water depth. The torsion moment for a curved routing scenario is below the critical value of the torsion moment, and hence is defined as feasible.

For umbilical 1 the imposed torsion moments resulting from an end cap turn is lower than the critical torsion moment. The same holds for the case of curved routing. Hence the two installation scenarios are executable for umbilical 1.

6.2.2 Critical torsion moment and curvature capacity

The following subsections present the torsion moments and total curvature which the cables experience during the simulated sea states for each installation scenario. These results will be compared with the critical values presented earlier in this chapter to define the feasibility of carrying out the operation in each sea state. A sea state will be defined as acceptable if a stable value of the maximum curvature is obtained without kink formation and the standard maximum curvature design criteria is not exceeded.

Umbilical 1 - End Cap Turn

In Figure 6.12 the distribution of the torsion moment as a function of time for the various sea states can be found in (a), while (b) presents the variation in maximum resultant curvature for the same time period. Table 6.10 presents the numerical values of the mean and maximum values of the torsion moment and the resultant curvature.

(a) Torsion moment

(b) Resultant curvature
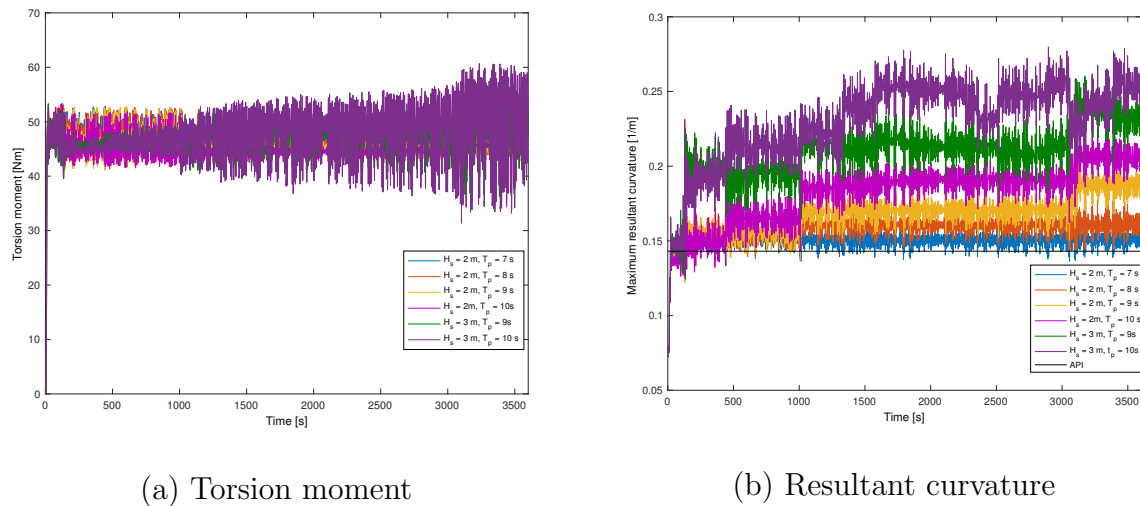
Figure 6.12: Dynamic torsion moment and curvature, umbilical 1 - end cap turn

It is observed that the torsion moment oscillates around a mean of approximately 50 Nm for all sea states. From Figure 6.12 (b) it is seen that the maximum resultant curvatures exceeds the API criterion at an early stage in the analyses. The mean maximum curvature for a certain significant wave height is increasing in magnitude with increasing peak period, while increasing the significant wave height also indicates an increase in curvature magnitudes. As the API criterion is exceeded after such a short duration, it might indicate that the horizontal bottom tension in the cable is too low initially. The bottom tension applied is the lowest possible with respect to criterion for minimum radius of curvature, and must potentially be increased. With respect to fulfillment of the dynamic curvature criterion, none of the sea states can be defined as feasible for an end cap turn.

Table 6.10: Dynamic torsion moment and resultant curvature, umbilical 1 - end cap turn

$\mathbf{H_s}$ [m]	$\mathbf{T_p}$ [s]	Torsion moment [kNm]		Resultant curvature [1/m]	
		Mean	Max	Mean	Max
2	7	47.72	53.12	0.1503	0.1717
2	8	46.49	53.40	0.1585	0.1854
2	9	45.82	53.2	0.1683	0.2103
2	10	45.36	53.26	0.1828	0.2310
3	9	47.47	57.99	0.2094	0.2629
3	10	48.07	60.68	0.2303	0.2798

Umbilical 1 - Curved routing

For the curved routing installation scenario, the resulting torsion moment and curvature is presented graphically in Figure 6.13 (a) and (b), while Table 6.11 shows the mean and maximum value for each sea state.

(a) Torsion moment   (b) Resultant curvature
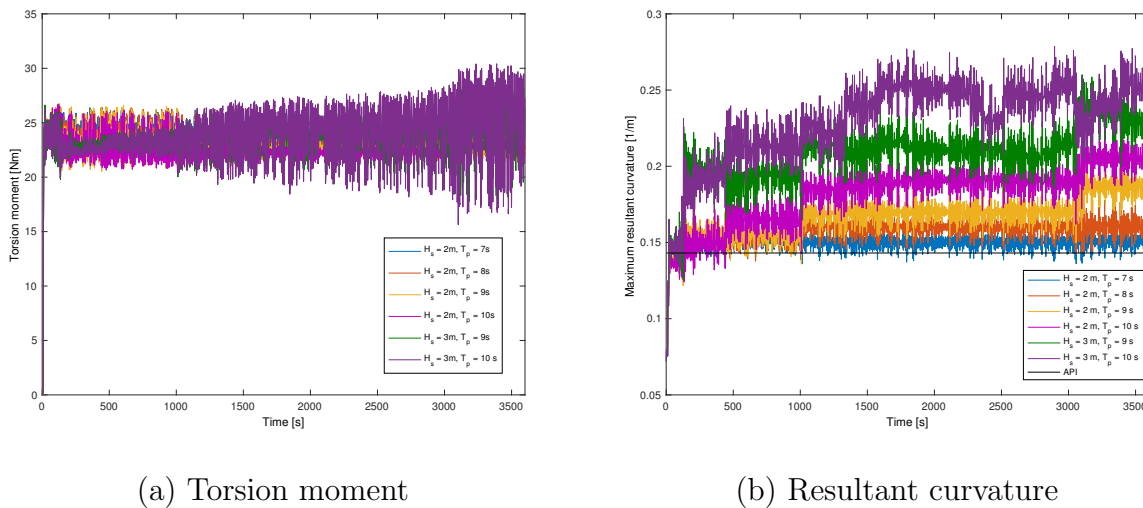
Figure 6.13: Dynamic results umbilical 1 - curved route

The maximum resultant curvature in the cable during the simulation time is presented in Figure 6.13 (b). It is easily observed that the maximum resultant curvature for all sea states exceed the API criterion in an initial state of the analyses, as was the case for an end cap turn. This can once again indicate that the applied bottom tension initially is too low for the operation to be executable. XPOST shows that the cable is experiencing deformations which should be categorized as non-acceptable. Neither of the sea states can be defined as acceptable with respect to the dynamic curvature criterion.

Table 6.11: Dynamic torsion moment and resultant curvature, umbilical 1 - curved routing

H_s [m]	T_p [s]	Torsion moment [kNm]		Resultant curvature [1/m]	
		Mean	Max	Mean	Max
2	7	23.86	26.67	0.1498	0.1712
2	8	23.25	26.75	0.1580	0.1852
2	9	22.93	26.61	0.1676	0.2097
2	10	22.70	26.53	0.1825	0.2302
3	9	23.74	29.09	0.2079	0.2611
3	10	24.04	30.41	0.2296	0.2785

Umbilical 2 - Curved routing

Figure 6.14 (a) illustrates the variations in torsion moment for the various sea states. As is seen from the figure, the torsion moments for the simulations with equal significant wave height oscillate around approximately the same mean value. It is also observed that increasing the wave height from 2 m to 3 m induces a decrease in the mean value of the torsion moment. Still the values for all analyses are far away from the critical torsion moment of 52.89 kNm. Hence with respect to torsion moment this gives no indication of loop formation.

(a) Torsion moment

(b) Resultant curvature
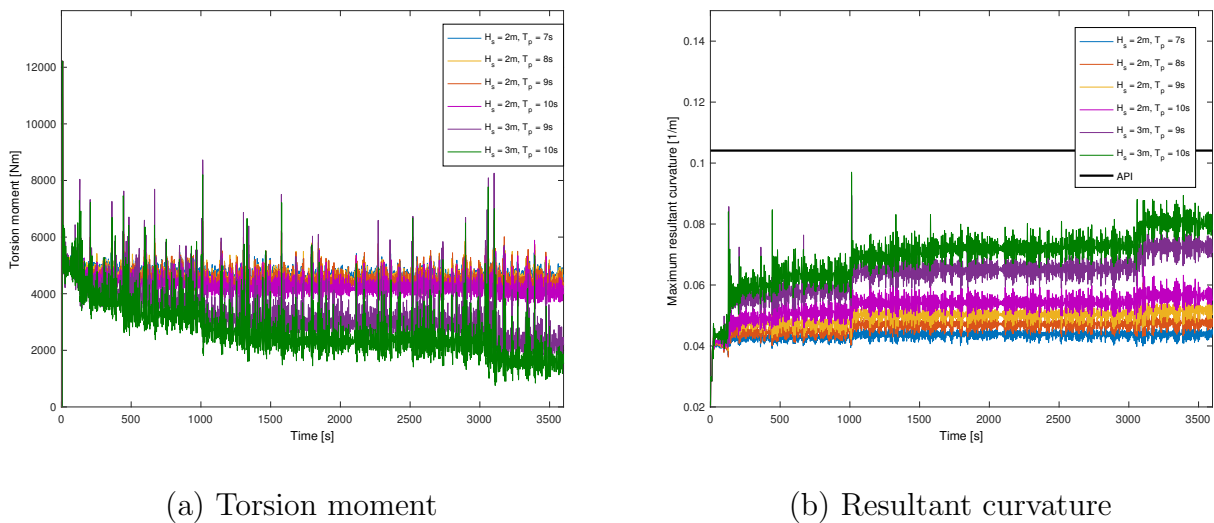
Figure 6.14: Dynamic results umbilical 2 - curved route

Figure 6.14 (b) illustrates the distribution of the maximum total curvature as a function of time. The curvature in the cable steadily increases until it oscillates around a constant mean value. The mean values, along with the maximum values obtained of curvature, are presented in Table 6.12. The magnitude of the maximum resultant curvature for all sea state is found to be lower than the dynamic curvature criterion. The resultant curvature is

found to be dependent on both the spectral period and significant wave height. An increase of either parameter yield an increase in the resultant curvature, where the significant wave height is found be yield largest variations. The magnitudes of the resultant curvature have such a good margin with respect to the dynamic API criterion that all sea states are defined as acceptable.

Table 6.12: Dynamic torsion moment and resultant curvature, umbilical 2 - curved routing

H_s [m]	T_p [s]	Torsion moment [kNm]		Resultant curvature [1/m]	
		Mean	Max	Mean	Max
2	7	1.3642	2.380	0.0436	0.0483
2	8	1.5872	3.1656	0.0465	0.0557
2	9	1.7541	3.8961	0.0496	0.0607
2	10	1.7576	4.0080	0.0531	0.0669
3	9	1.8651	7.3003	0.0637	0.0894
3	10	2.7226	12.216	0.0696	0.0970

For all sea states for the three cases presented it is observed that the resultant curvature values have not reached steady state. One might expect that if a simulation duration of 3 hours had been carried out, this state would have been reached. It might hence occur that even higher magnitudes of the curvature are experienced.

6.2.3 Compression in the touch down zone

Even though the dynamic curvature criterion is fulfilled for a cable, current practice defines an operation as unfeasible if compression in the TDZ occurs. This is since axial compression is known to trigger local buckling. Hence to investigate whether an eventual compressive force will be critical for the cable, the design check includes a comparison with critical buckling loads for tensile armour buckling.

As mentioned in Section 2.5.2, there exist two relevant failure modes for the tensile armour; radial and lateral buckling. Table 6.13 presents the calculated critical buckling loads for the two cable cross-sections for each failure mode. The occurrence of axial compression will be

Table 6.13: Buckling loads for tensile armour failure modes

	Failure mode	Buckling load [kN]
Umbilical 1	Radial failure	349
	Lateral failure load	3678
Umbilical 2	Radial failure	235
	Lateral failure load	2184

investigated for the same sea states as earlier. If axial compression is present the magnitude of the force will be compared with the analytical values presented in table 6.13 to check whether the compressive force indicates local buckling.
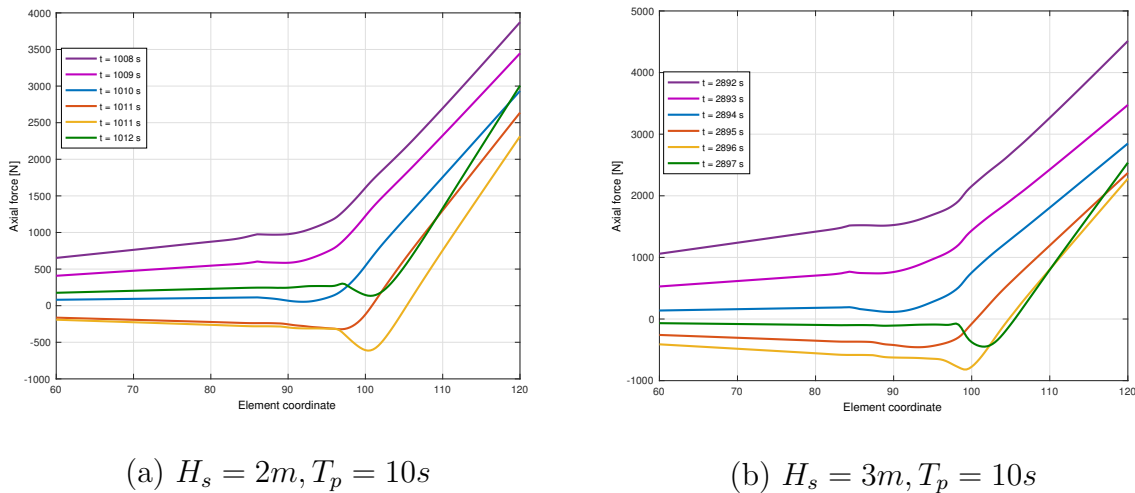
Umbilical 1 - End cap turn

For umbilical 1 installed with an end cap turn, it is found that each sea state analyzed experience axial compression of some extent in the TDZ. Table 6.14 presents the minimum and maximum tensile force experienced during the various sea states, while figure 6.15 presents the axial force distribution in the TDZ for the time steps around the obtained maximal compressive force.

Table 6.14: Axial force extremes for umbilical 1 - end cap turn

H_s [m]	T_p [s]	Compression	
		Min axial force [N]	Max axial force [N]
2	7	-234.33	16683
2	8	-430.79	17894
2	9	-543.85	16852
2	10	-613.98	16883
3	9	-1487.1	18294
3	10	- 1583.1	18178

The figure presents the axial force distribution for the sea states $H_s = 2m, T_p = 10s$ and $H_s = 3m, T_p = 10s$ which corresponds to the most severe sea states for the significant wave height analyzed. The results for the remaining sea states are presented in Appendix E.4. The magnitudes of the minimum axial force for the various sea states are all in a range away from the critical buckling loads inducing local armour buckling. The deformation which the umbilical experiences as a combination of the occurrence of compression and curvature levels is not acceptable.

(a) $H_s = 2m, T_p = 10s$ (b) $H_s = 3m, T_p = 10s$

Figure 6.15: Tensile force distribution in TDZ, umbilical 1 - end cap turn
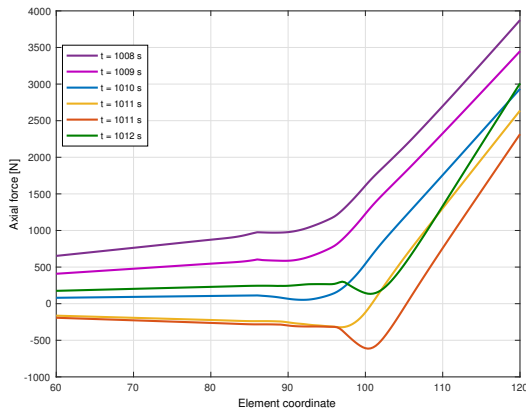
Umbilical 1 - Curved route

For the case of a curved route during installation of umbilical 1, the tensile force extremes are as presented in Table 6.15. In Figure 6.16 the variations in tensile force in the TDZ with a time range of 5 seconds are illustrated for the sea states $H_s = 2m, T_p = 10s$ and $H_s = 3m, T_p = 10s$. In Appendix B the axial force distribution for all sea states are presented.

Table 6.15: Axial force extremes for umbilical 1 - curved route

H_s [m]	T_p [s]	Compression	
		Min axial force [N]	Max axial force
2	7	-235.85	16686
2	8	-430.15	17898
2	9	-542.12	16854
2	10	-614.11	16885
3	9	-1480.7	18301
3	10	-1580.4	18177

It is observed a compressive axial force for all simulated sea states. The magnitudes of the compressive force are below the necessary loads to induce buckling, and hence the presence of compression in the touch down zone is not critical with respect to local buckling. Due to the high curvature values this cable experiences it's interesting to investigate whether the occurrence of compression is because the API criterion is not fulfilled, or only due to the presence of dynamic loading. Such an investigation will be presented in a later section.
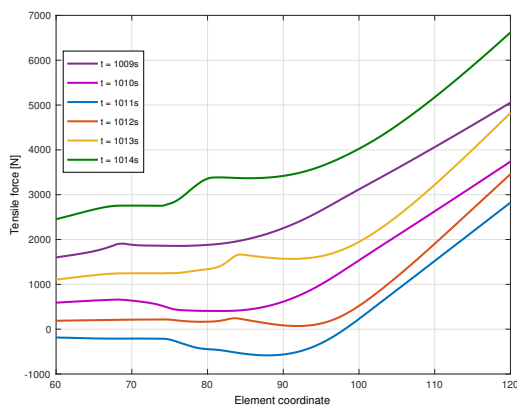
(a) $H_s = 2m, T_p = 10s$
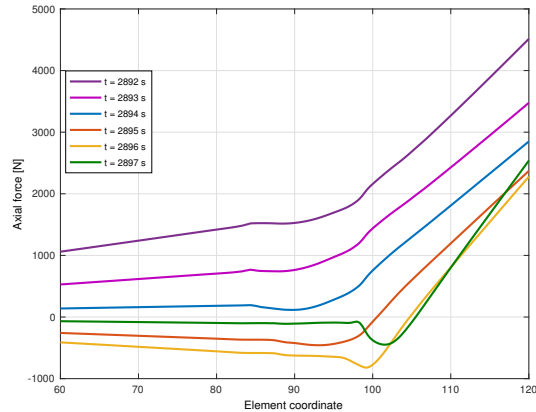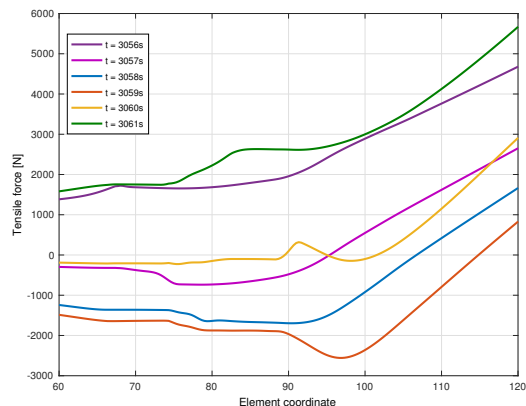
(b) $H_s = 3m, T_p = 10s$

Figure 6.16: Axial force distribution in TDZ for various sea states, umbilical 1 - curved routing

Umbilical 2 - Curved routing

Based on the dynamic analyses, occurrence of compression in the TDZ for umbilical 2 is investigated. Figure 6.17 illustrates that the axial force varies between positive and negative values for various time steps. For umbilical 2, all simulated sea states except $H_s = 2m, T_p = 7s$ experience compressive forces in the touch down zone. Table 6.16 presents the minimum and maximum value of the axial force for the various sea states. As seen from the table, the minimum axial force and the maximum compressive force increases with the severity of the sea state.

(a) $H_s = 2m, T_p = 10s$

(b) $H_s = 3m, T_p = 10s$

Figure 6.17: Axial force distribution in TDZ, umbilical 2 - curved routing

The compressive loads presented in Table 6.16 are compared with the buckling loads for

tensile armour failure in Table 6.13. The magnitudes of the compressive tensile force do not exceed the buckling loads. Thus, it is possible to conclude that the cable can experience compression in the TDZ without experiencing dramatic deformation or loop formation. Based on this, along with fulfillment of the API criterion, the sea states for umbilical 2 are all denoted as acceptable.

**Table 6.16:** Axial force extremes for umbilical 2

H_s [m]	T_p [s]	Compression	
		Min axial force [N]	**Max axial force**
2	7	2.51	19433
2	8	-196.50	19433
2	9	-476.68	19725
2	10	-584.12	19761
3	9	-2295.7	21651
3	10	-2557.6	21823

6.2.4   Effect of wave heading

The effect of wave heading is investigated by carrying out several analyses with constant significant wave height and peak period, while varying the heading. The definition of the wave heading is according to Figure 2.5. The analyses are carried out for the most severe sea state, with $H_s = 3m, T_p = 10s$. Results from the heading simulation are presented in Table 6.17, while the Figure 6.18 illustrates the development of the torsion moment and the maximum resultant curvature as a function of time for the various cases of wave heading with $H_s = 3m, T_p = 10s$.

Table 6.17: Results from simulation with various headings

| Wave Heading | Torsion moment [kNm] | | Maximum resultant curvature [1/m] | |
	Mean	Max	Mean	Max
0 deg	2.72	12.21	0.0695	0.0970
45 deg	3.52	14.12	0.0755	0.0960
90 deg	3.02	12.22	0.0568	0.0725
135 deg	3.32	12.58	0.0499	0.0641
180 deg	2.65	12.22	0.0651	0.085
225 deg	2.09	25.01	0.1349	0.1828
270 deg	1.60	20.47	0.1527	0.1981
315 deg	3.72	23.62	0.1085	0.1620

(a) Torsion moment

(b) Resultant curvature
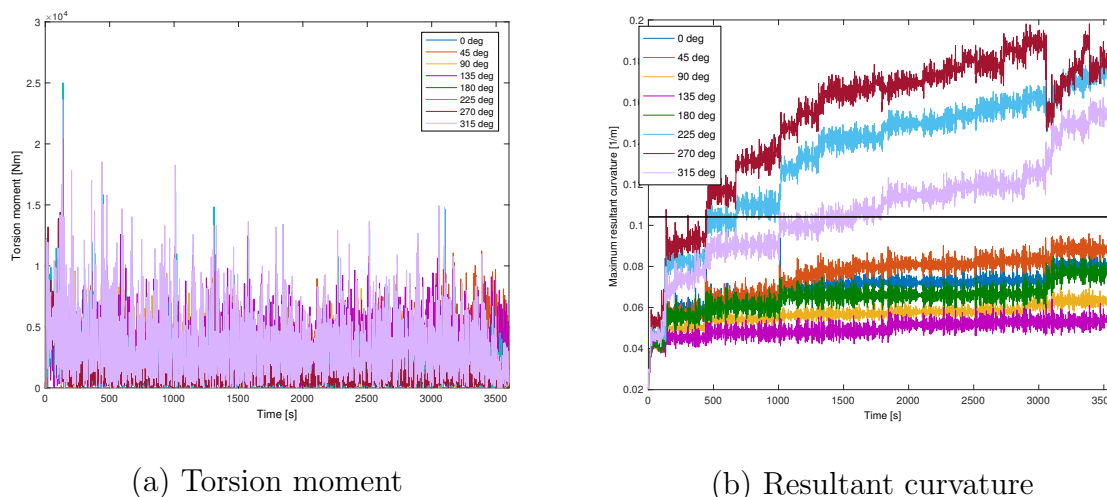
Figure 6.18: Dynamic results for $H_s = 3m, T_p = 10s$ with varying wave heading

From the figures some observations can be made; head sea (heading of 0°) and following sea (heading of 180°) yield very similar resultant curvature levels, while the direction of beam sea is critical and might induce unacceptable curvature levels. As seen from Figure 6.18 (b) the magnitudes of the maximum resultant curvature for the cases of 90° and 270° are very different. This can be explained by the configuration of the touch down point when applying the dynamics. In Figure 6.19 the configuration of the TDZ in the time step before and after activation of the wave load is illustrated. As seen from the figure activation of the wave dynamics induces a shift in the configuration, yielding a s slight bend in the TDZ. A result of this is asymmetry of the cable around the cable center line. When the wave loading is applied in the same direction as the bend, heading equal to 90°, the geometric stiffness of the cable restrains the deformation. For wave loading from the opposite direction, beam sea of 270°, the stiffness properties in this direction is lower and the cable will experience more severe deformation. This argumentation holds for the cases of heading 225° and 315° as well.

6.2.5 Effect of sea current

The above-mentioned analyses are carried out without the presence of current. This to intent to isolate the effect of the wave sea state. A normal installation conditions consist of both a wave excitation as well as current loading. Hence this section will discuss how additional current will affect the process of kink formation, to present a more realistic installation scenario. Presenting the sea current using Morison equation yields a mean drag effect, which will yield changes in the tension distribution in the structure, which might influence the riser

(a) t = 10 s   (b) t = 11 s
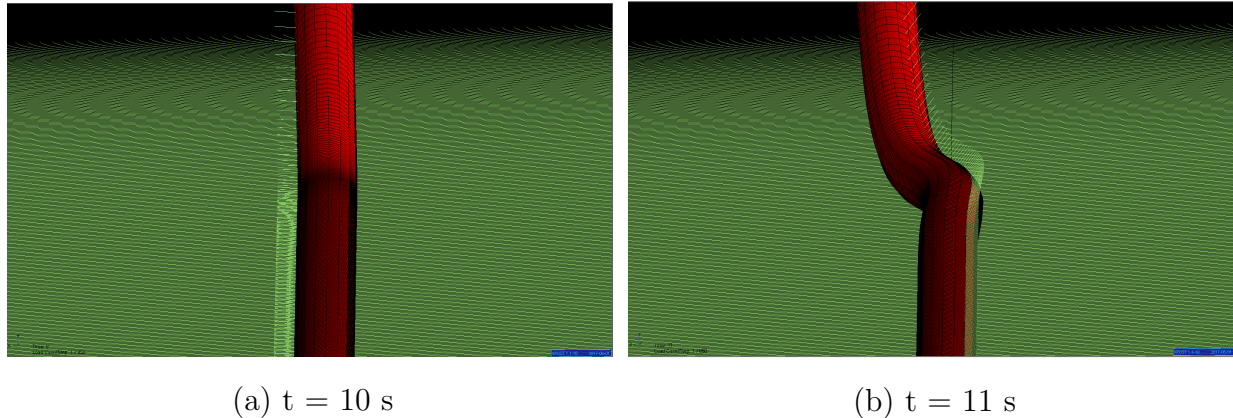
Figure 6.19: Cable configuration (a) right before and (b) after implementation of dynamics

loop formation [14].

The analyses with sea current are carried out for umbilical 2, subjected to the harshest sea state. This corresponds to $H_s = 3m, T_p = 10s$. This sea state is chosen as the resultant curvature in this sea state is the highest. The waves are applied with heading of 0°.

Figure 6.20 illustrates how the torsion moment and the maximum total curvature varies with the current velocity. The mean and maximum obtained values for the torsion moment and the resultant curvature are presented in Table 6.18. As seen the effect of the presence of current is dependent on current heading. Current and waves in the same direction yields lower resultant curvature for the cable. Current applied orthogonal to the wave direction yields higher torsion moment and resultant curvature. This is due to an increase in the drag forces. The most critical scenario is a wave heading of 180 °, which yields the highest resultant curvature levels. This is because the current "lifts" the umbilical such that the effective weight of the cable is reduced, and the cable is more prone to deform.

Table 6.18: Torsion moment and maximum resultant curvature with current

| Current heading	Torsion moment [kNm]		Maximum resultant curvature [1/m]	
	Mean	Max	Mean	Max
0 degrees	3.24	12.22	0.0627	0.1046
90 degrees	6.37	14.98	0.0795	0.1149
180 degrees	1.50	14.52	0.0865	0.1617
270 degrees	2.90	14.97	0.0727	0.1158
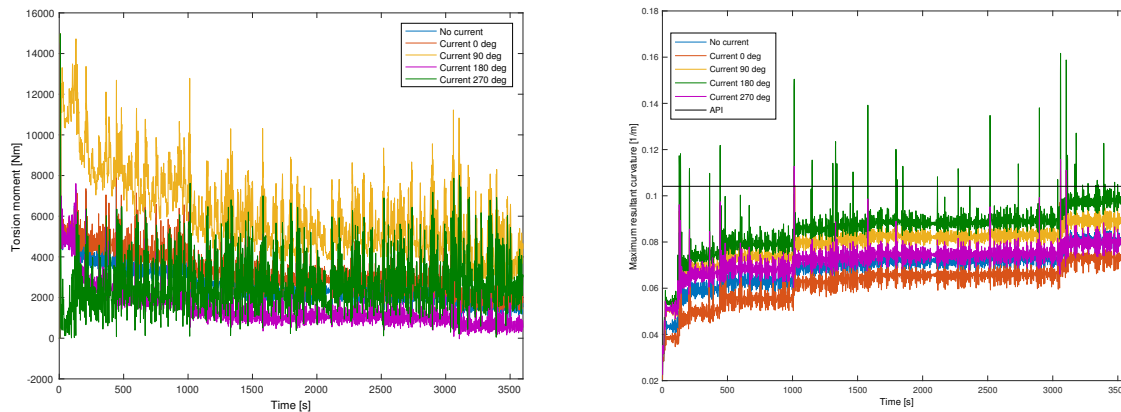
Figure 6.20: Torsion moment and maximum resultant curvature with current

## 6.2.6   Effect of horizontal bottom tension

As mentioned earlier, the resultant curvature for umbilical 1 for the case of both curved routing and end cap turn does exceed the API curvature criterion at an early stage of the dynamic analyses. These analyzes are carried out with as small horizontal bottom tension as the API standard allows. Hence it might be necessary operate with a higher initial tension. This yields directly from the catenary equations presented in Section 5.2.2. The curvature in the touch down point is defined by $\kappa = \frac{w_s}{T_0}$, which indicates that the curvature is inversely proportional with the bottom tension. An increase in T_0 yields a decrease in the theoretical curvature. Hence analyses for the same sea states as earlier are now carried out with a horizontal bottom tension of 5 kN for both cross-sections, to investigate how this affects the cable behavior.

Umbilical 1

Figure 6.21 (a) and (b) presents the resulting maximum resultant curvature and torsion moment for the case of an end cap turn, while Figure 6.21 (c) and (d) illustrates the variation of torsion moment of curvature for a curved routing scenario.
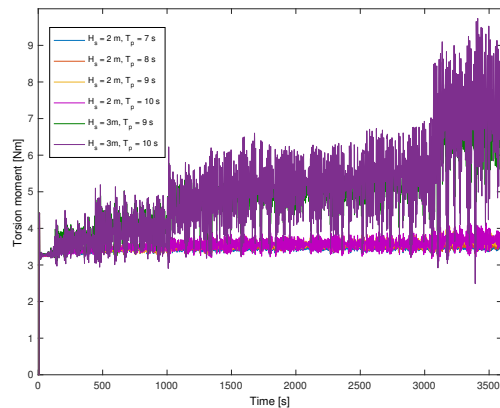
87
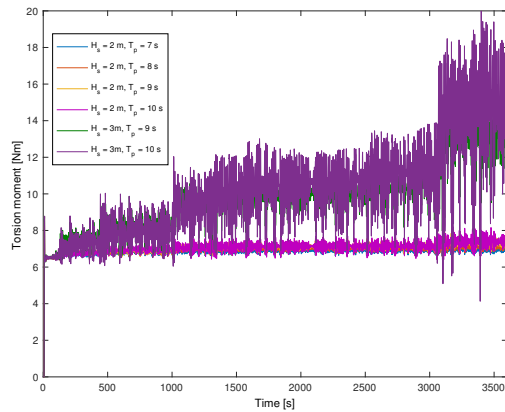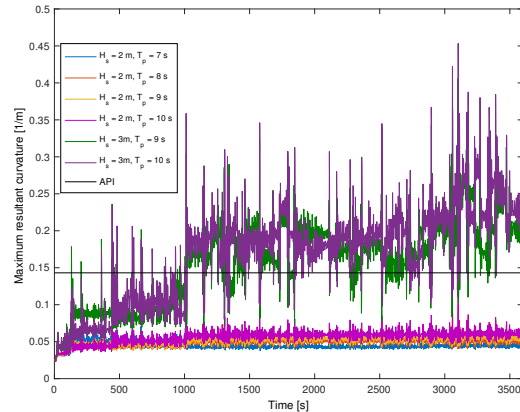
(a) Torsion moment

(b) Resultant curvature

End cap turn

(c) Torsion moment
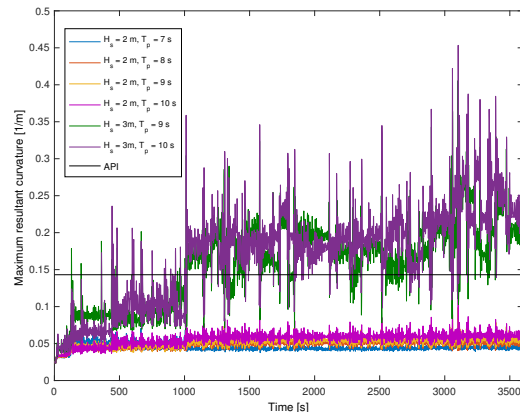
(d) Resultant curvature

Curved routing

Figure 6.21: Torsion moment and maximum resultant curvature for $T_0 = 5kN$, umbilical 1 - both installation scenarios

From the figures it is seen apparent differences between the sea states simulated sea states with various significant wave heading. The sea states with significant wave height of 2 meters are below the API criterion with a good safety margin, while the resultant curvature values for wave heights of 3 meters oscillate around the critical curvature value of 0.1041. This is apparent for both installation scenarios. The torsion moment follows the same scheme, with slight moment magnitude differences between the two installation scenarios. Hence increasing the horizontal bottom tension has a effect on the magnitude of the curvature over all, which is decreased for all sea states. Only for the sea states with significant wave

height of 2 meters the curvature levels are lowered to an acceptable level. Thus following the increase in tension, all sea states with significant wave height of 2 meter for this cable is defined as acceptable with respect to torsion and curvature, while a further increase of the bottom tension might be necessary for harsher sea states. .

In Appendix E.5 the axial force distributions for time steps in the region of the observed minimum axial force is presented for all sea states for an end cap turn and heading change respectively. From these figures its apparent that the occurrence of compression is less likely with a higher horizontal bottom tension. The magnitudes of the experienced compressive forces are also significantly lowered.

Umbilical 2

The same simulations are performed for umbilical 2. Figure 6.22 presents the resulting torsion moment and maximum resultant curvatures during an one hour sea state. As is apparent from the figure, the value of the horizontal bottom tension does not affect the resultant curvature in the same manner as for umbilical 1. The curvature values for the most severe sea states oscillate around the API criterion, which is an increase in the curvature levels compared with the results obtained with lower tension. The maximum value of the curvature increases with sea state severity. The sea states $H_s = 3m, T_p = 9s$ and $H_s = 3m, T_p = 10s$ do not fulfill the API criterion, and are not acceptable. In Appendix C the distribution of the axial force for the simulated sea states is given. From this it is seen that observations of compression follows the same scheme as for the case of lower tension.
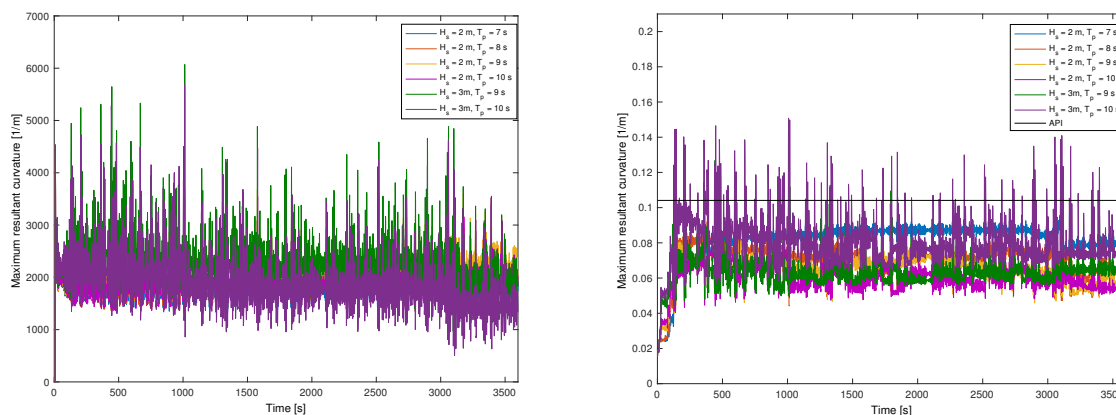

**Figure 6.22:** Torsion moment and maximum resultant curvature for $T_0 = 5kN$

Further investigations indicate that with the increase in horizontal bottom tension, the cable experiences that the resulting moment $M_{res} = \sqrt{M_y^2 + M_z^2}$ exceeds the friction moment in

certain regions. Figure 6.23 illustrates the variation of the resultant moment as a function of curvilinear element coordinate for the first 50 seconds. Of the 3600 seconds simulated, the friction moment is exceeded at 1073 and 1060 time steps for $T_0 = 1352N$ and $T_0 = 5000N$ respectively. The region experiencing yielding is most concentrated for the lowest bottom tension. The plasticity region is for that case located between element coordinates 70 - 75 m. For the case of $T_0 = 5000N$ the area is larger, corresponding to element coordinates 50 - 65 meters. The criticality of this plasticity region is assessed with respect to location proximity to the touch down point.

The tension is an important parameter in the catenary equation, and a change in this factor yield a different outlook of the catenary configuration. In this case, it yields a change in location of the touch down point. Hence based on the location of the elements which overstep the friction moment, the elements yielding for $T_0 = 5000N$ is directly in the touch down zone, while for $T_0 = 1352$ the elements are located just before the touch down zone. As the elements in the touch down zone are the most critical with respect to curvature, one can imagine that yielding in this area, as for $T_0 = 5000N$, is critical for the deformation and hence curvature the cable experiences. Figure 6.24 illustrates the deformation of the touch down zone for the two cases of tension, where it is seen that the highest initial tension yield largest deformation.
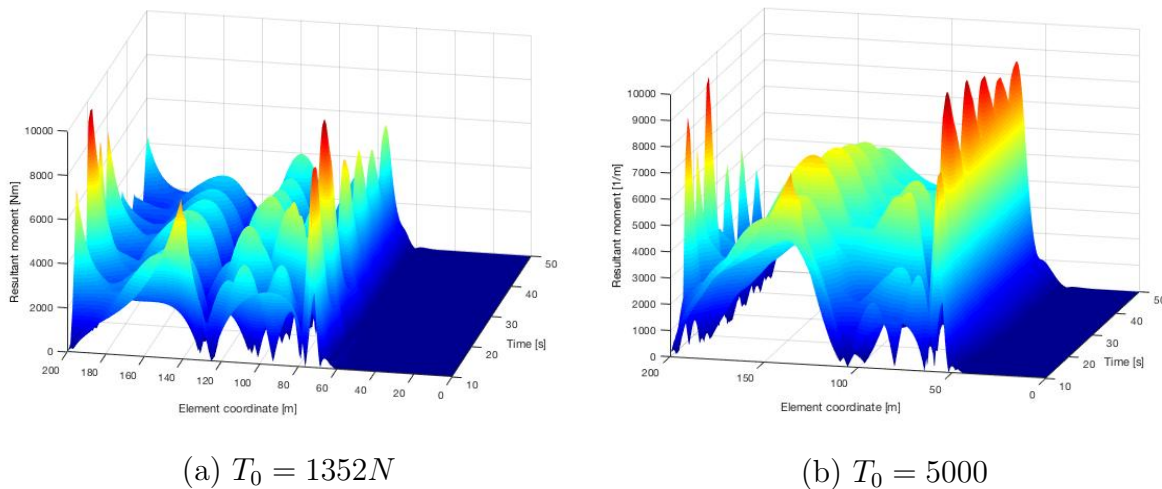
(a) $T_0 = 1352N$ (b) $T_0 = 5000$

Figure 6.23: Resultant moment distribution as function of element coordinate and time
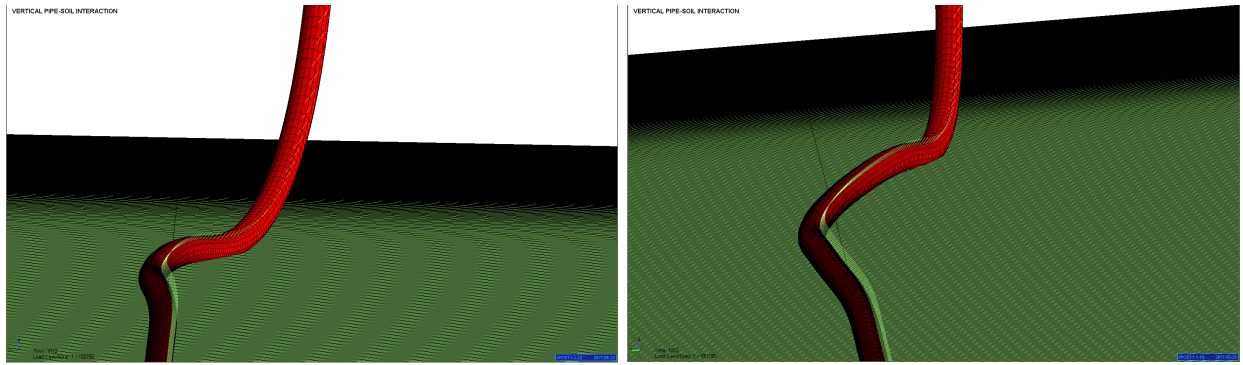
(a) $T_0 = 1352N$ (a) $T_0 = 5000N$

Figure 6.24: Deformation of the touch down zone with different horizontal bottom tension values

The moment the cable experiences at a certain curvature is a result of both elastic and plastic contributions, as defined in the following equation

$$M = M_e(\kappa) + M_p(\kappa) = EI\kappa + M_p(\kappa) \tag{6.2}$$

Table 6.19 presents the mean values of the resultant moment for the two cases of bottom tension, along with the elastic and plastic mean contributions. $T_0 = 5000N$ experiences higher curvature levels, which directly yields higher elastic moment contributions. Based on the values presented in the table, it can be established that with a higher horizontal bottom tension the plastic contribution will be less governing.

Table 6.19: Mean values of the resultant moment, and its elastic and plastic contributions

	T$_0$ = 1352N	**T$_0$ = 5000N**
Elastic moment	1.70 kN	1.98 kN
Plastic moment	4.83 kN	3.86 kN
Resultant moment	6.53 kN	5.84 kN

6.3 Discussion of design criteria

Up to now results obtained by following the design procedure proposed by Sævik [29] are presented. These results contribute to some concluding remarks with respect to prediction of loop formation.

1. The API criterion is the most limiting parameter in current practice. When performing the capacity analyses, it is found that the API criterion is surpassed at 70-80 % of the moment utilization for both cross-sections. This gives a good safety margin with respect to prevent operation with critical torsion moment levels. Keeping the curvature below this value indicates generally that the deformation can be kept to an acceptable level.

2. Koloshkin presented the critical curvature as a function of moment utilization. Utilizing this measure yields critical curvatures below the API criterion, indicating that the cable experience torsion buckling before the API criterion is exceeded. This measure does not capture the total behavior of the cable. Formation of a loop with larger diameter than the criterion will not be captured. Hence predicting the critical curvature is a difficult process, as it is not necessarily connected to the maximum torsion moment and highly dependent on the deformation pattern of the cable. It is important to constantly validate the cable behavior with visualization of the deformation, using for instance XPOST.

3. The critical torsion moment does not function as a measure of kink formation alone, and its difficult to predict the critical curvature based on obtained torsion moment values. The torsion moment and resultant curvature are not directly linked. Dynamic loading activates processes which affects the curvature in a more severe way than the torsion moments. Hence the critical curvature predicted can be exceeded, along with the API criterion, even though the torsion moment is far away form its maximum.

   For umbilical 1, the amount of imposed rotation necessary to induce maximum torsion moment is way above practical magnitudes, which might impact the results. The low torsional stiffness of umbilical 1 hence yields a very high capacity with respect to torsion buckling, where the amount of imposed rotation necessary to induce buckling is very large. It is hence difficult to apply the critical parameters found for this cable to real-life scenarios. If the maximum curvature criterion per API is fulfilled, the cable should be safe to operate.

4. Axial compression can safely occur without necessarily leading to loop formation. The results for umbilical 2 shows that the API criterion is fulfilled while the TDZ experiences axial compression without severe deformation. The magnitude of the compressive load is increasing with the severity of the sea state. It should be noted that the combination of axial compression and severe curvature makes loop formation favorable. As the curvature is kept below the API criterion, the curvature is not severe enough to induce

loop formation. Hence, if the dynamic curvature criterion is fulfilled axial compression can occur for the cables.

5. A horizontal bottom tension calculated based on the catenary equations as well as the minimum radius of curvature based on API standards does not necessarily indicate sufficiently low resultant curvature during dynamic cyclic loading. Investigations of the dynamic behavior of a cable to safely predict sufficient tension are necessary.

   It is hard to predict whether the severe deformation of umbilical 1 is due to the axial compression or the curvature level. Analyses with a higher initial bottom tension T_0 indicate a lower curvature level in the system, along with less frequent occurrence of compression. Carrying out the same analyses for umbilical 2 does not yield the same scheme, and the effect of tension must hence be evaluated for each individual case.

6. The results from the operation analyses carried out in this thesis brings up the question of validity of ULS analyses. As the resulting curvatures for the most common sea states in the northern North Sea already is on the limit of the API criterion, one can say that the dynamic maximum curvature criterion limits the possibilities for extreme sea state analyses. The sea states simulated are far away from long-term statistics extremes for the same area.

6.4   Uncertainties

An installation of a cable is a complex task with various elements included. When trying to represent a realistic scenario with a simplified simulation model there exists several uncertainties Some of the uncertain aspects in this thesis will be presented below.

6.4.1   Material properties

A cable cross-section is a complex structure with several layers and complex in-between layer interaction. Sævik [27] has established analytical expression to determine the flexural properties of the cross-sections due to axi-symmetric and bending loads. The properties of the two cables in this thesis are determined based on these expressions. These expressions are based on straight beam theory. Due to limited time scope and as the analysis is a global analysis, the mesh size is chosen relatively coarse to reduce computational time. It might be that the mesh size is chosen too coarse for the applied theory to be valid.

It should also be noted that the dimensions of the various layers are measured by hand, yielding uncertainties in the input values of when calculating the cross-section properties.

6.4.2   Modelling

The analyses are carried out with the program SIMLA. SIMLA is based on the non-linear finite element method, which is a well-developed method but at the same time is an approximate approach to realistic scenarios. The accuracy of the representation of the scenario is dependent on user-made selections, through selection of element type, mesh size and implementation of nonlinearities to mention some. The composition of the model in this scope is based on the selections made by Koloshkin in this thesis.

In SIMLA the cable cross-section is modelled as a thin-walled pipe using PIPE31/COMPIPE42 pipe elements, which is a very simplified representation of the complex geometry. This representation does not consider behavior in-between layers, which might be relevant for local behavior due to global loading. Using specialized FE software to accurately consider the composition of the umbilical can be preferable. Such programs also contain in-built methods for calculating the structure properties, which yield comparative values for the hand-calculations.

6.4.3   Environmental condition

The cable is subjected to irregular waves during a one hour sea state. Irregular wave theory assumes of short duration of maximum 3 hours. Hence by only simulating one hour, all possible wave elevations are not represented, and the results loses some of its validity due to lack of full statistical coverage. The utilized significant wave height and peak periods are based on a scatter diagram for the northern North Sea [11]. Scatter diagrams are based on historical data and presents probabilities for occurrence of various sea states. Hence there exist some uncertainty related to whether the sea states simulated will correspond to the actual wave environment.

6.4.4   Seed number

The waves are also generated by using the same seed number. The seed numbers generate the random phase angles of the wave components. Zhang [33] established that "the seed number had considerably impact on the tails of the probability distribution, i.e only on the largest peak values of the time history". The peak values yield displacements extremes which corresponds to peak values in the force distributions, hence running the analyses with various seed numbers would be advised. As this thesis focused on the effect of the cable capacity with respect to maximum resultant curvature as well as the maximum value of the compressive forces experienced, this might affect the results.

6.5 Limitations

Due to a limited duration of this thesis, some limitations have been made during the work. As a global analysis, only desires to capture the global behavior of the cable due to environmental loading and vessel motions, the global model is simplified as much as possible to reduce computational time without interfering with the validity of the results. The effect of some main parameters is investigated; inherent torque, severity of sea state, wave heading, presence of sea current and horizontal bottom tension. Regarding all the mentioned parameters, more cases could have been carried out to investigate trends in a larger extent. This was not possible due to limited time.

The dynamic results are limited to six sea states, based on the assumption that an installation will not be carried out in sea states of significant wave height larger than 3 meters. With respect to an operation analysis, this yields a good representation as these are the most probable sea states for the given region.

The focus is put on the global behavior of the cable, hence little attention is given to the local behavior of cable due to the loading and deformations. The cable is modelled as a thin-walled pipe despite its complex layer structure, and inter-layer interaction is neglected. Building a local model with a specialized FE software would have been a time-demanding task, which was not doable nor the focus for this thesis.

Chapter 7

Conclusion

In this thesis, a review and discussion of the torsion instability issue related to cable installations is presented. The aim has been to study how various loading parameters affect the process of loop formation due to severe curvature and axial compression in the touch down zone during installation. This is carried out by following a design procedure proposed by Sævik.

Numerical studies have been carried out with the purpose of investigating how parameters as cross-section friction moment, inherent torque and environmental conditions affect the process of kink formation during installation scenarios. Two cable-cross sections were subjected to axial rotation until the torsion capacity was exceeded. From this the critical torsion moment and curvature associated with the initiation of kink formation were established. This is then, along with the dynamic curvature criterion based on API standards, used to evaluate the feasibility of various dynamic sea states.

The critical torsion moment and curvature associated with kink formation are presented as potential measures of the kink formation process. The development of the torsion moment while gradually applying rotation to the system follows the same scheme for both cross-sections; the moment gradually increases until it reaches a maximum capacity. When the maximum value is surpassed, the loop formation process is initiated and the cable experience severe deformation. The effect of both material model and cross-section friction moment on the cable capacity in torsion is investigated. It is found that the composition of the cross-section greatly affect the capacity of a cable.

The dynamic analyses are carried out with an irregular sea state with a one hour duration. Two different installation scenarios are also simulated yielding different initial torque level in the cable. Based on this, it is found that umbilical 1 experiences too severe curvature according to current criteria to be feasible during installation. It is established that this is due to too low bottom tension. The results for umbilical 2 shows that there is no loop formation during the simulated time. The maximum resultant curvature in the system is kept below the API criterion for all sea states, and the magnitudes of the torsion moments are kept below the critical capacity of the cable. Predicting the critical curvature based on

critical torsion moment is found to be difficult as the critical torsion moment not necessarily coincide with the point of loop formation. Hence no good estimator for the critical curvature is established.

It is found that incoming waves are most critical when applied with angles in the range $[\pi, 2\pi]$. This is due to fact that the cable experiences a bend in the touch down zone due to applied torsion moment. It is also established that to predict the total response of a cable, a realistic current loading must be implemented in the figure. Current with heading of 180° is found as the most critical scenario.

Current practice does not allow for axial compression in the touch down zone. The numerical analyses show that some degree of axial compression is present in nearly all simulated load cases. It is also shown that the magnitudes of the axial compression are outside the critical range for local tensile armour buckling. The analyses show that the trend is an increasing compressive tension with increasing severity of the environmental condition. Hence it should be investigated whether a relation is found between experienced compressive load and sea state parameters. As the results for umbilical 2 illustrates acceptable conditions while experiencing severe compression, it can be discussed whether prohibition of compression for all sea states is a too conservative criterion.

To summarize, it can be concluded that installation in certain sea states can be stated as acceptable with respect to experienced torsion moment and curvature if the API criterion is fulfilled. It is also shown that axial compression in the touch down zone is very common for the sea states simulated, without associated loop formation. Hence it is shown with numerical analyses that installation scenarios which current practice does not allow due to compression, not necessarily induce cable failure and can be defined as feasible. This validation can be a step in the direction of increasing the weather window and thus reducing installation costs. With respect to Sævik's proposed design procedure, it is establshed that fulfillment of the dynamic curvature criterion yield acceptable installation conditions and good prediction of avoidance of loop formation. It is though difficult to predict the critical torsion moment and curvature associated with loop formation on a general basis.

Chapter 8

Recommendations for further work

The scope of this thesis is investigated by carrying out numerical analyses using SIMLA. If possible, it would be very interesting to validate the results obtained with scale laboratory experiments. By representing the cable properties in a scaled dimension, it is possible to verify the accuracy of the numerical analyses as well as observing the development of deformation in a more realistic manner.

The results in this thesis are obtained by following a design procedure proposed by Sævik. Here prediction of the critical curvature is a crucial step. In this thesis the resultant curvature at the point of critical torsion moment is proposed as critical curvature parameter. It is found that this does not accurately predict the curvature yielding torsion buckling, and hence it proposed to further investigate how the critical curvature can be more accurately predicted generally.

Due to limited time and computer capacity, the main dynamic simulations in this thesis were carried out with a simulation time corresponding to one hour. Irregular wave statistics assume that a sea state endure for three hours. A simulation time of three hours should hence have been carried out. This will ensure full statistical coverage of possible wave elevations corresponding to the given combination of wave height and period. The simulated sea states assume that an installation in the North Sea will not be carried out in wave heights larger than 3 meters. This is a choice made in cooperation with the supervisor, based on his experience in the field. Simulating more sea states would have made it easier to make more reasoned conclusion with respect to the validity of current practice, and hence easier to propose a design criterion.

As it is found that axial compression might be present without necessarily induce loop formation, the focus of further work should be to carry out a more comprehensive parametric study. The effect of more severe sea states should be carried out with the goal to establish a relation between applied environmental state and resulting deformation. In addition, the results obtained when varying the wave heading should be confirmed for more cross-sections, as the bend umbilical 2 experiences necessarily not will be the case for all cross-sections

dependent of its properties.

The analyses performed in this thesis are operational analyses, with calm sea conditions. As seen these sea states yield in curvature levels already on the verge of the API criterion. In addition, it is found that the magnitude of the curvature and axial compression obtained is highly dependent on severity of the sea state. Hence it would be very interesting to investigate how the cable behaves during storm conditions. It is thus proposed to carry out an ultimate limit state analysis with extreme wave conditions, in combination with extreme values of the current.

The analyses of this thesis are carried out in relatively shallow water. Torsion buckling is mostly associated with deep waters, and local buckling of tensile armours is a frequently encountered problem in deeper waters. Analyzing whether the instability problem is mostly associated with deep water operations for operational sea states is of great interest, and can contribute to establishment of a design criterion as a function of water depth.

The conclusions from this thesis are not generalized as they are carried out using two very specific cross-sections. Two cross-sections of very different composition were chosen. Due to the critical differences in composition it was hard to draw conclusions with regards to the behavior of a general cable. It is favorable to cover a wider range of compositions to investigate whether some effects are one-offs, or common for all cables.

The analyses carried out are global analyses a cable during installation. Hence the inter-layer behavior will not be accountable, and the effect of this relation is interesting. By building a model in a specialized FE software which includes every layer component would give a more realistic representation of the cable, and how the cable structure is affected by loop formation. It is hence proposed that in a future analysis local and global analysis are combined to more realistically present the complexity of an umbilical.

Bibliography

[1] API. *API 17J Specification for Unbonded Flexible Pipe, Fourth Edition, Includes Errata 1.* 2014.

[2] API. *API RP 17B Recommended Practice for Flexible Pipe, Fifth Edition.* 2014.

[3] Yong Bai and Qiang Bai. *Subsea Pipelines and Risers.* Mechanics of Offshore Pipelines. Elsevier Science, Burlington, 2005.

[4] Yong Bai and Qiang Bai. *Subsea engineering handbook.* Elsevier, Amsterdam, 2012.

[5] K. J. Bathe. *Finite element procedures.* Prentice Hall, Englewood Cliffs, N.J, 1996.

[6] Zdeněk P. Bažant and Luigi Cedolin. *Stability of structures : elastic, inelastic, fracture, and damage theories*, volume 26 of *The Oxford engineering science series.* Oxford University Press, New York, 1991.

[7] Cygwin. www.cygwin.com, Accessed date: 02.15.2017.

[8] DNV. *DNV-OSS-302: Offshore Riser Systems.* 2003.

[9] DNV. *Subsea Power Cables in Shallow Water Renewable Energy Applications.* 2014.

[10] Natalia S. Ermolaeva, Jeroen Regelink, and Martijn P. M. Krutzen. Hockling behaviour of single- and multiple-rope systems. *Engineering Failure Analysis*, 15(1):142–153, 2008.

[11] Odd M. Faltinsen. *Sea loads on ships and offshore structures.* Cambridge ocean technology series. Cambridge University Press, Cambridge, 1990.

[12] J. J. Feret and C. L. Bournazel. Calculation of stresses and slip in structural layers of unbonded flexible pipes. *Journal of Offshore Mechanics and Arctic Engineering*, 109(3):263–269, 1987.

[13] Alfredo Gay Neto. Dynamics of offshore risers using a geometrically-exact beam model with hydrodynamic loads and contact with the seabed. *Engineering Structures*, 125:438–454, 2016.

[14] Alfredo Gay Neto and Clóvis de Arruda Martins. Structural stability of flexible lines in catenary configuration under torsion. *Marine Structures*, 34:16–40, 2013.

[15] J.M.J. Journée, W.W. Massie, Faculty of Civil Engineering Delft University of Technology, and Geosciences. *Offshore Hydromechanics.* TU Delft, 2000.

[16] J.W. Johnson S.A. Schaaf J.R. Morison, M.P. O'Brien. The force distribution exerted by surface waves on piles. 1953.

[17] N. Ohle E. Tautenhain K.-F. Daemrich, S. Mai. Influence of spectral density distribution on wave parameters and simulation in time domain. 2006.

[18] Evgenii Koloshkin. Torsion buckling for dynamic flexible risers. 2016.

[19] PhD Tian Ran Lin, PhD Boyun Guo, Ph D. Shanhong Song, PhD Ali Ghalambor, and Jacob Chacko. *Offshore Pipelines.* Elsevier Science, Burlington, 2005.

[20] F.C Liu. Kink formation and rotational response of single and multistrand electromechanical cables. Technical report, Naval Facilities Engineering Command, 1975.

[21] Raymond F. McAllister, John J. Myers, and Carl H. Holm. *Handbook of ocean and underwater engineering.* McGraw-Hill handbooks. McGraw-Hill, New York, 1969.

[22] Torgeir Moan. *Finite Element Modelling and Analysis of Marine Structures.* Prentice Hall, 2003.

[23] Alfredo Gay Neto, Clóvis A. Martins, and Paulo M. Pimenta. Static analysis of offshore risers with a geometrically-exact 3d beam model subjected to unilateral contact. *Computational Mechanics*, 53(1):125–145, 2014.

[24] F. Rosenthal. Application of greenhill's formula to cable hockling. *Journal of Applied Mechanics, Transactions ASME*, 43(4):681–683, 1976.

[25] A. L. Ross. Cable kinking analysis and prevention. *Journal of Engineering for Industry*, 99(1):112, 1977.

[26] Ir. JAAP De RUITER and DENYS A. FOX. Site investigations for the north sea forties field. Technical report.

[27] S. Sævik. Lecture notes in offshore pipeline technology. 2015.

[28] Svein Sævik. Simla - theory manual. 2008.

[29] Svein Sævik and Evgenii Koloshkin. Torsion instability of offshore cables during installation. 2017.

[30] Svein Sævik and Mats. J Thorsen. Techniques for predicting tensile armour buckling and fatigue in deep water flexible pipes. 2, 2012.

[31] J. A. Witz and Z. Tan. On the flexural structural behaviour of flexible pipes, umbilicals and marine cables. *Marine Structures*, 5(2):229–249, 1992.

[32] Thomas Worzyk. *Submarine Power Cables*. Submarine Power Cables : Design, Installation, Damages and Repair, Environmental Aspects. Springer, Dordrecht, 2009.

[33] Yucheng Hou Jiabei Yuan Yanqiu Zhang, Zhimin Tan. A study for statistical characteristics of riser response in global dynamic analysis with irregular wave. 2014.

[34] Niels Højen Østergaard, Anders Lyckegaard, and Jens H. Andreasen. On lateral buckling failure of armour wires in flexible pipes. 4:289–298, 2011.

[35] Niels Højen Østergaard, Anders Lyckegaard, and Jens H. Andreasen. On modelling of lateral buckling failure in flexible pipe tensile armour layers. *Marine Structures*, 27(1):64–81, 2012.

Appendix A

Umbilical cross-section properties

Umbilical 1	**Umbilical 2**
OD = 79 mm	OD = 143 mm
mass per unit length = 9.56 kg/m	mass/unit length = 32.58 kg/m

Layer 1: Outer protection sheet
OD = 79 mm, ID = 67 mm
Cross- sectional area $A = 0.0014m^2$
Inertia $I = 9.2279 * 10^{-7}m^4$

Layer 1: Outer protection sheet
OD = 143 mm, ID = 134 mm
Cross- sectional area $A = 0.0020m^2$
Inertia $I = 4.6998 * 10^{-6}m^4$

Layer 2: Helical steel tubes, n = 10
OD = 16 mm, ID = 12 mm
Cross- sectional area $A = 8.796 10^{-5}m^2$
Inertia $I = 2.1991 * 10^{-9}m^4$

Layer 2: Outer tensile armour layer, n = 95
OD = 4 mm
Cross- sectional area $A = 1.2566 10^{-5}m^2$
Inertia $I = 2.0106 * 10^{-10}m^4$

Layer 3: Inner plastic sheath
OD = 38 mm, ID = 21 mm
Cross- sectional area $A = 7.8775 10^{-4}m^2$
Inertia $I = 9.2807 * 10^{-8}m^4$

Layer 3: Inner tensile armour layer, n = 87
OD = 4 mm
Cross- sectional area $A = 1.2566 10^{-5}m^2$
Inertia $I = 2.0106 * 10^{-10}m^4$

Layer 4: Center tube
OD = 16 mm, ID = 12 mm
Cross- sectional area $A = 8.796 10^{-5}m^2$
Inertia $I = 2.199 * 10^{-9}m^4$

Layer 4: Inner plastic sheath
OD = 117 mm, ID = 110 mm
Cross- sectional area $A = 0.0012m^2$
Inertia $I = 2.0115 * 10^{-6}m^4$

Layer 5: Helical steel tubes, n = 10
OD = 22 mm, ID = 18 mm
Cross- sectional area $A = 1.2566 * 10^{-4}m^2$
Inertia $I = 6.346 * 10^{-9}m^4$

Layer 6: Center tube
OD = 22 mm, ID = 18 mm
Cross- sectional area $A = 1.2566 * 10^{-4}m^2$
Inertia $I = 6.346 * 10^{-9}m^4$

Appendix B

SIMLA input file

```
HEAD CABLE INSTALLATION
HEAD Catenary Shape Formation (STATIC)

#      MAX_ITER  NDIM ISOLVR NPOINT  IPRINT CONV_RAD  GRAV ISTRES
CONTROL  100     3   2    16     1    1e-5   9.81 stressfree

#Dynamic Analysis criteria
#      Lumped mass  alfa1  alfa2  HHT-alfa parameter
DYNCONT   2       0.0   0.051  -0.05

#Result visualization definition
VISRES integration 1 sigma-xx

ENVRES_E    2           1     600   1    1     1
ENVRES_E    2           1     600   1    4     1
ENVRES_E    2           1     600   1    5     1
ENVRES_E    3           1     600   1    1     1
ENVRES_E    3           1     600   1    2     1
ENVRES_E    3           1     600   1    3     1


#========================================================================
#GEOMETRY DATA
#========================================================================
# Vessel
# ----------------------------------------------------------------------------------------
#                            node  x-cor    y-cor      zcor
NOCOOR     COORDINATES    7001  241.00   -13.92     -96.582
                          7002  200.000   0.0        -99.942
#
#           group        elty        material    no    n1    n2
ELCON      vessel1      pipe31       vesselmat   7000  7001  7002
#
#                          element    x     y     z
ELORIENT   COORDINATES    7000      0.0   0.0   0.0
#
#    name   type   poiss talfa  tecond heatc beta ea     eiy   eiz    git   em  gm
MATERIAL vesselmat linear 0.0  1.17e-5  50   800 0  194e10 5.14e11 5.14e11   3.96e3  2e11 8e10
#    name   type   r    t    CDr Cdt CMr CMt wd    ws     ODp    ODw   rks
ELPROP vessel1  PIPE   1.0  0.01  1.0 0.1 2.0 1.0 0.0      0.0 10.0    10.0   0.5
#
#PIPE
#-------------------------------------------------------------------------
#           type         NodeID     X     Y      Z
NOCOOR     COORDINATES    1        0     0    -99.942
                          601  200.0  0     -99.942
```

107

```
#ELCON DATA for PIPE
ELCON  pipe1  COMPIPE42  pipemat1 1 1 2
REPEAT 595 1 1
ELCON          pipe2  COMPIPE42    pipemat2     596     596 597
ELCON          pipe3  COMPIPE42    pipemat3     597     597 598
ELCON          pipe4  COMPIPE42    pipemat4     598     598 599
ELCON          pipe5  COMPIPE42    pipemat5     599     599 600
ELCON          pipe6  COMPIPE42    pipemat6     600     600 601


#                              elno      x      y      z
ELORIENT      COORDINATES      1        0.0    1.000  -99.942
REPEAT        600 1 0 0 0


#    name    type    poiss talfa  tecond heatc beta ea    eiy  eiz    git  em gm
MATERIAL pipemat1 RESULTANT  0.30    0 1.17e-5  50   800  0     1    1      1    1  1 0
      0    0    0    0  axmat1 tomat1  bendmat1
MATERIAL pipemat2 RESULTANT  0.30    0 1.17e-5  50   800  0     1    1      1    1  1 0
      0    0    0    0  axmat2 tomat2  bendmat2
MATERIAL pipemat3 RESULTANT  0.30    0 1.17e-5  50   800  0     1    1      1    1  1 0
      0    0    0    0  axmat3 tomat3  bendmat3
MATERIAL pipemat4 RESULTANT  0.30    0 1.17e-5  50   800  0     1    1      1    1  1 0
      0    0    0    0  axmat4 tomat4  bendmat4
MATERIAL pipemat5 RESULTANT  0.30    0 1.17e-5  50   800  0     1    1      1    1  1 0
      0    0    0    0  axmat5 tomat5  bendmat5
MATERIAL pipemat6 RESULTANT  0.30    0 1.17e-5  50   800  0     1    1      1    1  1 0
      0    0    0    0  axmat6 tomat6  bendmat6


 #   name    type   rade radi  CDr Cdt CMr CMt wd    ws      ODp   ODw   rks PHIST MHIST
ELTIME AUTOPLAST TCURV
ELPROP pipe1   COMPIPE 0.0715  0.018  1.0 0.1 2.0 1.0 3.08e1 1.436e1  0.12  0.12  0.5
eltime=5.1
ELPROP pipe2   COMPIPE 0.0715  0.018  1.0 0.1 2.0 1.0 3.08e1 1.436e1  0.12  0.12  0.5
eltime=5.1
ELPROP pipe3   COMPIPE 0.0715  0.018  1.0 0.1 2.0 1.0 3.08e1 1.436e1  0.12  0.12  0.5
eltime=5.1
ELPROP pipe4   COMPIPE 0.0715  0.018  1.0 0.1 2.0 1.0 3.08e1 1.436e1  0.12  0.12  0.5
eltime=5.1
ELPROP pipe5   COMPIPE 0.0715  0.018  1.0 0.1 2.0 1.0 3.08e1 1.436e1  0.12  0.12  0.5
eltime=5.1
ELPROP pipe6   COMPIPE 0.0715  0.018  1.0 0.1 2.0 1.0 3.08e1 1.436e1  0.12  0.12  0.5
eltime=5.1


MATERIAL  axmat1    hycurve         -100.0      -760e8
                                     100.0       760e8


MATERIAL  tomat1    hycurve         -100.0      -8.27e9
                                     100.0       8.27e9


MATERIAL  bendmat1  epcurve  1       0.0         0.0
                                     0.0067      6.6590e3
                                     0.0075      7.0965e3
```

			0.0107	7.6385e3
			0.0128	7.6925e3
			0.100	9.8319e3
MATERIAL axmat2	hycurve		-100.0	-760e8
			100.0	760e8
MATERIAL tomat2	hycurve		-100.0	-8.27e9
			100.0	8.27e9
MATERIAL bendmat2	epcurve	1	0.0	0.0
			0.0067	6.6590e3
			0.0075	7.0965e3
			0.0107	7.6385e3
			0.0128	7.6925e3
			0.100	9.8319e3
MATERIAL axmat3	hycurve		-100.0	-760e8
			100.0	760e8
MATERIAL tomat3	hycurve		-100.0	-8.27e9
			100.0	8.27e9
MATERIAL bendmat3	epcurve	1	0.0	0.0
			0.0067	6.6590e3
			0.0075	7.0965e3
			0.0107	7.6385e3
			0.0128	7.6925e3
			0.100	9.8319e3
MATERIAL axmat4	hycurve		-100.0	-760e8
			100.0	760e8
MATERIAL tomat4	hycurve		-100.0	-8.27e9
			100.0	8.27e9
MATERIAL bendmat4	epcurve	1	0.0	0.0
			0.0067	6.6590e3
			0.0075	7.0965e3
			0.0107	7.6385e3
			0.0128	7.6925e3
			0.100	9.8319e3
MATERIAL axmat5	hycurve		-100.0	-760e8
			100.0	760e8
MATERIAL tomat5	hycurve		-100.0	-8.27e9
			100.0	8.27e9
MATERIAL bendmat5	epcurve	1	0.0	0.0
			0.0067	6.6590e3

0.0075	7.0965e3
0.0107	7.6385e3
0.0128	7.6925e3
0.100	9.8319e3

MATERIAL axmat6   hycurve   -100.0   -760e8
                                    100.0   760e8

MATERIAL tomat6   hycurve   -100.0   -8.27e9
                                     100.0   8.27e9

MATERIAL bendmat6 epcurve 1   0.0   0.0
                                   0.0067   6.6590e3
                                   0.0075   7.0965e3
                                   0.0107   7.6385e3
                                   0.0128   7.6925e3
                                   0.100   9.8319e3
#---
#SEABED
#---
#	Name	TYPE	SurfaceID	ElemID	NodeID
ELCON	seabed	cont126	cosurf1	10001	1
REPEAT	601	1	1		

#seabed		elno	tx	ty	tz
ELORIENT	eulerangle	10001	0.000	0.000	0.0
REPEAT	601	1	0	0	0

#---
#SEASURFACE
#---
#	type		NodeID	X	Y	Z
NOCOOR	COORDINATES		20001	0	-200	0
			20100	1607	-200	0
REPEAT	3	100	0	200.0	0	

#	Name	TYPE	MatID	ElemID	NodeID			
ELCON	SEA1	SEA150	seamat	20001	20001	20002	20102	20101
REPEAT	99	1	1					
REPEAT	2	99	100					

MATERIAL seamat sea 1024
#===
#BOUNDARY CONDITION
#===
#	COSYS	NODEID	DOF	
BONCON	GLOBAL	1	2	repeat 601 1
BONCON	GLOBAL	1	4	repeat 601 1
BONCON	GLOBAL	1	6	repeat 601 1
#				
BONCON	GLOBAL	7001	1	
BONCON	GLOBAL	7001	2	
BONCON	GLOBAL	7001	4	
BONCON	GLOBAL	7001	5	

```
BONCON      GLOBAL    7001     6
#CONSTR CONEQ LOCAL SLNOD SLDOF C0 MNOD1 MDOF1 C1
constr coneq         global        601 1  0.0  7002  1      1.0
constr coneq         global        601 2  0.0  7002  2      1.0
constr coneq         global        601 3  0.0  7002  3      1.0
#
BONCON  GLOBAL  20001    1
REPEAT 300 1
BONCON  GLOBAL  20001    2
REPEAT 300 1
BONCON  GLOBAL  20001    3
REPEAT 300 1
#
#===============================================================================
#SEABED DATA/CONTACT ELEMENT
#===============================================================================
#                 name       data file            nlin  kp0 x0  y0  fi   route_id
COSURFPR          cosurf1    "seabed_deep_flat.txt" 3   0.0 0.0 0.0  0    100 101 102
#
#          route id    kp1     kp2  soiltype
COSUPR     100        0.0   100000.0  soil1
COSUPR     101        0.0   100000.0  soil1
COSUPR     102        0.0   100000.0  soil1
#
#          name   type       MUX   MUY   MUTX XNAME      YNAME      ZNAME TXNAME
MATERIAL   soil1  R_CONTACT  0.4   1.0   1.0  soilx      soily      soilz soilrx
#
#          name   type      IHARD    EPS    SIGMA
MATERIAL   soilx  epcurve    1       0.00   0.0
                                     0.005  1.0
                                     2.00   1.01
#
MATERIAL   soily  epcurve    1       0.00   0.0
                                     0.02   1.0
                                     2.00   1.01
#
MATERIAL   soilz  hycurve           -1000.0  -65e6
                                     1000.0   65e6

MATERIAL   soilrx hycurve           -1000.0   0.
                                     1000.0   0.

#CONTACT INTERFACE DATA
#          groupn   mname      name  is1 isn  istx isty istz maxit igap
CONTINT    seabed   pipe1    cosurf1  1  596  5.0  5.0  0.0  60   0
CONTINT    sea1     sea1     pipe1

CONTINT    seabed   pipe2    cosurf1  1  597  5.0  5.0  0.0  60   0
CONTINT    sea1     sea1     pipe2

CONTINT    seabed   pipe3    cosurf1  1  598  5.0  5.0  0.0  60   0
CONTINT    sea1     sea1     pipe3
```

```
CONTINT     seabed    pipe4     cosurf1  1  599   5.0 5.0  0.0  60   0
CONTINT     sea1      sea1      pipe4


CONTINT     seabed    pipe5     cosurf1  1  600   5.0 5.0  0.0  60   0
CONTINT     sea1      sea1      pipe5


CONTINT     seabed    pipe6     cosurf1  1  601   5.0 5.0  0.0  60   0
CONTINT     sea1      sea1      pipe6
#==========================================================================
#LOAD INPUT
#==========================================================================

#External Pressure and Gravity Load
#           dmhist        b&pehist
PELOAD      100           100
# Tension
CLOAD       150    1     1       -1352.0

#PRESCRIBED DISPLACEMENT
CONSTR      PDISP  GLOBAL      7001  3      100     300

#WAVELO ELGRP IRREGULAR WAVENO WAVEHIST X0    Y0  ANG  TP HS  D DT   TSIM T0   DKIN SEED TYPE
WAVELO      sea1  IRREGULAR 100    700    241.084 0.0 0.0  10 3  100 0.25 4096 5.1   100  1   1
#
#==========================================================================
#ANALYSIS TIME CONTROL
#==========================================================================
#           T    DT   DTVI      DTDY  DT0
TIMECO      5.0
0.1    1.0    1.0     201.0 static nohla AUTO none ALL 100 5 1e-5


#==========================================================================
# HISTORY DATA
#==========================================================================
#           no     istp   fac
THIST       100    0.0    0.0
                   0.1    1.0
                   1.0    1.0


THIST       150    0.0    1.0
                   5.0    1.0


THIST       300    0.0    0.0
                   0.1    0.1
                   5.0    1.0


THIST_r     400    5.0    15.0    rampcos      1.0


THIST_r     700    100.0  200.0  rampcos      1.0
```

Appendix C

SIMPOST results file

```
ELPLOT "input"   "mpf-momx598" "Load step    " LOADSTEP "Torsion moment (Nm)"   ELMOM-X 598 598   1  1
ELPLOT "input"   "mpf-momx300" "Load step    " LOADSTEP "Torsion moment (Nm)"   ELMOM-X 300 300   1  1
ELPLOT "input"   "mpf-momy300" "Load step    " LOADSTEP "Torsion moment (Nm)"   ELMOM-Y 300 300   1  1
ELPLOT "input"   "mpf-momz300" "Load step    " LOADSTEP "Torsion moment (Nm)"   ELMOM-Z 300 300   1  1
#
GLPLOT "input"   "mpf-curvy"    "Element coorindate" E-COR "Curvatue y-direction" ELCUR-Y 1 600 1 1
GLPLOT "input"   "mpf-curvz"    "Element coorindate" E-COR "Curvatue z-direction" ELCUR-Z 1 600 1 1
ELPLOT "input"   "mpf-tens1"    "Element coorindate" TIME "Curvatue z-direction" ELFORCE-X 280 280 1 1 2
ELPLOT "input"   "mpf-tens2"    "Element coorindate" TIME "Curvatue z-direction" ELFORCE-X 300 300 1 1 2
#
#GLPLOT "input" "mpf-momxecor"  "Element coorindate" E-COR "Curvatue y-direction" ELMOM-X 1 600 1 1
GLPLOT "input"   "mpf-tensecor""Element coorindate" E-COR "Tensile force" ELFORCE-X 1 600 1 1
```

Appendix D

CYGWIN script for parametric study

```
#--------------------------------------------------------------------------------------------------------------------------------
#Analyse: Hs = 2 m, Tp = 7 s
#--------------------------------------------------------------------------------------------------------------------------------
mkdir Analyse_Hs2_Tp7
cp      go-analyze                Analyse_Hs2_Tp7/go-analyze
cp      initialconfig2.sif        Analyse_Hs2_Tp7/initialconfig.sif
cp      dynamic1.sif              Analyse_Hs2_Tp7/dynamic1.sif
cp      dynamic2.sif              Analyse_Hs2_Tp7/dynamic2.sif
cp      seabed_deep_flat.txt      Analyse_Hs2_Tp7/seabed_deep_flat.txt
cp      vessel_rao.trf            Analyse_Hs2_Tp7/vessel_rao.trf
cp      mpfdyn.spi                Analyse_Hs2_Tp7/mpfdyn.spi
#
cd Analyse_Hs2_Tp7
#
erzatz        "#Hs"        "2"    initialconfig.sif
erzatz        "#Tp"        "7"    initialconfig.sif
#
cp      initialconfig.sif        input.sif
#
simla   <<      eod
input
eod
#
erzatz        "#Hs"        "2"     dynamic1.sif
erzatz        "#Tp"        "7"     dynamic1.sif
#
cp      dynamic1.sif  input.sif
#
simla << eod
input
eod
#
erzatz        "#Hs"        "2"    dynamic2.sif
erzatz        "#Tp"        "7"    dynamic2.sif
cp      dynamic2.sif  input.sif
#
simla   <<      eod
input
eod
#
simpost <<      eod
mpfdyn
eod
#
cd ..
```

115

Appendix E

Plots

E.1   Critical torsion moment - PIPE31

A   Umbilical 1
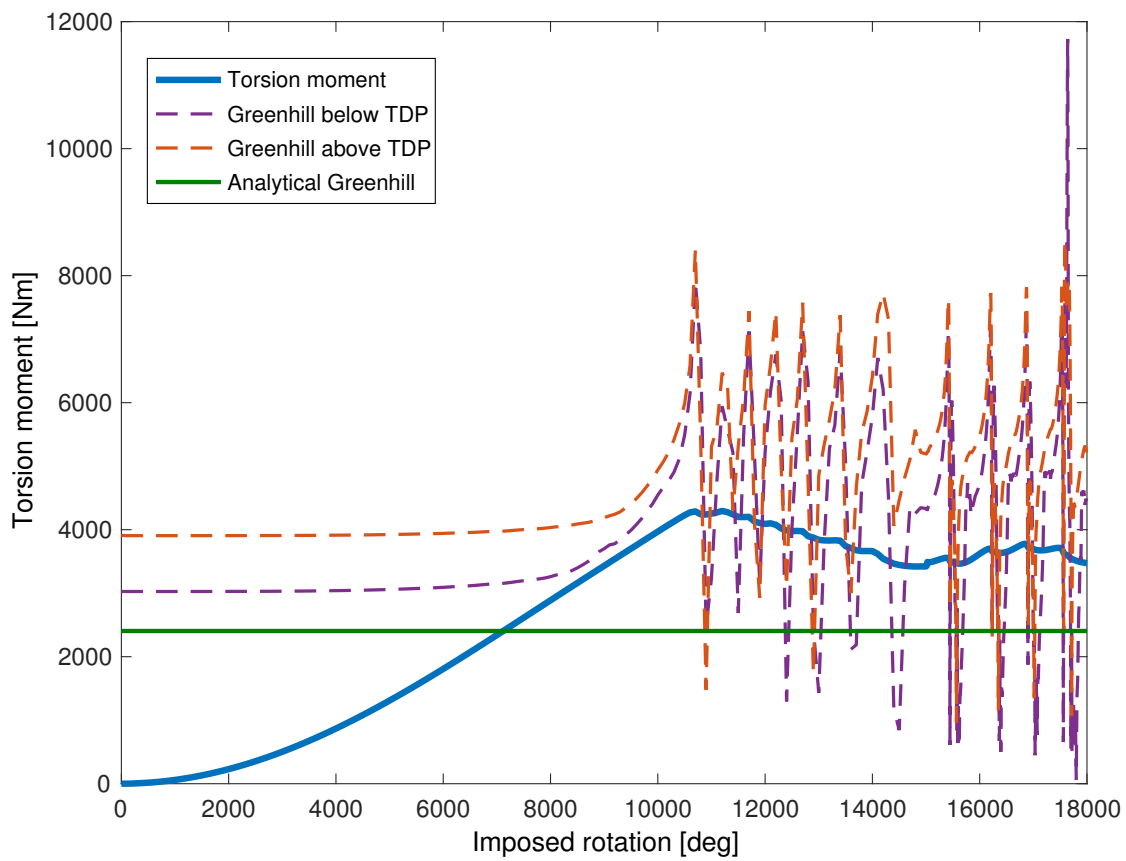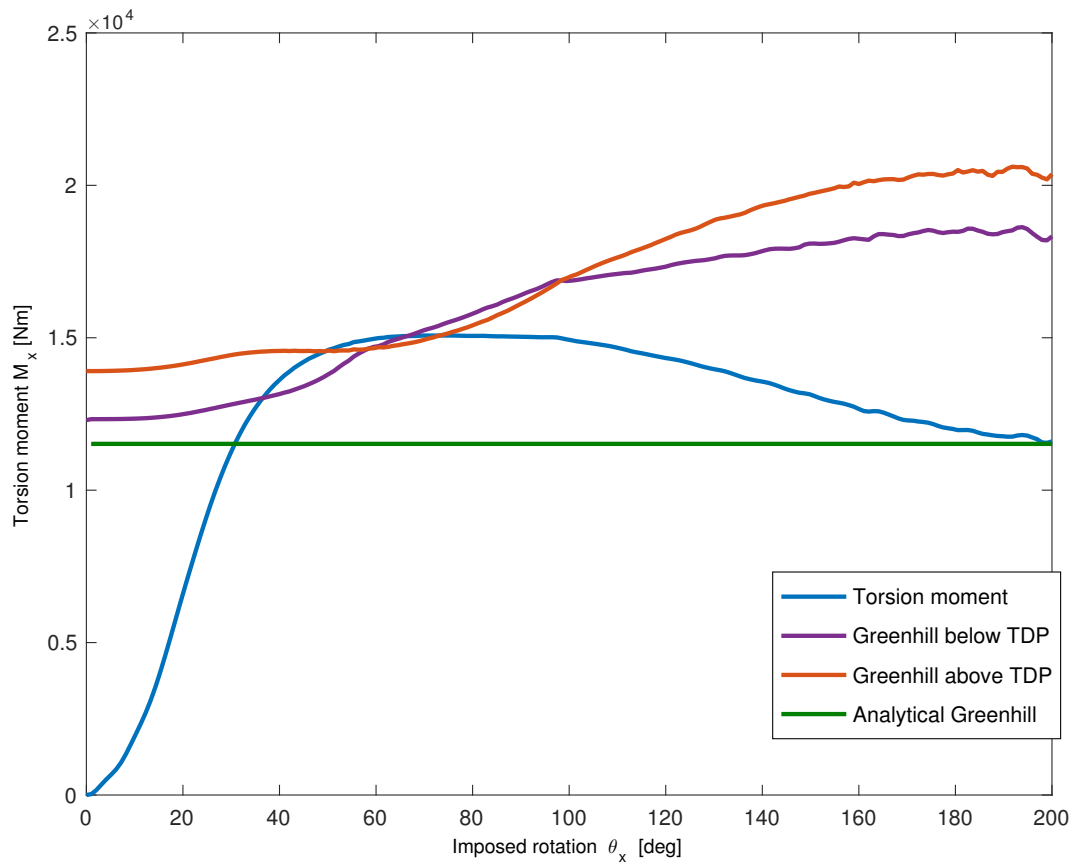
B   Umbilical 2

E.2 Resultant curvature distribution as a function of element coordinate and time

A Umbilical 1 - COMPIPE42
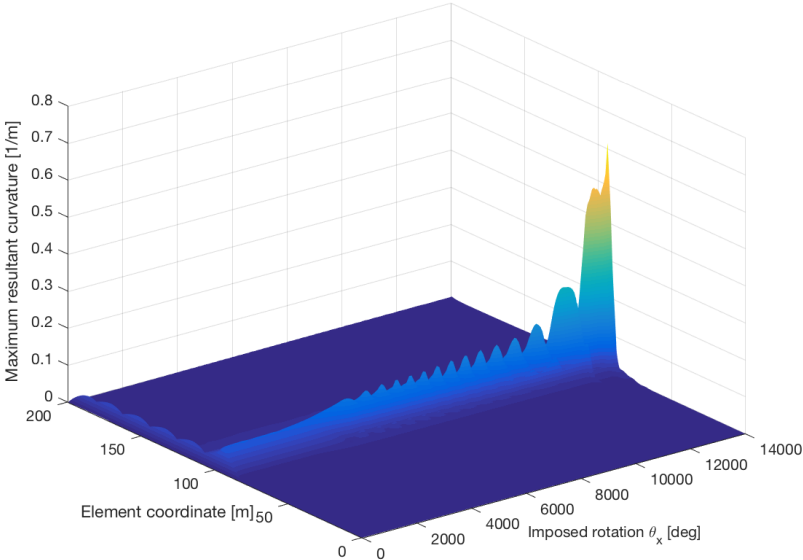
B Umbilical 2 - COMPIPE42
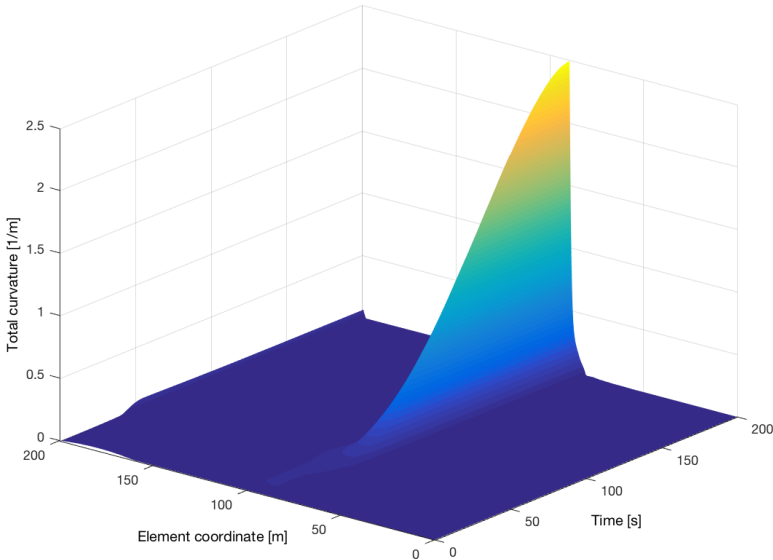
E.3   Maximum resultant curvature - PIPE31

A   Umbilical 1
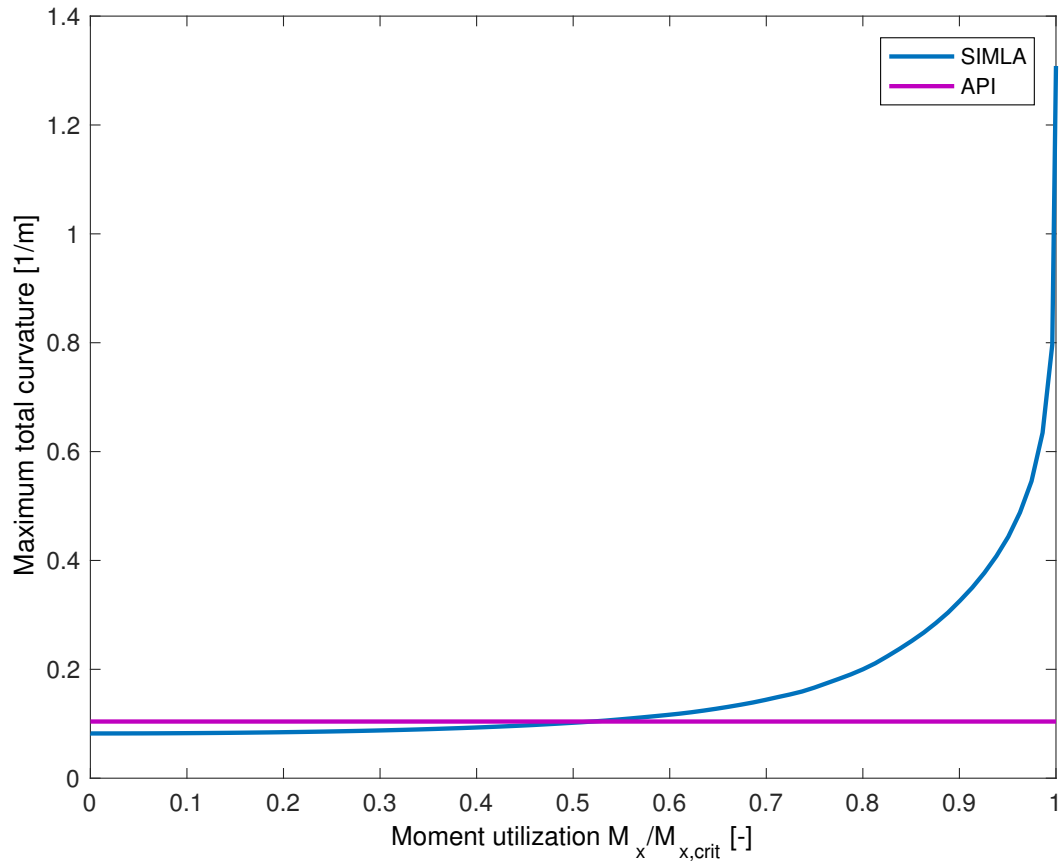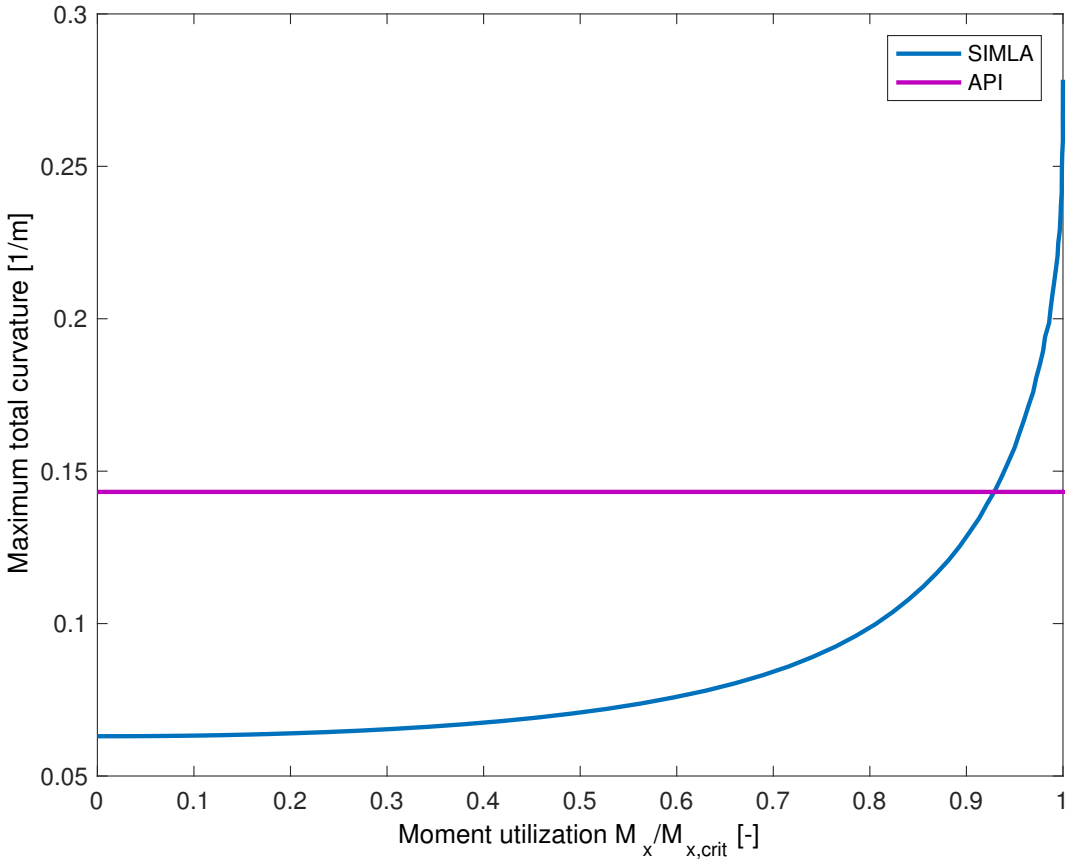
B   Umbilical 2

E.4 Tensile force distribution

A Umbilical 1 - end cap turn
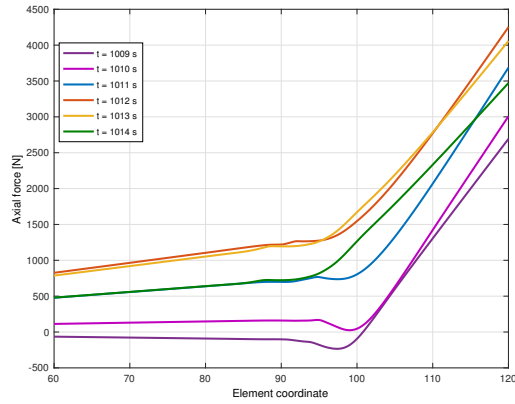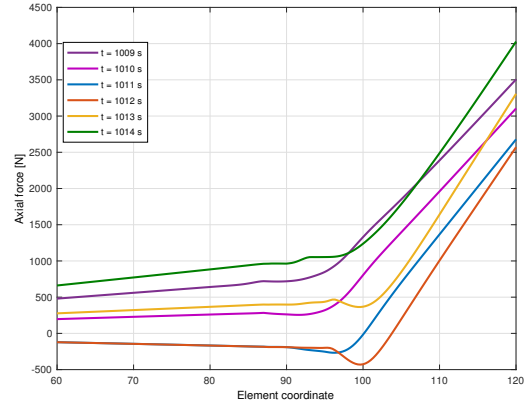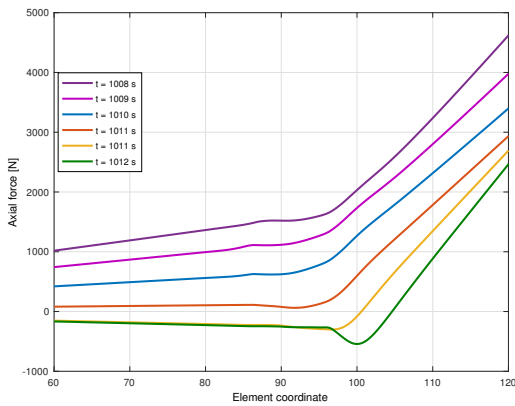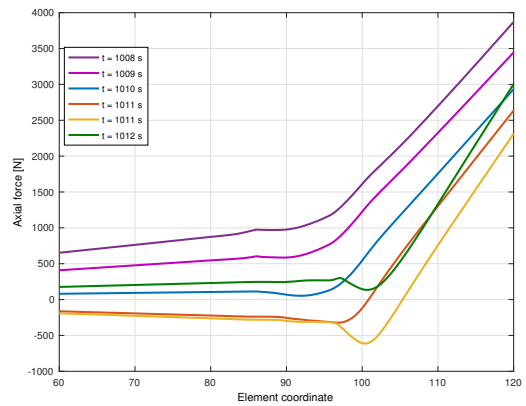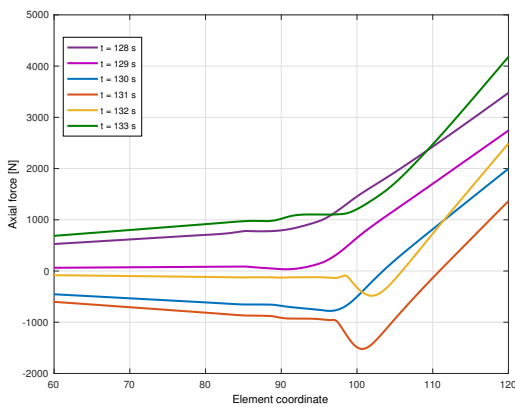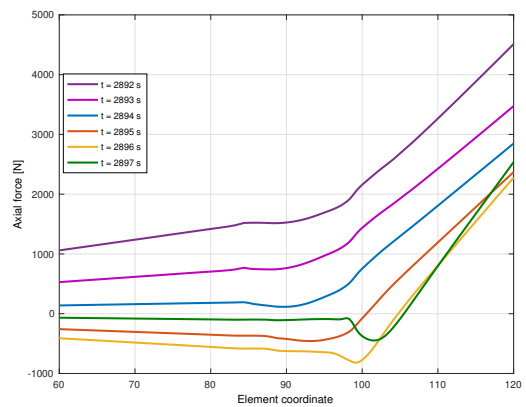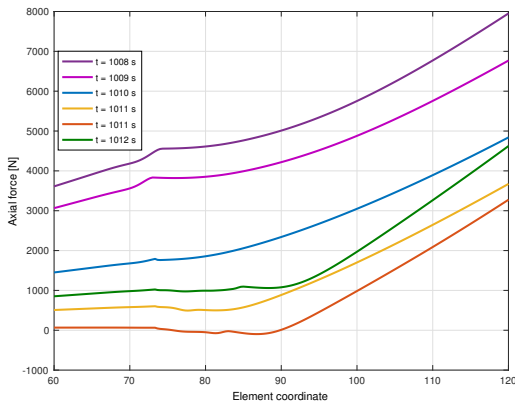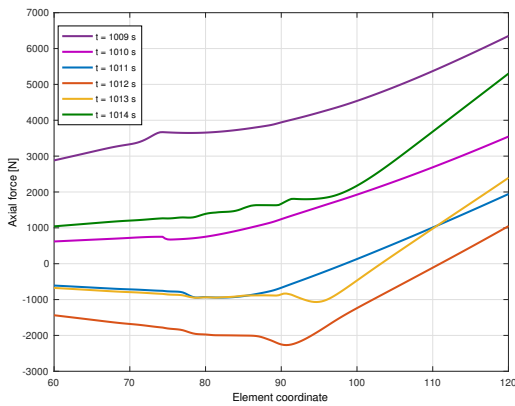

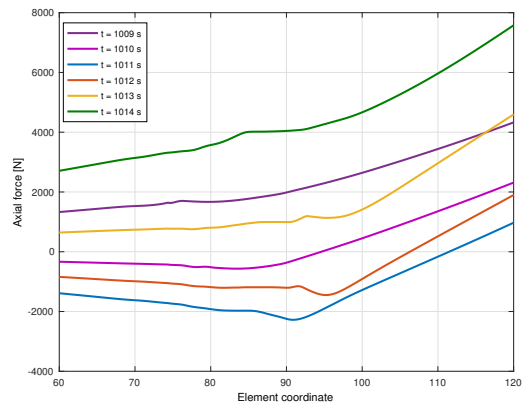(a) $H_s = 2m, T_p = 7s$

(b) $H_s = 2m, T_p = 8s$

(c) $H_s = 2m, T_p = 9s$

(d) $H_s = 2m, T_p = 10s$

(e) $H_s = 3m, T_p = 9s$

(f) $H_s = 3m, T_p = 10s$

B Umbilical 1 - curved routing
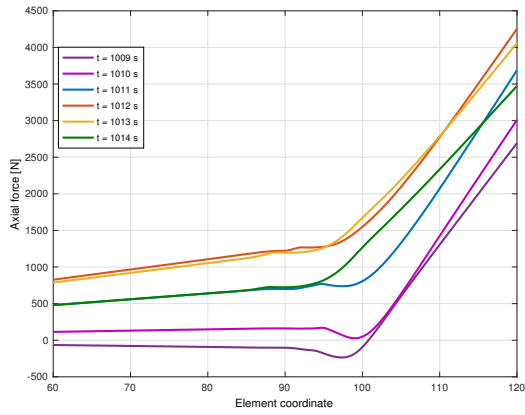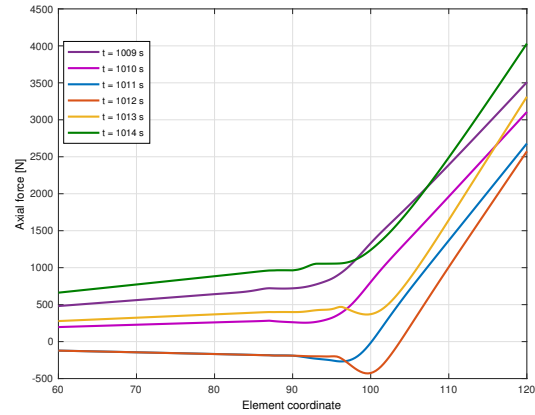
(a) $H_s = 2m, T_p = 7s$
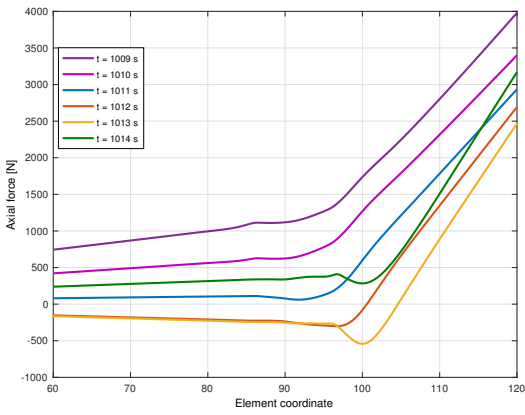
(b) $H_s = 2m, T_p = 8s$
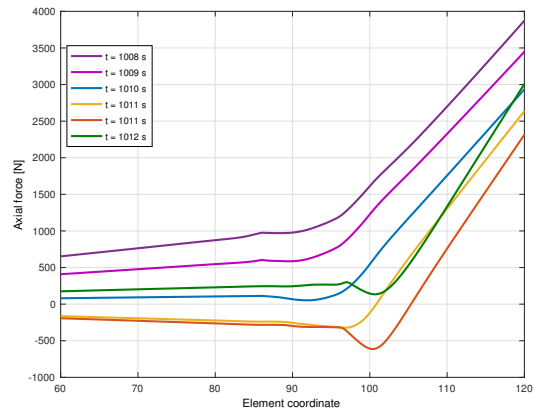
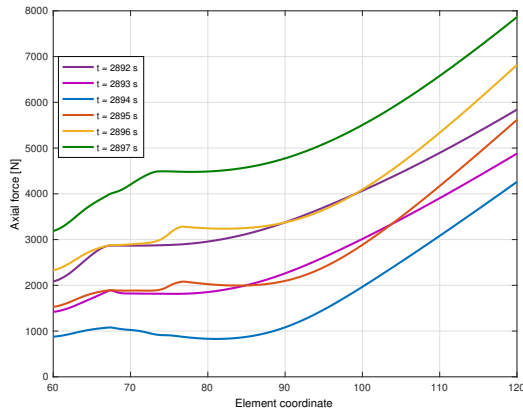(c) $H_s = 2m, T_p = 9s$
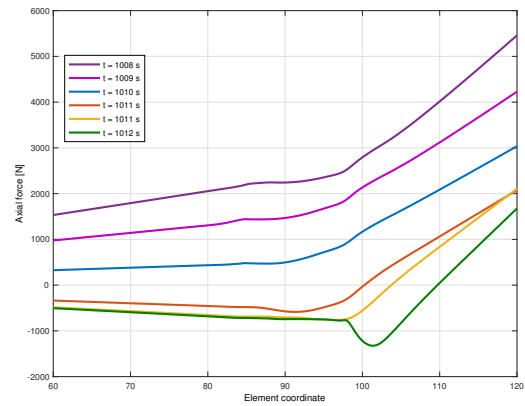
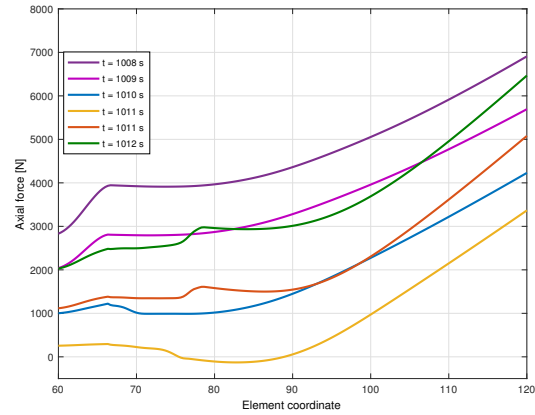(d) $H_s = 2m, T_p = 10s$
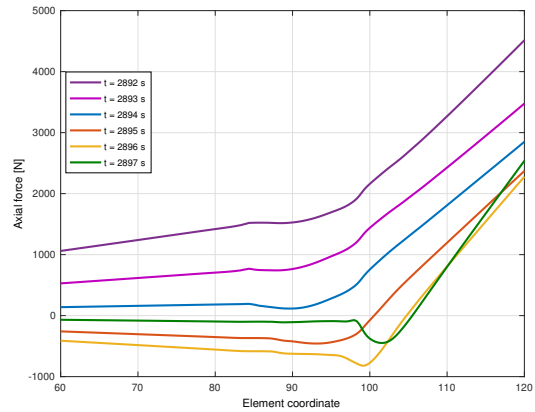
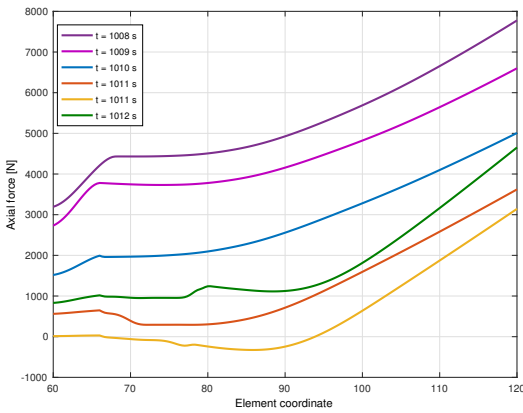(e) $H_s = 3m, T_p = 9s$

(f) $H_s = 3m, T_p = 10s$

C Umbilical 2 - curved routing
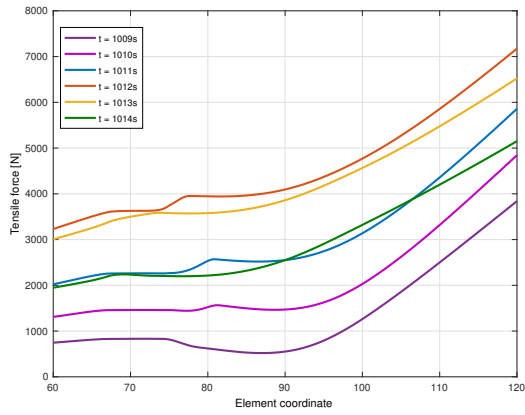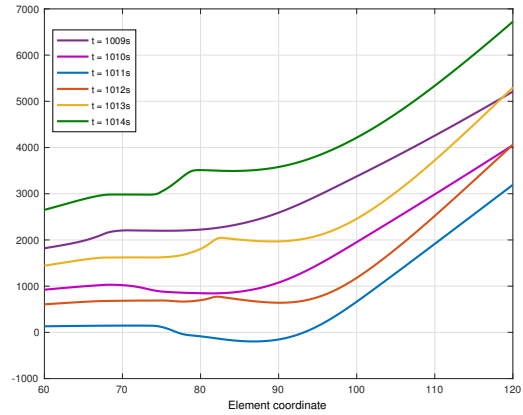
(a) $H_s = 2m, T_p = 7s$
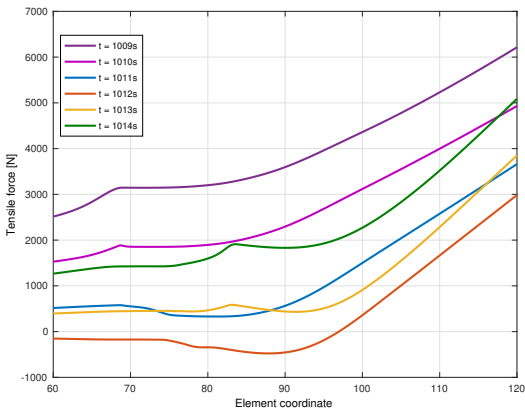
(b) $H_s = 2m, T_p = 8s$
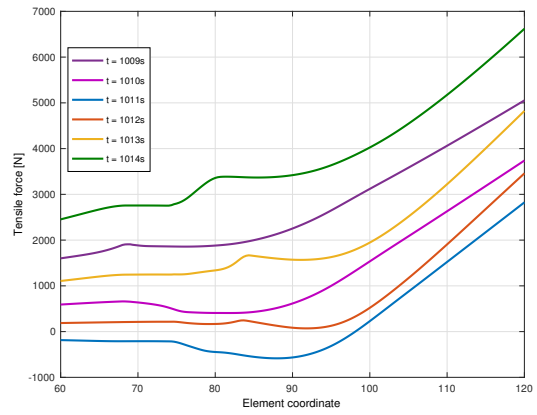
(c) $H_s = 2m, T_p = 9s$
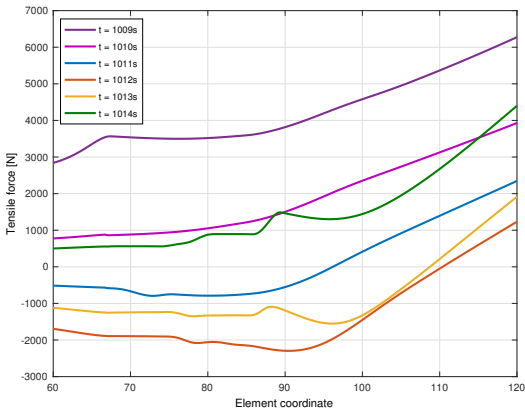
(d) $H_s = 2m, T_p = 10s$
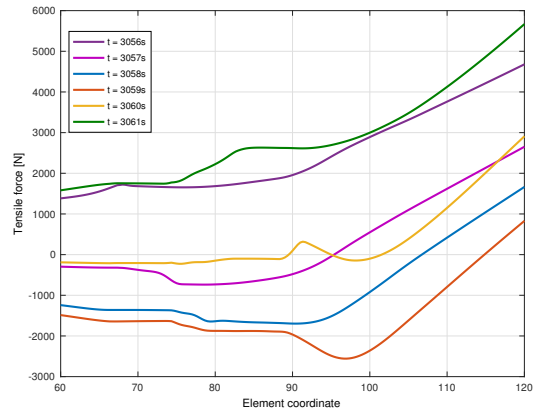
(e) $H_s = 3m, T_p = 9s$

(f) $H_s = 3m, T_p = 10s$

E.5 Tensile force distribution, $T_0 = 5000N$

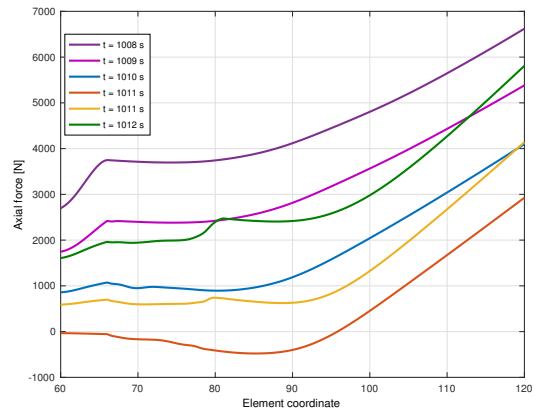## A Umbilical 1 - end cap turn
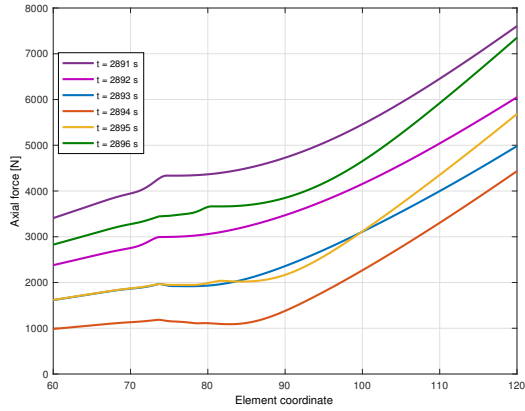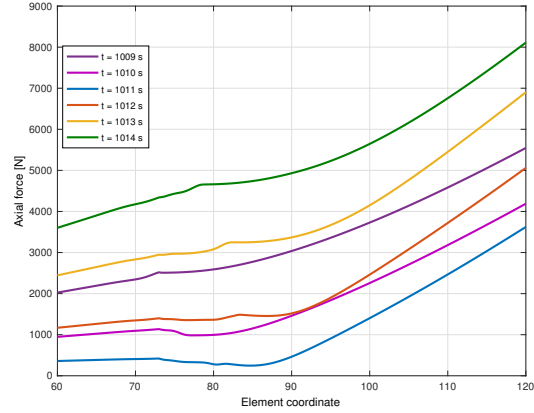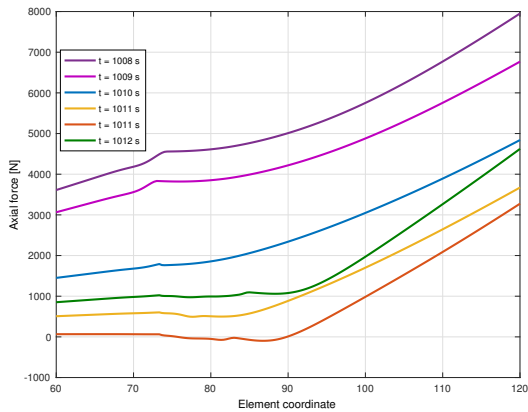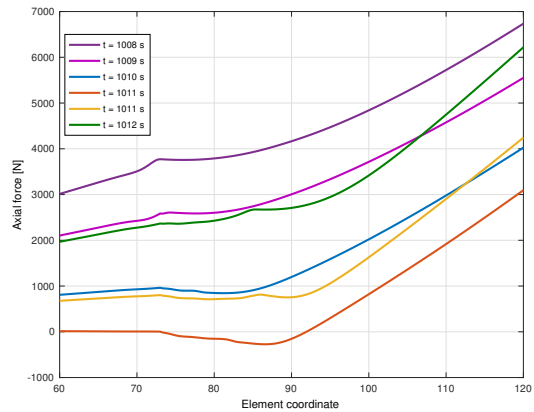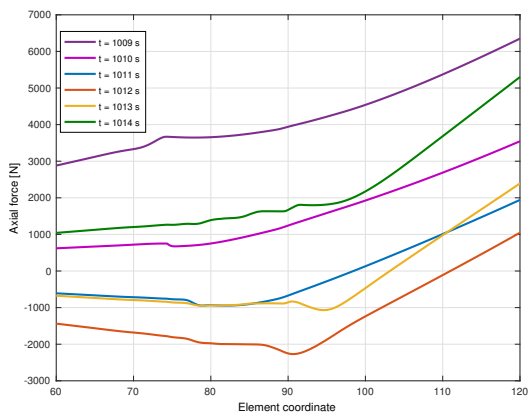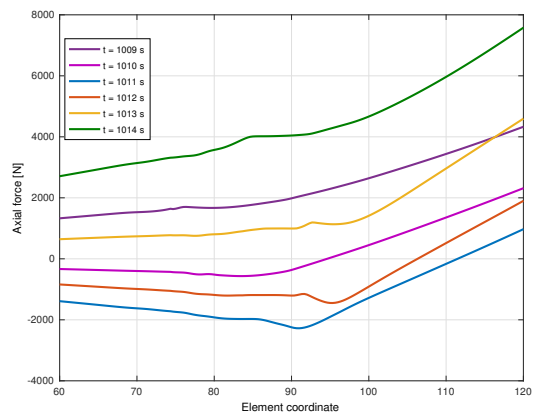
(a) $H_s = 2m, T_p = 7s$

(b) $H_s = 2m, T_p = 8s$

(c) $H_s = 2m, T_p = 9s$

(d) $H_s = 2m, T_p = 10s$

(e) $H_s = 3m, T_p = 9s$

(f) $H_s = 3m, T_p = 10s$

B   Umbilical 1 - curved routing
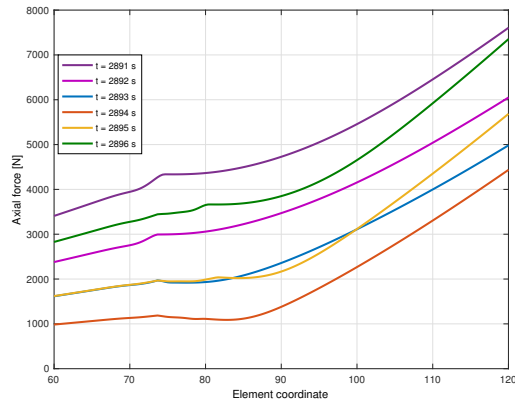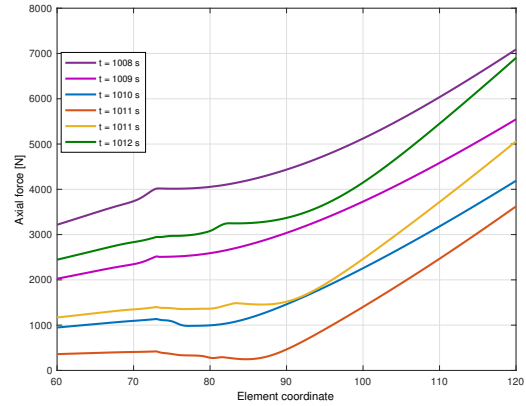
(a) $H_s = 2m, T_p = 7s$

(b) $H_s = 2m, T_p = 8s$
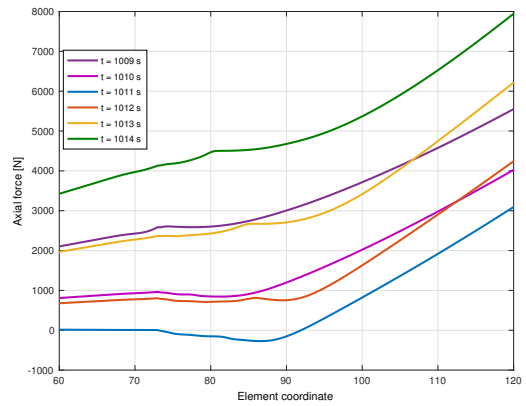
(c) $H_s = 2m, T_p = 9s$

(d) $H_s = 2m, T_p = 10s$

(e) $H_s = 3m, T_p = 9s$

(f) $H_s = 3m, T_p = 10s$

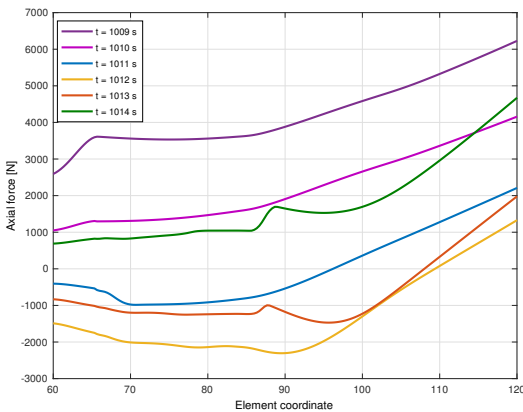## C   Umbilical 2 - curved routing

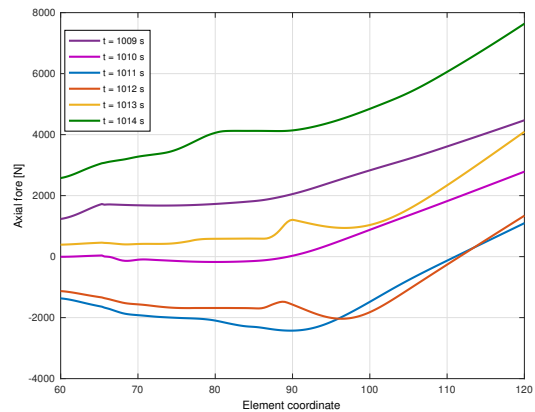

(a) $H_s = 2m, T_p = 7s$

(b) $H_s = 2m, T_p = 8s$

(c) $H_s = 2m, T_p = 9s$

(d) $H_s = 2m, T_p = 10s$

(e) $H_s = 3m, T_p = 9s$

(f) $H_s = 3m, T_p = 10s$

Appendix F

Input files

Attached with this thesis is a .zip-file containing all the input files for the various analyses carried out, as well as a excel worksheet containing relevant calculations for the values presented in this thesis. The .zip-file contains the following

Folder name	Description of file
Capacity_analysis	A folder containing the input files for analyses where the capacity of the cable with respect to torsion buckling is established. See ReadMe for more details.
Dynamic_analysis	Folder containing input files for the dynamic parametric studies carried out. The parametric studies comprehend variation of sea state, variation of heading, current direction as well as horizontal bottom tension. The script utilized in Cygwin for running consecutive analyses is also attached. See ReadMe for further explanation of the input files.
Relevant calculations	This folder contains the relevant calculations performed in context with this thesis. Two matlab-scrips calculating the flexural properties of the cross-sections. An excel sheath containing the relevant calculations of the catenary parameters and the torsion moment induced by installation scenario, as well as buckling loads associated with radial and lateral buckling of tensile armour wires.
Poster	A poster made for the Master Thesis Poster Exhibition, summarizing the main findings.